In-depth B cell analysis to determine pre-existing B cell immunity against SARS-CoV-2

Inaugural-Dissertation

zur

Erlangung des Doktorgrades

der Mathematisch-Naturwissenschaftlichen Fakultät

der Universität zu Köln

vorgelegt von

Meryem Seda Ercanoglu

aus Köln

Köln

2022

In-depth B cell analysis to determine pre-existing B cell immunity against SARS-CoV-2

Inaugural-Dissertation

zur

Erlangung des Doktorgrades

der Mathematisch-Naturwissenschaftlichen Fakultät

der Universität zu Köln

vorgelegt von

Meryem Seda Ercanoglu

aus Köln

Köln

2022

Gutachter:	Prof. Dr. Florian Klein Prof. Dr. Michael Nothnagel
Datum der mündlichen Prüfung:	18.03.2022

No te pierdas los detalles de tu vida. No son las grades cosas las que determinan.
Sino esos pequeños microinstantes de no se qué.
Y la vida se hace de momentos y momentitos que hacen momontones.
Asi que no te dejes pasar de largo. Y sentí, rebobiná, re reproducí, enlaza, delirate…
Recordá (como también leí alguna vez por ahi- re cordis-)
Volvé a pasar por el corazón.

-Natalia Vargas

Acknowledgments

I would like to express my special thanks and gratitude to my supervisor Prof. Dr. Florian Klein who gave me the opportunity to conduct my thesis research in his laboratory. It was his continuous guidance, support and trust that amplified my strengths to develop new skills and to grow as a scientist. His full commitment to science and his endless curiosity inspired me to this day and was a driving force behind my research. Having contributed to the substantial translational research of his laboratory fills me with pride.

Furthermore, I want to thank the Graduate School of Biological Sciences for offering many interesting workshops to improve and expand my skill set with special thanks to Dr. Isabell Witt for supporting me. I also want to thank Prof. Dr. Michael Nothnagel and Prof. Dr. Clara Lehmann for having been a member of my thesis committee for reviewing, exchanging insights and providing valuable comments.

I want to express my gratitude to all current and former members of the Klein laboratory and the Institute of Virology at the University of Cologne. I am grateful to have worked with such wonderful, open-minded, inspiring and funny people. My special thanks and appreciation to Janina Malenica, Franziska Bach, Hanna Janicki, Julian Potthoff, Till Schoofs, Nathalie Lehnen, Carola Ruping, Silvia Gulisano-Laudani, Felix Dewald, Henning Grüll, Philipp Schommers, Maike Schlotz, Sabrina Dähling, Nareshkumar Poopalasingam, Michael Korenkov, Susanne Detmer, Leona Dold, Matthias Zehner, Kanika Vanshylla and Timm Weber. On a more personal note, I would like to thank Christoph Kreer and Lutz Gieselmann for their endless support, encouragement and friendship. You filled each day with good laughs, dad jokes and weird conversations that made the laboratory unique and special. Christoph – to me, you are the kindest and one of the most inspiring and sharp-minded scientists and I am very thankful for everything you taught me.

Through close collaborations and the friendly and connective atmosphere at the CMMC I met wonderful people that enriched my days at work and personal life and I want to mention and thank them here: Kat Folz-Donahue, Christian Kukat, Hanna Ludwig, Lydia Meder, Marieke Nill, Carolin Selenz, Sebastian Theobald, Deniz Bartsch, Wenjie Yao, Leo Kurian, Max Augustin, Carola Horn, Clara Lehmann.

I am lucky that I have many, beloved and special people in my life and I want to thank them for accompanying me: Kader Sara Tutar, Sinan Ercanoglu, Asena Ercanoglu, Seyma Yücel, Sophia Pourdas, Dana Dajani, Mareike Richter, Henning Guthoff, Sabine Wollnik, Margret

Asmuth, Reza Aminnezhad, Maria José Vargas, Karosh Taha, Simona Müller, Johanna Hagemeier and Mona Heep.

Mein größter Dank gilt dir, Mama. Du hast dir ein besseres Leben für mich gewünscht und mir dafür den Weg geebnet. Es ist allein Dir zu verdanken, dass ich Zugang zu Bildung hatte und in meiner Entfaltung, Freiheit und Sicherheit empfinden durfte. Du hast mir gezeigt, wie man Hindernisse meistert und dabei niemals die Freude und Dankbarkeit für das Leben verliert. Mama, Kader, Sinan. Ohne euch bin ich nicht vollständig. Zuhause seid immer nur ihr.

I dedicate this work to my mother.

Table of Contents

1. List of Figures

2. List of Tables

3. Summary

The B cell-mediated humoral immune response is a major part of the human immune system and shapes disease progression and severity. Hallmark of an effective B cell response is the development of pathogen-specific antibodies after an infection or vaccination. Understanding the B cell response is critical for improving vaccine design and implementation of vaccine-strategies. In the past, pathogen-specific, neutralizing antibodies have been successfully identified and demonstrated to be a promising new therapeutic option to treat infectious diseases. A comprehensive and in-depth B cell receptor repertoire analysis therefore expands our knowledge and provides new insights about how these antibodies evolve and how they can be elicited.

In this thesis, I implemented and advanced techniques to study the B cell immune response and applied these to highly relevant infectious diseases. I investigated pathogen-driven alterations in the B cell receptor repertoire and isolated potent and broadly neutralizing antibodies as potential therapeutic agents. To this end, I co-established protocols for B cell subset identification and characterization on a cellular and sequence level by improving FACS sorting strategies and extracting B cell receptor sequence information on a single cell level and from bulk sorted cells. We revealed a convergent antibody evolution against an Ebola virus vaccine and SARS-CoV-2 and demonstrated that elicited antibodies show partly low levels of somatic hypermutation. Moreover, this thesis contributed critical techniques to identify and to analyze novel potential therapeutic antibodies against Ebola virus, HIV-1 and SARS-CoV-2. With the emerge of the COVID-19 pandemic, particular focus was set on the investigation of a pre-existing immunity against SARS-CoV-2 since these findings can be critical for vaccine strategies.

Taken together, this thesis provides detailed insights into B cell immune responses against viral infections with important implications for the development of vaccines as well as new drugs for therapy and prevention.

4. Zusammenfassung

Die B-Zell abhängige Immunantwort stellt einen wesentlichen Bestandteil des menschlichen Immunsystems dar und bestimmt Verlauf und Schwere einer Erkrankung. Ein Merkmal für eine effektive B-Zell Antwort ist die Entwicklung von erregerspezifischen Antikörpern nach einer Infektion oder Impfung. Das Verständnis der B-Zell-Antwort ist entscheidend für die Herstellung von Impfstoffen und der Implementierung von Impfstoffstrategien. In der Vergangenheit wurden erregerspezifische, neutralisierende Antikörper erfolgreich identifiziert und als vielversprechende neue Therapieoption zur Behandlung von Infektionskrankheiten nachgewiesen. Eine umfassende und tiefgreifende Analyse des B-Zell-Rezeptor-Repertoires erweitert daher unser Wissen und liefert neue Erkenntnisse darüber, wie sich diese Antikörper entwickeln und wie sie freigesetzt werden können.

Zielsetzung dieser Dissertation war es, Techniken zur Untersuchung der B-Zell-Immunantwort zu implementieren und weiterzuentwickeln, um sie auf relevante Infektionen anzuwenden. Ich untersuchte pathogen-bedingte Veränderungen im Repertoire von B-Zell-Rezeptoren und unterstützte die Analyse potenter und breit neutralisierender Antikörper. Dafür habe ich Protokolle zur Identifizierung und Charakterisierung von B-Zell-Subsets auf Zell- und Sequenzebene mit etabliert, indem ich FACS-Sortierstrategien verbessert und B-Zell-Rezeptorsequenzinformationen, auf Einzelzellebene und aus im Zellverband sortierten Zellen extrahiert habe. Wir konnten so eine konvergente Antikörperentwicklung gegen den Ebola-Virus Impfstoff rVSV-ZEBOV und SARS-CoV-2 zeigen und beobachteten dabei, dass die gebildeten Antikörper zum Teil wenige somatische Hypermutationen aufweisen. Diese Arbeit lieferte damit auch wesentliche Techniken zur Identifizierung potenzieller therapeutischer Antikörper gegen Ebola-Virus, HIV-1 und SARS-CoV-2. Mit Beginn der COVID-19-Pandemie wurde ein besonderer Fokus auf die Untersuchung einer vorbestehenden B Zell Immunität gegen SARS-CoV-2 gelegt, da diese Untersuchungen neue wertvolle Erkenntnisse für die Planung von Impfstoffen liefern können.

Zusammengefasst liefert diese Dissertation detaillierte Einblicke in die B-Zell-Immunantwort gegen virale Infektionen mit wichtigen Implikationen für die Entwicklung von Impfstoffen sowie neuen Medikamenten für Therapie und Prävention.

5. List of Abbreviations

ACE2	Angiotensin-converting enzyme 2
ADCC	Antibody-dependent cell-mediated cytotoxicity
ADCP	antibody-dependent cellular phagocytosis
AID	Activation-induced deaminase
AIDS	Acquired immunodeficiency syndrome
ART	Antiretroviral therapy
AU	Arbitrary units
AUC	Area under the curve
B cells	Bursa-derived cells
BC	Buffy Coat
BM	Bone marrow
bNAb	Broadly neutralizing antibody
CD	Cluster of differentiation
cDNA	Complementary DNA
CDR	Complementarity determining region
CH	Constant domain of the heavy chain
CL	Constant domain of the light chain
CoV-AbDab	Coronavirus antibody database
COVID-19	Coronavirus disease 2019
CPE	Cytopathic effect
DAPI	4’,6-Diamidin-2-phenlindol
DC	Dendritic cell
DNA	Deoxyribonucleic acid
E	Envelope
EBOV	*Zaire ebolavirus*
EBV	Epstein-Barr virus
ELISA	Enzyme-linked immunosorbent assay
EVD	Ebola virus disease
Fab	Fragments with specific antigen binding
FACS	Fluorescence-activated-cell-sorting
Fc	Fragment crystallizable
FDA	Food and drug administration
FSC-A	Forward-scatter-area
FSC-H	Forward-scatter-height

FWR	Framework region
GC	Germinal center
HC	Heavy chain
HCMV	Human cytomegalovirus
HIV-1	Human immunodeficiency virus 1
HSC	Hematopoietic stem cells
Ig	Immunoglobulin
IRB	Institutional Review Board
LC	Light chain
M	Membrane
mAbs	Monoclonal antibodies
MERS-CoV	Middle East respiratory syndrome coronavirus
MID	Molecular identifier
mRNA	Messenger RNA
N	Nucleocapsid
NK cells	Natural killer cells
NSP	Nonstructural proteins
nt	Nucleotide
ORF	Open-reading-frame
ORF	Open-reading-frame
PES	polyethersulfone
RAG1/2	Recombination genes 1/2
RBD	Receptor-binding-domain
RNA	Ribonucleic acid
RTC	Replicase-transcriptase complex
rVSV-ZEBOV	recombinant vesicular stomatitis virus - Zaire ebolavirus
S	Spike
SARS-CoV	Severe acute respiratory syndrome coronavirus
SHIV	Simian-human immunodeficiency virus
SHM	Somatic hypermutation
SSC-A	Side-scatter-area
T cells	Thymus-derived cells
TCID50	50% tissue culture infectious doses

TdT	terminal deoxynucleotidyl transferase
TMPRSS2	Transmembrane protease serine 2
UMI	Unique molecular identifier
V(D)J	Variable Diversity Joining
VH	Variable domain of the heavy chain
VL	Variable domain of the light chain
WHO	World Health Organization

6. Introduction

6.1. Basics of our immune system

Protection and clearance from viral infections is accomplished by a healthy immune system. Based on the levels of specificity the immune system can be divided into functions and components of the innate and adaptive immune system. The innate immune system includes various different cell types carrying receptors recognizing patterns on antigens that are germline-encoded, restricting them to a genetically-determined specificity [1-4]. The adaptive immune system mainly includes T cells and B cells which have highly variable antigen receptors accomplished by a complex gene segment rearrangement allowing for the generation of large receptor repertoires [5]. This diversity plays a major role for the ability of the immune system to detect any possible antigen [6]. Although not all infections are life-threatening, studying the pathogenesis and understanding the immune response against a particular virus provides an understanding of the human immune response. As represented by the ongoing global pandemics, including HIV-1 and SARS-CoV-2, this substantially shapes the way towards treatment options, limiting the spread of a virus and influencing vaccine design [7, 8]. Regarding the complexity of the human immune system, I focused in this thesis on adaptive immunity and specifically on the identification and characterization of the B cell mediated antibody immune response. The lymphocytes of the adaptive immune system provide an effective and highly specific immune response, able to recognize antigens from invading pathogens [6]. In 1890 Shibasaburo Kitasato and Emil von Behring proved the existence of protective substances circulating in the blood by transferring serum from animals, immunized against diphtheria, to infected animals. The infected animals were healed [9] and it was Paul Ehrlich in 1900 to propose the first model of an antibody molecule [10]. It was Max Cooper and his colleagues back in 1965 who discovered the function of B cells by conducting chicken experiments proving that B cells derive from the chickens' bursa and are therefore called B (bursa-derived) cells. Removal of the bursa results in lack of antibody production in those animals and overall impaired immune response [11, 12]. It was 1974 when scientists found out that the bone marrow serves as the bursa equivalent organ in humans [13, 14].

6.2. Antibody structure

Antibodies are the secreted form of the B cell receptor and therefore carry a hydrophilic sequence patch at the C-terminus instead of a hydrophobic membrane-anchoring one [6]. An antibody or an immunoglobulin (IG) with the molecular weight of ~150 kDa is composed of two identical heavy chains (HC), each ~50 kDa, linked to two identical light chains (LC), each 25 kDa, giving the molecule its characteristic Y-shape (Figure 1, A and B) [15]. Antibodies can be separated into three parts based on proteolytic cleavage with the enzyme papain: (i) the

two arms of the Y-shape which are identical and the so called “Fragments with specific antigen binding” (Fab). The N-terminal part of the heavy chain and the light chain make up the Fab. (ii) And into the C-terminal half of the heavy chains which is called “Fragment crystallizable” (Fc) (Figure 1, A). Fab arms and the Fc part are joined together by disulfide bonds in the so-called hinge region [6]. This region gives the antibody molecule its flexibility allowing independent movements of the two arms and the identical Fabs to facilitate potential simultaneous binding. Each chain itself can be divided into different domains: the light chains contain one variable domain (VL) and one constant domain (CL). For the heavy chain it is one variable domain (VH) but up to four constant domains (for IgG: CH1, CH2, CH3). The V gene sequence itself can be divided into structurally relevant regions called complementarity determining regions (CDR1, CDR2 and CDR3) that are flanked by so called framework regions (FWR) that mainly function as scaffold [16] (Figure 1, A). Taken together the CDRs provide the most critical structures for antigen-binding and are the most diverse component of the IG molecule. While the sequences for the CDR1 and CDR2 are germline encoded the CDRH3 results from multiple gene rearrangements and unencoded nucleotide insertions or deletions [17]. There are five heavy-chain isotypes (IgG, IgM, IgD, IgA and IgE) defining the functional antibody molecule activity which can change along the B cell receptor development process or after antigen-encounter [18-22]. And there are two types of light chains: kappa and lambda [23]. There is no functional difference between those chain types.

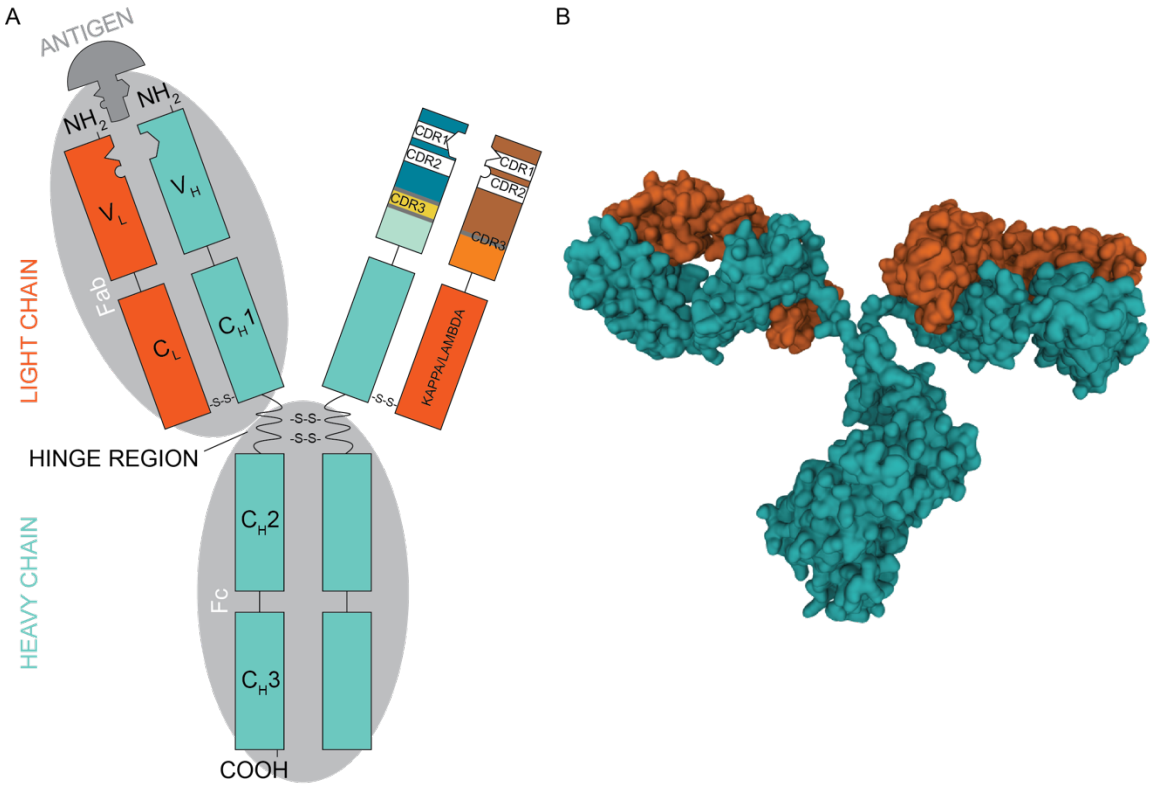

Figure 1: Antibody molecule structure

Schematic illustration (A) and crystal structure (B) of a typical IgG antibody molecule. An antibody molecule is made up of two heavy (green) and two light (orange) chains that are joined together through disulfide bonds (-S-S-). The chains comprise a constant domain (CH for the heavy chains and CL for the light chain) and a variable domain (VH for the heavy chain and VL for the light chain). It is the antibodies variable region, composed of VH and VL, where antigen binding occurs and which is therefore the most variable part of an antibody. (B) The crystal structure shows an intact, anti-canine lymphoma monoclonal IgG2a antibody (Mab231). PDB file format was obtained from the RCSB Protein data bank and modified using the PyMOL software [24].

6.3. B cell development and diversity

B cell development starts in the fetal liver before birth and after birth in the bone marrow where hematopoietic stem cells (HSC) differentiate into immature B cells before leaving the bone marrow (BM) (Figure 2) [25-27]. The different stages of B cell development are typically characterized by the B cell receptor formation and other cell surface molecules (Figure 2) [27]. Some of these surface molecules are assigned a “CD”-designation (cluster of differentiation). The markers CD19 and CD20 can be used for positive identification of cells of the B cell lineage except for antibody-secreting cells like plasma cells that lack CD20 [28]. Human CD19 is a 95 kDa transmembrane glycoprotein of the immunoglobulin superfamily with only one transmembrane domain, a cytoplasmic C-terminus and extracellular N-terminus [29]. CD20 is an approximately 33 kDa membrane protein only expressed on the surface of B cells which

made CD20 a promising target for immunotherapy against B cell lymphomas and autoimmune diseases [30]. Most prominent, the B cell-depleting monoclonal antibody rituximab, an anti-CD20 antibody to treat B cell tumors like Burkitt lymphoma, non-Hodgkin lymphoma and chronic lymphocytic leukemia [31, 32]. The B cell receptor facilitates binding to a specific antigen and therefore, varies considerably between individual B cells. The specificity is a result of variability in the antibody part that binds the antigen. The B cell receptor is composed of different germline-encoded gene segments [27, 33]. For the heavy chain the gene segments are variable (V), diversity (D) and joining (J). For the light chain variable region, it is V and J gene recombination. The different gene segments are combined to form heavy and light chain. For the heavy chain it is one random gene out of 56 functional heavy chain V genes which is coupled with one out of 23 random D genes and then coupled to one out of 6 J genes [23]. During kappa/lambda chain recombination it is pairing of one out of 41 V_{kappa} / 33 V_{lamdba} genes with one out of 5 $J_{kappa/lambda}$ genes [23].

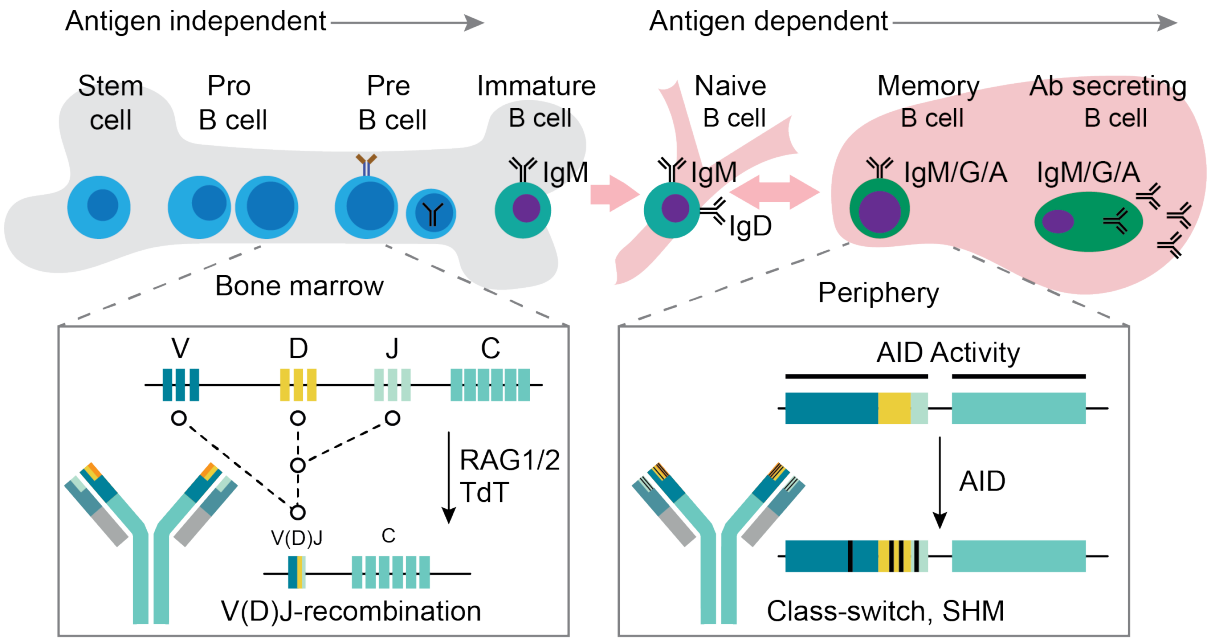

Figure 2: B cell development and subsets

B cell development starts in the bone marrow with a hematopoietic stem cell becoming an immature B cell before leaving the bone marrow site. B cell receptor formation is shaped by rearrangement of V, D and J gene segments during development. Further maturation takes place in the periphery and after entering the spleen or other secondary lymphoid organs such as lymph nodes. Upon antigen-encounter they differentiate into class-switch memory B cells and/or antibody-secreting B cells (Figure adapted from [27]).

By leaving the BM and entering the lymphoid and blood stream to the peripheral lymphoid organs (e.g., lymph nodes, spleen) the cells will undergo further maturation as in acquiring

IgD on its surface. These B cells are also known as naïve B cells that circulate between the blood and the lymphatic system until they encounter antigen or antigen-presenting cells [34]. Upon antigen encounter, the naïve B cell undergoes cell division (clonal expansion) and receptor sequence alterations in special lymphatic structures called germinal centers (GCs) [27]. In the GCs the enzyme activation-induced cytidine deaminase (AID) introduces random mutations, insertions and deletions into the variable regions (Figure 2) and diversifies the clonal population [35]. Simultaneously, cells switch from IgM and IgD heavy chain receptor types to IgG, IgA or IgE, leaving a molecular mark for affinity maturation [27, 36]. In contrast to naïve B cells, having a lifespan of a few weeks [37], memory B cells are long-lived and antigen-specific lymphocytes that provide an enhanced and rapid immune response upon reencounter of cognate antigen. Therefore, they represent a part of immunological memory and can protect the body from reinfection and related complications mediated by the same or a similar pathogen [34]. It is the combination of the following processes that is necessary to generate the B cell receptor repertoire diversity that is required: (i) random shuffling of gene segments during V(D)J recombination. (ii) heavy and light chain pairing [23]. (iii) somatic hypermutation (SHM) during affinity maturation upon antigen contact [35]. (iv) AID-mediated class-switch [36]. Up to 20 % of peripheral blood B cells in adults are memory IgG^+ B cells with four different IgG subclasses: Ig1, IgG2, IgG3 and IgG4 which is very rare [38, 39]. IgA memory B cells can also be found in the periphery but are predominantly in mucosa-associated lymphatic tissues [40]. IgE memory B cells are known to be involved in asthma and allergic diseases and hardly detectable in the periphery [41]. Taking these processes into account, the body can produce an almost infinite number of different B cell receptors [42]. To ultimately clear an infection, pathogen-specific antibodies are released by plasmablasts and plasma cells into the blood stream that target pathogens throughout the body [43].

6.4. Antibody effector functions

Antibodies have a variety of effector functions that can differ among the different antibody types and subclasses and physiological compartment where the infection occurs [44]. Antibodies can inhibit pathogens or their toxins by directly binding to them. While binding occurs with the Fab part, the Fc part of the antibody can bind to Fc receptors on other immune cells, such as macrophages and neutrophils, and activate phagocytosis or release of chemokines and cytokines. For example antibody-dependent cell-mediated cytotoxicity (ADCC) is the process when innate immune cells like NK cells, are activated by the Fc part of an antibody attached to an antigen and induce secretion of cytotoxic granules that result in killing of infected cells [45]. The destruction of infected cells through phagocytosis triggered by antibodies coating the infected cell or pathogen is known as antibody-dependent cellular

phagocytosis (ADCP) and another effector function [46, 47]. Another possible defense mechanism is the so-called complement activation. 'Complement' is a complex interaction of plasma proteins resulting in inflammatory and cytolytic immune responses [48, 49]. This broad spectrum of effector functions and their target specificity makes antibodies valuable for research, diagnostics, and therapeutic applications.

6.5. Advanced methods for B cell receptor analysis and monoclonal antibody identification

There are different approaches and methods to address scientific questions regarding B cell immune responses. For example, secreted antibodies in serum samples can be tested for binding (for example by ELISA and affinity chromatography) and for neutralizing activity using pseudovirus particle-based or authentic virus assays. Such experiments can inform on the presence of antibodies targeting a specific antigen and are useful in large-cohorts as screening approach or to understand infection dynamics [50]. This proved particularly useful during the ongoing COVID-19 pandemic, as the analysis of 2,146 SARS-CoV-2 convalescent serum samples revealed that advanced age, a symptomatic progression and severity of disease are predictive for SARS-CoV-2 neutralization. Neutralizing activity of serum and purified IgGs had half-lives of 14.7- and 31.4-weeks. The analysis further described an exceptional SARS-CoV-2 neutralization in approximately 3% of individuals. These individuals are called elite neutralizer and are interesting for the identification and isolation of potent antibodies for therapeutic approaches [51]. For the isolation of potent antigen-specific antibodies from elite neutralizer, fluorescence-activated cell sorting (FACS) can be used to sort single reactive B cells. An antigen-derived bait is used that can be a fluorescently-labeled protein such as a part of a receptor, antigens presented on virus-like particles or pathogens themselves ((reviewed in [50]). Alternative methods for the identification and analysis of reactive B cells, however in throughput relatively low, are B cell cultures of single and Epstein-Barr Virus (EBV) immortalized B cells [52-54]. A more advanced, alternative methods is LIBRA-seq using multiple fluorescently-labeled antigens simultaneously, since they are distinguishable by individual oligonucleotide-barcodes, to generate large high-throughput B cell-antigen libraries on single-cell level [55]. To extract antibody sequence information from the sorted B cells, designing the correct PCR-primers for amplification is critical, since the sequences can be highly mutated and all different V genes need to be covered. Current approaches for sequence identification and PCR-based amplification are Primer-design tools such as openPrimeR to generate optimized multiplex primer sets [56]. Isolated and *in vitro* produced antibodies from a single B cell clone that target a specific antigen are called monoclonal antibodies (mAbs) [57]. Standard research techniques as immunocytochemistry,

western blotting, enzyme-linked immunosorbent assays (ELISA) and flow cytometry use this feature to study protein and molecule interaction. In 1986 the first therapeutic monoclonal antibody was approved for kidney transplant patients threatened by graft lost and since then the interest and search for new potent mAbs has grown [58]. In 2019 over 90 mAbs have been approved by the US Food and Drug Administration and numbers are growing [59]. They interact with specific targets in targeted cancer therapy (e.g. Rituximab) [60, 61] and find clinical application in infectious diseases to target and neutralize infectious pathogens like Ebola viruses and the recent severe acute respiratory syndrome coronavirus 2 (SARS-CoV-2) [62-69], stimulate an autologous immune response [70, 71] and even prevent infections in animal models [72-75]. In this thesis we demonstrate single B cell analysis to infectious pathogens including Ebola virus, HIV-1 and SARS-CoV-2.

6.6. Ebola virus

Infections with *Ebolavirus* species such as *Zaire ebolavirus* (EBOV) can cause the severe and life-threatening Ebola virus disease (EVD) [76]. More thn 11,000 infected individuals died during the largest outbreak in West Africa in 2014-2016 (https://www.who.int/health-topics/ebola#tab=tab_1). The virus is initially transmitted to humans from wild animals and spreads by direct human to human contact or by contact with infected tissues or body fluids [77]. Mild and severe symptoms include fever, fatigue, muscle pain, headache, vomiting, diarrhea, impaired kidney and liver function and internal and external bleeding [76]. Current treatment options include the monoclonal antibodies Inmazeb [78] and Ebanga [79] approved by the FDA in late 2020. The most recent achievement from December 2020 is the FDA approval of the Ebola virus vaccine Ervebo [80] which has been administrated in the 2018-2020 Ebola virus outbreak in the Democratic Republic of the Congo and has been shown effective (https://www.who.int/emergencies/disease-outbreak-news/item/2021-DON351).

6.7. Human immunodeficiency virus 1 (HIV-1)

The human immunodeficiency virus 1 (HIV-1) infects immune cells and causes the life-threatening acquired immunodeficiency syndrome (AIDS) with 36.3 million deaths to date (World Health Organization, July 2021). It is transmitted by exchanging body fluids such as blood, breast milk, semen, and vaginal secretions. AIDS is defined by an impaired immune system leading to the development of cancers and opportunistic diseases caused by other infections. Infection with HIV-1 can be treated with the administration of antiretroviral therapy (ART) that suppresses the virus effectively. However, ART requires a life-long medication and can be associated with long-term side effects and drug resistance [81, 82]. There is currently no vaccine available. However, bNAbs directed against HIV-1 have been isolated and tested

in humans and are promising candidates in terms of feasibility, safety and efficiency in suppressing viral replication [64, 65, 83, 84]. Passive administration of bNAbs was shown to prevent against simian-human immunodeficiency virus (SHIV) infection in a macaque model [74, 85, 86]. Despite the promising findings, studies showed acquisition of viral escape mutations that lead to resistance, resulting in the ongoing search for new broadly neutralizing antibodies [64, 83].

6.8. Severe acute respiratory syndrome coronavirus 2 (SARS-CoV-2)

6.8.1. Epidemiology and pathogenesis

The severe acute respiratory syndrome coronavirus 2 (SARS-CoV-2), a member of the family of coronaviridae, was identified in December 2019 in Wuhan, China in patients suffering from pneumonia with a seafood market being identified as a potential first spreading spot [87]. On March 11, 2020 the World Health Organization (WHO) declared the novel coronavirus outbreak a global pandemic [88]. Since the start of the pandemic 275.54 million infections have been reported with 5.36 million reported deaths (at the timepoint of 21th of December 2021; https://coronavirus.jhu.edu/map.html). Coronaviruses are enveloped positive stranded RNA viruses that can infect humans, other mammals and birds and cause respiratory, enteric, hepatic, and neurologic diseases [89]. They are divided into four genera: alpha, beta, gamma, and delta coronaviruses (https://talk.ictvonline.org/files/master-species-lists/m/msl/12314). Most abundant coronavirus species that can cause common cold symptoms in humans are HCoV229E (alpha), HCoVNL63 (alpha), HCoVOC43 (beta) and HCoVHKU1 (beta) [90-93]. While most infections are not life threatening, a coronavirus outbreak in 2002/2003 with a member of the betacoronaviruses named severe acute respiratory syndrome coronavirus (SARS-CoV) caused 8096 cases with 774 related deaths [94, 95]. Another ongoing outbreak since 2012, with a species of coronaviruses named Middle East respiratory syndrome coronavirus (MERS-CoV), lead to (as of December 2021) more than 2,595 cases and 941 deaths (https://www.ecdc.europa.eu/en/publications-data/distribution-confirmed-cases-mers-cov-place-infection-and-month-onset-6) [96, 97]. SARS-CoV-2 is transmitted through respiratory intake of infected fluids. Thus, the most common route of transmission is any form of contact with exposure to aerosols (e.g. emitted when breathing, coughing, talking or sneezing) [98-100]. Most infections show no or mild symptoms such as fever, fatigue, cough, sore throat and headache [101]. Some individuals develop these symptoms but progress into acute respiratory distress, pneumonia, renal failure and death [102-104].

6.8.2. Structure

SARS-CoV-2 is a spherical enveloped virus with a diameter of 60-140 nm [87]. It contains a single-stranded positive-sense ribonucleic acid (RNA) genome [105] that encodes for 16 nonstructural proteins (NSP1-NSP16) essential for replication and transcription of viral proteins (for example NSP3 and NSP5 encoding for proteases or NSP12 for the RNA polymerase) and the structural proteins: spike (S), envelope (E), membrane (M) and nucleocapsid (N) (Figure 3). Corona-virions are covered with the spike (S) surface glycoprotein giving the virus family its crown (lat. *corona*) -like shape [106]. The S protein is essential for viral entry to the host cell and consists of two subunits: S1- subunit containing the receptor-binding-domain (RBD) and S2-subunit for viral- and host-membrane fusion [107]. The M interacts with all other structural proteins and promotes completion of viral assembly, host cell attachment and entry of the virions [108, 109]. The E protein is involved in assembly and releasing processes of the virus [110]. Essential for genome packaging and interaction with RNA is the nucleocapsid (N) protein [111].

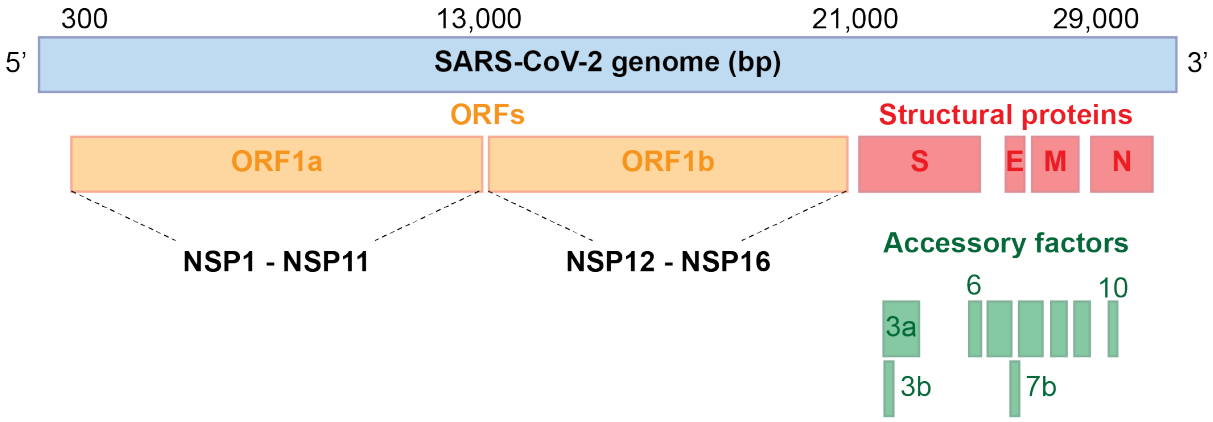

Figure 3: SARS-CoV-2 genome organization

The SARS-CoV-2 single-stranded positive-sense RNA genome encodes the two large open-reading-frames ORF1a and ORF1b which encode 16 non-structural proteins (NSP1-NSP16) (yellow). The structural genes are color coded in red and encode for the spike (S), envelope (E), membrane (M) and nucleocapsid (N). The accessory factor genes are displayed in green and encode for proteins that are not essential for viral replication (Figure adapted from [112]).

6.8.3. Life cycle of SARS-CoV-2

SARS-CoV-2 enters the host cell by attaching to angiotensin-converting enzyme 2 (ACE2) as entry receptor together with a cell host factor such as transmembrane protease serine 2 (TMPRSS2) expressed on cells like ciliated bronchial epithelial cells and type II pneumocytes, [113-115]. This binding leads to viral entry via membrane fusion or endocytosis. Once the virus has entered, the RNA genome is released in the cytosol and translation of ORF1a and

ORF1b into viral replicase proteins is initiated [116]. Host and viral proteases (e.g. NSP2 and NSP5) cleave the proteins into individual NSPs [117]. The viral protein NSP1 suppresses the host immune mechanisms by blocking the ribosomes to interfere with host mRNA-translation and promoting its degradation [118]. Some of those NSPs build a replicas-transcriptase complex (RTC) which is responsible for RNA replication and transcription of sub-genomic RNAs which serve as messenger RNAs (mRNAs) for structural and accessory genes [119]. Budding of new virions is processed at the endoplasmic reticulum–Golgi intermediate compartment (ERGIC). Assembled virions, mainly controlled by M and E protein functions, are transported to the cell surface in vesicles and released by exocytosis [120].

6.8.4. Treatment and prevention

At the time of conducting the SARS-CoV-2-related projects for this thesis, there was no vaccine or therapy available for patients suffering from COVID-19 (January 2020 – August 2020). We and other research groups worked on the identification and isolation of potent neutralizing antibodies targeting SARS-CoV-2 to implement a potential treatment option [62, 121-125]. In October 2020 the FDA approved the antiviral drug Remdesivir (also called Veklury) [126]. By the end of 2020 the FDA issued Emergency Use Authorizations (EUA) for the monoclonal antibodies REGEN-COV (Casirivimab and Imdevimab) that were tested in clinical trials and showed to reduce COVID-19-related hospitalization [127]. Followed by authorization of the monoclonal antibodies Bamlanivimab and Etesevimab in February 2021 [128] and the antibody Sotrovimab in May 2021 [129]. There are 3 vaccines approved by the FDA for full use. The Pfizer-BioNTech-vaccine Comirnaty was the first vaccine with an EUA by the FDA [130], followed by the Moderna-vaccine mRNA-1273 (Spikevax) in December 2020 [131] and the Janssen COVD-19 vaccine from Johnson & Johnson [132].

7. Aim of this thesis

Previous pathogen-encounters are memorized by B cells to provide protection after reencounter with the same or a similar pathogen [34]. Pathogen-specific B cells secret antibodies to neutralize the antigen and activate other immune mechanisms [133]. Analyzing the antibody-sequence information of different B cell subsets informs on B cell-antigen dynamics that impact our understanding of disease severity and progression and influence the development of vaccines and therapeutic options. In this thesis I aimed to study B cell responses against different pathogens (Ebolavirus, HIV-1 and SARS-CoV-2) and therefore implement and advance functional immunoassays. The specific aims are as follows:

1. Establishing protocols to study B cell immune responses in healthy and infected individuals on a single cell level and in bulk. We established and advanced protocols for the isolation of PBMCs from whole blood and buffy coat samples, followed by the purification of B cells to detect and isolate B cell subsets using fluorescence-activated cell sorting. Subsequently, I aimed to amplify the B cell receptor sequences for repertoire comparison of pathogen-specific B cell subsets to the overall repertoire. We utilized the advanced single cell cloning method to extract the pathogen-specific antibodies and next generation sequencing for the bulk sorted B cell subsets. Using these methods, we aimed to provide new insights into the B cell immune response against Ebolavirus and HIV-1.

2. Describing the B cell immune response of SARS-CoV-2 infected individuals. With the emergence of the novel SARS-CoV-2 pandemic we applied the methodologies and insights from aim one to identify potent neutralizing antibodies against SARS-CoV-2 and described repertoire characteristics to eventually find unique and pathogen-driven alterations in the B cell immune response of SARS-CoV-2 infected individuals over the course of several timepoints post infection.

3. Determining pre-existing B cell immunity against SARS-CoV-2. Based on the findings in aim two, we aimed to perform detailed B cell response analyses against SARS-CoV-2 in unexposed individuals, who provided blood samples before the COVID-19 pandemic. We aimed to explore SARS-CoV-2 directed reactivity on plasma and cellular level by establishing and using different advanced immunoassays and by identifying and eventually isolating putatively SARS-CoV-2-reactive B cells on a single cell level using FACS. This information was used to provide more data and insights towards the presence and clinical relevance of a pre-existing B cell immunity.

8. Material and Methods

Parts of the methods and used materials described here and showed in *9.1. Results-Part I* and discussed in *10.Discussion-Part I* are included in [63, 134, 135]. This includes text as well as figures. See also *14. Detailed description of work performed for this thesis.*

8.1 Part I: In-depth B cell analysis

8.1.1. Blood samples

Study participants were recruited at the University Hospital Cologne. 24 Buffy coats from study participants were collected according to a study protocol approved by the Institutional Review Board (IRB) of the University of Cologne (study protocol 16-054). Buffy coats were provided as residual products in the context of regular blood donations from the Institute for Transfusion Medicine at the University Hospital of Cologne.

Individuals participating in the study of Ehrhardt *et al.* 2019 initially enrolled in a Phase I trial study of an Ebola Virus Vaccine (rVSV∆G-ZEBOV-GP;NCT02283099). Whole blood and/or leukapheresis samples were collected under the IRB-approved study-protocol 16-054. All individuals provided written informed consent before participation [134].

Individual IDC561 in the study of Schommers *et al.* 2020 participated with a leukapheresis sample collected at the University Hospital Cologne under the study protocols 13-364 and 16-054 approved by the IRB. At the timepoint of participation, IDC561 was a male, 48-year-old, HIV-1-positive individual, who provided written informed consent [63].

8.1.2. Isolation of PBMCs

Peripheral blood mononuclear cells (PBMCs) were isolated from buffy coats/whole blood samples/leukapheresis samples by density gradient separation using Histopaque separation medium (Sigma-Aldrich) and Leucosep cell tubes (Greiner Bio-one). Briefly, Lecosep cell tubes were prefilled with 15 ml Histopaque separation medium and centrifuged for 1 minute at 800 *g* to transfer the medium underneath the separation barrier of the tube. Subsequently, blood products were poured above the separator and centrifuged for 15 minutes, 400 *g*, no brakes, no acceleration at room temperature. Erythrocytes are collected at the bottom of the tube and the PBMCs layer should be clearly visible in the middle of the tube above a layer of Histopaque solution and underneath the plasma layer. Plasma can be collected and long-term stored at -80 °C. PBMCs were carefully collected and washed twice in 1 x PBS before cryopreservation at -150 °C in 90 % fetal bovine serum (FBS) supplemented with 10 %

dimethyl sulfoxide (DMSO) (Sigma-Aldrich) until further use. If conducted, cell counts were performed using a Neubauer cell count chamber [135].

8.1.3. B cell enrichment

B cell enrichment from PBMCs was performed using magnetic CD19-Microbeads (Miltenyi Biotec) according to the manufacturer's instructions. Briefly, freshly isolated or thawed PBMCs were resuspended in MACS buffer and precalculated amount of CD19-Microbeads (20 µl beads per 10^7 cells). After incubation for 15 minutes at 4 °C and protected from light, cell suspension was washed with MACS buffer. LS MACS columns were equilibrated with MACS buffer and placed into the magnetic separator. Cell suspension was applied to the columns, so that $CD19^+$ B cells were positively selected using magnetic forces. To access the B cells, the LS column is removed from the separator and flushed with MACS buffer into a collection tube. Cell number was determined and cells were pelleted for 10 minutes at 400 *g* at 4 °C in preparation for FACS staining [134, 135].

For the study of Schommers *et al.* 2020 B cell enrichments were conducted using the negative selection B cell enrichment kits from Miltenyi Biotec (Pan B Cell Isolation Kit, B cell Isolation Kit II or IgG^+ Memory B Cell Isolation Kit) [63].

8.1.4. Single cell sorts

For bait-specific single B cell sorts as conducted in Ehrhardt *et al.* 2019 B cells were mixed with a fluorescence staining mix containing 4′,6-diamidino-2-phenylindole (DAPI) (Thermo Fisher), anti-human CD20-Alexa Fluor 700 (AF700) (BD), anti-human IgG-APC (BD) and the *Zaire ebolavirus* bait protein EBOV GPΔTM coupled to DyLight 488 (Microscale Antibody Kit, Thermo Fisher). Cell were incubated for 20 minutes on ice and washed with FACS buffer (1 x PBS, containing 2 % FBS and 2 mM EDTA). Gating strategy for single cell sorts was: forward-scatter-area (FSC-A) against side-scatter-area (SSCA-A) for lymphocyte identification, SSC-A against DAPI to gate into DAPI-negative events as a live/dead-marker. Doublet-events were excluded using FSC-A plotted against FSC-height (FSC-H). Human CD20-AF700 positive events were plotted against human IgG-APC for antigen-experienced B cells, before gating to the final sorting gate of EBOV GPΔTM-DyLight 488 against human IgG-APC. $DAPI^-$ $CD20^+$ IgG^+ EBOV $GP\Delta TM^+$ cells were sorted in a single cell manner into a 96-well PCR plate filled with 4 µl lysis buffer (0.5 x PBS, 0.5 U/µl RNAsin (Promega), 0.5 U/µl RNaseOut (Thermo Fisher Scientific), and 10 mM DTT (Thermo Fisher Scientific) per well. Plates were stored at -80 °C until further use [134, 135].

For bait-specific single B cell sorts as conducted in Schommers *et al.* 2020 B cells were mixed with a fluorescence staining mix containing 4′,6-diamidino-2-phenylindole (DAPI) (Thermo Fisher), anti-human CD19-AF700 (BD), anti-human IgG-APC (BD) and the respective HIV-1 Env bait-protein ($BG505_{SOSIP.664}$-GFP or biotinylated $YU2_{gp140}$). For the staining mix containing $YU2_{gp140}$ Streptavidin-PE (BD) was added as consecutive binding for detection. $DAPI^-$ $CD19^+$ IgG^+ HIV-1 Env bait-$protein^+$ cells were sorted in a single cell manner into a 96-well PCR plate filled with 4 µl lysis buffer per well. Plates were stored at -80 °C until further use [63]. All sorts were performed on a BD FACSAria Fusion Flow cytometer using the 100 micron nozzle in single-cell precision mode. FACS images were evaluated and exported using BD FlowJo v9/v10.

8.1.5. Antibody cloning and production from single cell sorted B cells

For antibody production heavy and light chain sequence information was amplified by first generating cDNA of the sorted single cells. Therefore, cells were mixed with Random Hexamer Primers (Thermo Fisher), NP-40 (Thermo Fischer) and RNase-free water for 1 minute at 65 °C. Followed by the addition of 5 x RT Buffer (Thermo Fischer), dNTPs (Thermo Fischer), DTT (Sigma Aldrich), RNase-free H2O, RNasin (40 U/ml, Promega), RNaseOUT (40 U/ml, Promega) and Superscript IV (200 U/ml, Thermo Fisher) and incubation at 42°C for 10 min, 25°C for 10 min, 50°C for 10 min, and 94°C for 5 minutes. By using a semi-nested PCR approach with a Platinum Taq DNA Polymerase or Platinum Taq Green Hot Start DNA Polymerase (Thermo Fisher) we amplified antibody sequences for further sequence analysis and cloning. We used previously described primers, including novel optimized V gene-specific primer mixes [56]. The optimized primer and CG_RT 50-AGGTGTGCACGCCGCTGGTC [136] were used for the 1st PCR, and the optimized primer and IgG_Internal RT 50-GTTCGGGGAAGTAGTCCTTGAC [137] for the 2nd PCR. PCR products were sequenced by Sanger sequencing. The 1st PCR product served as template for sequence and ligation independent cloning (SLIC). Briefly, cloning amplicons were produced by PCR using Q5 Hot Start High Fidelity DNA Polymerase (New England Biolabs) and specific forward- and reverse primers designed for the nucleotide sequence of the V- and J-regions [137] and including expression vector overhangs for the SLIC reaction. PCR was run at 98 °C for 30 s; 35 cycles of 98 °C for 10 s, 65 °C for 30 s, and 72 °C for 30 s; and 72 °C for 2 min. With the SLIC approach PCR products were cloned into IgG1, kappa or lambda chain human antibody expression vectors [138]. 293-6E cells (National Research Council Canada) were used for antibody production by co-transfection of heavy and light chain-encoding plasmids with polyethylenimine (PEI) reagent (Sigma-Aldrich). Cell were cultured at 37 °C and 6 % CO2 in FreeStyle 293 Expression Medium (Thermo Fisher) and 0.2% penicillin/streptomycin (Thermo Fisher) for 7 days. Supernatants were filtered and antibody was purified with protein G

Sepharose and incubation overnight at 4 °C. Protein G beads were transferred to chromatography columns for two washing steps with sterile PBS. 0.1 M glycine with pH = 3.0 was used to elute IgG from the column. 0.1 M Tris with pH = 8.0 served as buffer and was placed into the elution tube ahead. To exchange the buffer to PBS and to concentrate the antibodies, 30 kDa Amicon spin membranes (Millipore) were used that required multiple centrifugation steps, depending on the antibody-amount of a sample. Concentration was measured by UV/Vis spectroscopy using a Nanodrop (A280) [63, 134].

8.1.6. Bulk sorts for the unbiased B cell repertoire analyses

B cells were stained with a fluorescence mix containing DAPI (Thermo Fisher), anti-human CD20-AF700 (BD), anti-human IgG-APC (BD), anti-human IgM-FITC (BD), anti-human IgD-PE-Cy7 (BD) and anti-human CD27-PE (BD). Gating strategy for antigen-experienced B cells was $Dapi^-$, $CD20^+$, IgG^+ and for naïve B cells $Dapi^-$, $CD20^+$, IgM^+, IgD^+, $CD27^-$, IgG^-. The sorts were performed using the 4-way sort under 4-way purity precision mode into 2 mL collected tubes pre-coated with pure FBS using the 70 micron nozzle. Sorted cells were centrifuged for 5 minutes at 400 *g* at 4 °C. The supernatant was carefully discarded and cell pellets were immediately frozen on dry-ice and stored at -80 °C until further use. For the test experiments described in this thesis 100,000 antigen-experienced B cells and 100,000 naïve B cells were sorted. For the bulk sorts conducted in Ehrhardt *et al.* 2019 we collected 250,000 antigen-experienced B cells for each individual [134]. For the bulk sorts in Schommers *et al.* B cell enrichment was performed using CD19 microbeads as described in 8.1.3. as opposed to the negative B cell enrichment for the single cell sorts. B cells were stained with anti-human CD20-AF700 (BD), anti-human IgG-APC (BD), anti-human IgM-FITC (BD), anti-human IgD-PE-Cy7 (BD) and anti-human CD27-PE (BD) to isolate 200,000 antigen-experienced B cells ($Dapi^-$, $CD20^+$, IgG^+ IgM^-, IgD^-, $CD27^-$) [63].

8.1.7. Unbiased B cell repertoire analysis

RNA was isolated from bulk sorted antigen-experienced and/or naïve B cells with the RNeasy Micro Kit (QIAGEN) using the QiaCube (QIAGEN) instrument. To generate cDNA we used the template-switch reverse transcription according to the SMARTer RACE 50/30 manual using the SMARTScribe Reverse Tran- scriptase (Takara) with a template-switch oligo that included an 18-nucleotide unique molecular identifier (UMI). HC and LC (Kappa and lambda)-variable regions were amplified with a nested PCR using constant-region-specific primers. Amplicons were purified by gel-electrophoresis using [139] the Nucleo-Spin Gel and PCR clean up Kit (Macherey-Nagel). Purified heavy chain and light chains of the respective individual were

pooled and used for library preparation. Sequencing was done on an Illumina sequencer (MiSeq 2x300 bp) [63, 134].

8.1.8. Sequence evaluation

Initial processing and assembly of the raw sequencing reads was done with an in-house pipeline based on custom Python scripts, IgBLAST [140], Clustal Omega [139] and the pRESTO toolkit [141]. In brief, first step was to filter the raw reads by Phred quality score (mean of 25 or higher) and read length (250 bp or longer). Unique molecular identifiers (UMIs) were extracted and paired reads were pre-annotated with IgBLAST. Based on IgBLAST pre-annotation, an additional molecular identifier (MID) was extracted by taking consecutive 18 nucleotides (nt) starting 12 nt downstream of the end of framework region (FWR) 3. For error correction, reads with the same UMIs were grouped. Reads that did not match the most abundant V gene call or had more than 1 nt difference to any other read were removed from their assigned UMI group. Assuming that ungrouped and removed reads may result from RT, PCR, or sequencing errors within the UMI, the remaining single as well as the removed reads were re-grouped by their MID. MID groups with a unique V gene call and no more than 1 nt difference between included UMIs were re-defined as a novel UMI group. Clustal omega was used to align all reads within each corrected UMI group and aligned sequences were collapsed to build consensus reads. For consensus building, base calls were weighted by their quality (1 - error probability) and bases with the highest quality-weighted frequencies were taken as the consensus. Paired consensus reads were assembled with the pRESTO AssemblePairs module and a minimal overlap set to 6 nt. Assembled sequences were annotated with IgBLAST and productive sequences were kept for analyses. To minimize the influence of sequencing and PCR errors, NGS-derived sequences were only evaluated for UMI groups with at least three reads. This exact pipeline was previously described in [62, 63, 134].

8.2 Part II: B cell analysis of SARS-COV-2 infected individuals

All described methods and used materials described here and showed in *9.2. Results-Part II* and discussed in *10.Discussion-Part II* are included in [62] . This includes text as well as all figures. See also *14. Detailed description of work performed for this thesis.*

8.2.1. Blood samples

Blood samples from all 12 SARS-CoV-2 infected study participants were collected according to a study protocol approved by the Institutional Review Board (IRB) of the University of Cologne (study protocol 16-054) with written informed consent. Samples were collected in Munich Clinic Schwabing, University Hospital of Frankfurt and University Hospital Cologne.

Buffy Coats from 48 healthy individuals were collected before the SARS-CoV-2 outbreak from the Institute for Transfusion Medicine at the University Hospital of Cologne under the study protocol 16-054 [62].

8.2.2. Isolation of PBMCs and plasma

Peripheral blood mononuclear cells (PBMCs) and plasma were isolated from buffy coats and whole blood samples by density gradient separation using Histopaque separation medium (Sigma-Aldrich) and Leucosep cell tubes (Greiner Bio-one). For detailed description see also section “8.1.2. Isolation of PBMCs” and [62].

8.2.3. Isolation of total IgG from plasma

All plasma samples were heat-inactivated at 56 °C for 40 min before further use. Protein G Sepharose (GE Life Sciences) was mixed with 1 ml of heat-inactivated plasma overnight at 4 °C (GE Life Sciences) under constant rotation. Protein G beads were transferred to chromatography columns for two washing steps with sterile PBS. 0.1 M glycine with pH = 3.0 was used to elute IgG from the column. 0.1 M Tris with pH = 8.0 served as buffer and was placed into the elution tube ahead. To exchange the buffer to PBS and to concentrate the IgG extraction, 30 kDa Amicon spin membranes (Millipore) were used that required multiple centrifugation steps, depending on the IgG-amount of a sample. Concentration of purified IgGs was measured by UV/Vis spectroscopy using a Nanodrop (A280). Purified IgGs were stored at 4 °C [62].

8.2.4. Expression of SARS-CoV-2 S-protein and protein-purification

The construct used for the expression of the prefusion stabilized SARS-CoV-2 S ectodomain (amino acids 1-1208 of SARS-CoV-2 S; GenBank: MN908947) was kindly provided by Jason McLellan (Texas, USA) and described previously [107]. The construct contained two proline substitutions at residues 986 and 987 which were introduced for prefusion state stabilization. A ‘‘GSAS’’ substitution at residues 682–685 was introduced to eliminate the furin cleavage site and a C-terminal T4 fibritin trimerization motif. To ensure purification, the protein is fused to a TwinStrepTag and 8XHisTag at its C-terminus. HEK293-6E cells were transiently transfected with poly- ethylenimine (PEI, Sigma-Aldrich) and 1 µg DNA per 1 mL cell culture medium at a cell density of 0.8 x 10^6 cells/mL in FreeStyle 293 medium (Thermo Fisher Scientific) for protein production. Transfected cells were cultured for 7 days at 37 °C and 5 % CO2. Culture supernatant was harvested and filtered using a 0.45 mm polyethersulfone (PES) filter (Thermo Fisher Scientific) before the protein was purified by Strep-Tactin affinity chromatography (IBA lifescience, Göttingen Germany) according to the Strep-Tactin XT

intructions. Briefly, adding 100 mL 10x Buffer W (1 M Tris/HCl, pH 8.0, 1.5 M NaCl, 10 mM EDTA, IBA lifescience) the filtered medium was adjusted to pH 8 and loaded with a low pressure pump at 1 mL/min on 5 mL bedvolume Strep-Tactin resin. Washing of the column was done with 15 column volumes (CV) 1x Buffer W (IBA lifescience). Elution was conducted with 6x 2.5 mL 1x Buffer BXT (IBA lifescience). Elution fractions were collected and subsequently pooled. The buffer was exchanged to PBS with pH 7.4 (Thermo Fisher Scientific) by filtrating four times over 100 kDa cut-off cellulose centrifugal filter (Merck) [62].

8.2.5. SARS-CoV-2 S-protein ELISA

ELISA plates (Corning 3369) were coated with 2 µg/mL spike ectodomain protein of SARS-CoV-2 in PBS at 4 °C overnight. Plates were blocked with 5 % BSA in PBS for 60 min at RT before incubation with the fist antibody in 1 % BSA in PBS for 90 min, followed by anti-human IgG-HRP (Southern Biotech 2040-05) diluted 1:2500 in 1 % BSA in PBS for 60 min at RT. Development was done with with ABTS solution (Thermo Fisher 002024) and measured at an absorbance of 415 nm and 695 nm. Positive binding was defined by an OD ≥ 0.25 and an EC50 < 30 µg/mL [62]

8.2.6. SARS-CoV-2 neutralization assay with authentic virus

SARS-CoV-2 neutralization activity was determined by cytopathic effect (CPE) on VeroE6 cells (ATCC CRL-1586) in the presence of authentic SARS-CoV-2 (BavPat1/2020 isolate, European Virus Archive Global # 026V-03883). The protocol is based on a previously described protocol for MERS-CoV [142]. Starting concentration for plasma-isolated IgG samples was 1,500 µg/ml and for monoclonal antibodies 100 µg/ml. The samples were serially diluted in a 96-well plate and incubated for 1 h at 37 °C together with 100 50 % tissue culture infectious doses (TCID50) SARS-CoV-2. CPE was determined after 4 days. Absence of CPE was defined as neutralization. Neutralizing COVID-19 patient plasma was used as control in duplicates as an inter-assay neutralization standard [51, 62].

8.2.7. SARS-CoV-2-specific single cell sorts

For bait-specific single B cell sorts as conducted in Kreer *et al.* 2020, B cells were enriched as described in “8.1.3. B cell enrichment”. B cells were mixed with a fluorescence staining mix containing DAPI, anti-human CD20-AF700 (BD), anti-human IgG-APC (BD), anti-human CD27-PE (BD) and 10 µg/ml SARS-CoV-2 spike protein labeled with DyLight488. $DAPI^-$, $CD20^+$, IgG^+, $spike\ protein^+$ cells were sorted in a single cell manner into a 96-well PCR plate filled with 4 µl lysis buffer per well. Plates were stored at -80 °C until further use [62].

8.2.8. Antibody cloning and production of SARS-CoV-2-specific B cells

Antibody cloning and production of SARS-CoV-2-specific antibodies from the sorted B cells as conducted in Kreer *et al.* 2020 followed the protocol described in "8.1.5. Antibody cloning and production from single cell sorted B cells" and [63, 135] with some changes: PCR amplification for SLIC assembly was performed with extended forward primers based on 2nd PCR primers [56] covering the complete endogenous leader sequence of all heavy and light chain V genes [135] and reverse primers specific for the 5' end of heavy and light chain constant regions [62, 135].

8.3 Part III: Determining pre-existing B cell immunity against SARS-CoV-2

All described methods and used materials described here and showed in *9.3. Results-Part III* and discussed in *10.Discussion-Part III* are included in [143] that is (as of December 2021) under review at the iScience journal and available at biorxiv.org (https://doi.org/10.1101/2021.09.08.459398). This includes text as well as all figures and tables. See also *14. Detailed description of work performed for this thesis.*

8.3.1. Blood samples

Study participants were recruited at the University Hospital Cologne. 150 Buffy coats from study participants were collected according to a study protocol approved by the Institutional Review Board (IRB) of the University of Cologne (study protocol 16-054). Buffy coats were provided as residual products in the context of regular blood donations from the Institute for Transfusion Medicine at the University Hospital of Cologne. All study participants provided informed consent.

8.3.2. Isolation of PBMCs and plasma

Peripheral blood mononuclear cells (PBMCs) and plasma were isolated from all 150 buffy samples by density gradient separation using Histopaque separation medium (Sigma-Aldrich) and Leucosep cell tubes (Greiner Bio-one). For detailed description see also section "8.1.2. Isolation of PBMCs" and [62].

8.3.3. Isolation of total IgG from plasma

All 150 plasma samples were heat-inactivated at 56 °C for 40 min before total IgG isolation according to the protocol described in "8.2.3. Isolation of total IgG from plasma".

8.3.4. Expression of viral proteins and protein-purification

The following viral surface proteins were used in this study: (1) the stabilized spike protein ectodomain of the endemic HCoV-HKU1 (amino acids 1 – 1295, GenBank ID.: ABD75497). (2) the stabilized spike protein ectodomain of the endemic HCoV-OC43 (amino acids 1 – 1300, GenBank ID.: AAX84792). Both were kindly provided by Raiees Andrabi (California, USA) and Victor Corman (Berlin, Germany) and described previously [144-148]. (3) the prefusion stabilized SARS-CoV-2 S ectodomain (amino acids 1 – 1207; GenBank ID.: MN908947). The construct was kindly provided by Jason McLellan (Texas, USA) and Florian Krammer (New York, USA) and previously described [107, 149]. All of the human coronavirus constructs contain the following modifications: two proline substitutions for prefusion state stabilization (SARS-CoV-2: residues 986 and 987; OC43: residues 1078 and 1079; HKU1: residues 1071 and 1072) and the furin cleavage sites were mutated (SARS-CoV-2: ‘‘GGGG’’ substitution at residues 682–685; OC43: ‘‘GSAS’’ substitution at residues 762-766; HKU1‘‘GSAS’’ substitution at residues 756-760). The different coronavirus ectodomains were amplified from the synthetic gene plasmids by PCR and subsequently cloned into a modified sleeping beauty transposon expression vector containing a C-terminal T4 fibritin trimerization motif (foldon) followed by a Twin-Strep-Tag purification tag. This modification served for the recombinant protein productions by using stable HEK293 EBNA cells employing the sleeping beauty transposon system previously described [150]. HEK293 EBNA cells were transfected using FuGENE HD transfection reagent (Promega). After transfection cells were selected with puromycin and induced with doxycycline. The supernatants were harvested, filtered and recombinant proteins were purified via Strep-Tactin XT (IBA Lifescience) resin. For elution biotin-containing TBS-buffer was used (IBA Lifescience), and dialyzed against TBS-buffer. (4) the Ebola surface glycoprotein (EBOV Makona, GenBank ID.: KJ660347; amino acids 1 – 651) which was stabilized with GCN4 trimerization domain and expressed without the transmembrane domain as previously described [134] was used as negative control for HCoV S protein ELISAs.

8.3.5. SARS-CoV-2 and HCoV S-protein binding assays

ELISA plates (Greiner Bio-One 655092) were coated with 2 µg/ml (for IgG measurement) or 5 µg/ml (for IgM and IgA measurement) spike ectodomain protein of SARS-CoV-2, HKU1 and OC43 in PBS at 4°C overnight. Plates were blocked with 5% nonfat dried milk powder (Carl Roth T145.2) in PBS for 60 min at RT before incubation with plasma, polyclonal IgG or monoclonal antibody for 90 min at RT, followed by anti-human IgG-HRP (Southern Biotech 2040-05) diluted 1:2500 in blocking buffer (BB), anti-human IgM-HRP (Thermo Fisher Scientific A18835) diluted 1:2000 in BB or anti-human IgA-HRP (Thermo Fisher Scientific A18781) diluted 1:2000 in BB for 60 min at RT. Starting concentration for monoclonal

antibodies was 10 µg/ml in PBS with 1:5 serial dilutions. For polyclonal IgGs starting concentration was 500 µg/ml in BB and for plasma samples a starting dilution of 1:20 for IgG detection and 1:10 for IgM and IgA detection in BB. Polyclonal IgGs and plasma samples were diluted in 1:4 serial dilutions. Final reaction for development was done with adding ABTS solution (Thermo Fisher 002024) and read-out at an absorbance of 415 nm and 695 nm. Furthermore, we assessed IgG and IgM binding of all plasma samples against SARS-CoV-2 (S1/S2) by using the automated DiaSorin's LIAISON® at the Institute for Virology at the University Clinic of Cologne following the manufacturer's instructions. Cut-off values for IgG and IgM results were: negative < 12.0 AU/ml, equivocal ≥ 12.0 - < 15.0 AU/ml, and positive ≥ 15.0 AU/ml. To measure IgA antibody titers against SARS-CoV-2 (S1) in all plasma samples we used the automated Euroimmun Analyzer I system. Note here, that IgA was only measured against the S1 subunit of the SARS-CoV-2 S-protein. S/CO values were interpreted with the following cut-off values: negative S/CO < 0.8, equivocal S/CO ≥ 0.8 - < 1.1, positive S/CO ≥ 1.1.

8.3.6. Cell-surface expressed SARS-CoV-2 binding assays

TurboFect™ transfection of HEK293T cells with plasmids encoding for the full-length SARS-CoV-2 S-protein containing mCherry as reporter gene (GenBank ID.: MN908947) resulted in cell-surface expressed S-protein to assess binding of plasma antibodies by flow cytometry, as described previously [148, 151]. After 48 h post transfection at 37 °C and 5 % CO2, adherent cells were detached with PBS supplemented with 1 mM EDTA (pH = 7.4) and resuspended in FACS buffer (1x PBS, 2 % FCS, 2 mM EDTA). Plasma samples were tested in serial dilutions, starting with an initial dilution of 1:50 continuing in a 2-fold serial dilution for a total of 6 concentrations per sample. 3 x 10^4 cells per well were used in 50 µl of FACS buffer in a V-bottom-shaped 96 well plate. Cells and plasma dilutions were incubated on ice for 30 minutes, followed by a washing step with 100 µl FACS buffer per well. FACS staining mix was prepared for 50 µl per well with 1:160 dilution of anti-human Fc IgG-BV421 (Biolegend) and 1:100 dilution of anti-human IgM (Biolegend) [148]. After 30 minutes of staining with the FACS-antibodies, cells were washed and analyzed on a BD FACSAria Fusion instrument. FCS 3.1 files were analyzed using the FlowJo10 software (BD). For the analysis geometric mean values of all cells/single cells/mCherry positive (transfected cells) in APC-A channel (for IgM) and BV421-A channel (for IgG) were determined and graphically displayed using GraphPad Prism.

8.3.7. SARS-CoV-2 neutralization assay with authentic virus

All 150 plasma samples were tested against authentic SARS-CoV-2 following the protocol described in “8.2.5. SARS-CoV-2 neutralization assay with authentic virus” and [51, 62, 142]. With the following differences: Plasma samples were tested at a single dilution of 1:10 against 200 TCID50.

8.3.8. SARS-CoV-2 neutralization assay with pseudovirus

SARS-CoV-2 pseudovirus particles expressed the SARS-CoV-2 Wu01 spike protein (EPI_ISL_40671). It is produced by co-transfecting plasmids, using FuGENE 6 Transfection Reagent (Promega), for HIV Tat, HIV Gag/Pol, HIV Rev, luciferase followed by an IRES and ZsGreen, and the SARS-CoV-2 spike protein into HEK 293T cells. The pseudovirus particles were secreted into the supernatant and titrated after harvest by infecting HEK293T cells expressing human ACE2 [152]. Virus incubation was allowed for 48-hour at 37 °C and 5% CO2, luciferase activity was determined by addition of luciferin/lysis buffer (10 mM MgCl2, 0.3 mM ATP, 0.5 mM Coenzyme A, 17 mM IGEPAL (all Sigma-Aldrich), and 1 mM D-Luciferin (GoldBio in Tris-HCL) using a microplate reader (Berthold). For the final neutralization assays, a virus dilution was selected that had a 1000-fold increased relative luminescence unit (RLU) in infected cells compared to non-infected cells. Neutralization assays of plasma, polyclonal IgGs and monoclonal antibodies were conducted in single dilutions and/or serial dilutions. For single dilution assays polyclonal IgG samples (1000 µg/ml), plasma samples (1:10) and mAbs (50 µg/ml), were co-incubated with pseudovirus supernatants for 1 h at 37°C, followed by the addition of 293T-ACE-2 cells. After a 48 h incubation at 37 °C and 5 % CO2, luciferase activity was determined using the luciferin/lysis buffer. The background RLUs of non-infected cells were subtracted and % of neutralization was calculated. Each sample was tested in duplicates and the mean values were used for analysis. Serial dilution assays to determine Half maximal inhibitory concentration (IC50) values of mAbs comprised a dilution series of the antibody starting with a concentration of 50 µg/ml. IC50 values were calculated as the antibody concentration causing a 50 % reduction in signal compared the virus-only controls using a dose-response curve calculated in GraphPad Prism.

8.3.9. SARS-CoV-2-specific single cell sorts

For bait-specific single B cell sorts from 40 donors, B cells were enriched as described in “8.1.3. B cell enrichment”. B cells were mixed with a fluorescence staining mix containing DAPI, anti-human CD20-AF700 (BD), anti-human IgG-APC (BD), anti-human CD27-PE (BD) and 10 µg/ml SARS-CoV-2 spike protein labeled with DyLight488. $DAPI^-$, $CD20^+$, spike $protein^+$, IgG^+ and $DAPI^-$, $CD20^+$, spike $protein^+$, IgG^- cells were sorted in a single cell manner

into a 96-well PCR plate filled with 4 µl lysis buffer per well. Plates were stored at -80 °C until further use [62].

8.3.10. SARS-CoV-2 specific sequence amplification and analysis

For antibody production heavy and light chain sequence information was amplified as described in [62, 135]. Briefly, cDNA was generated as described in thesis section “8.1.5. Antibody cloning and production from single cell sorted B cells”. Heavy and light chain sequences were amplified from cDNA using optimized V gene-specific primer mixes [56] and Platinum Taq DNA Polymerase or Platinum Taq Green Hot Start Polymerase (Thermo Fisher Scientific) as previously described [56, 62, 63, 135]. For downstream sequence analysis only sequences with a mean Phred score of 28 and sequences with a minimal length of 240 nucleotides were selected. Sequences were annotated with IgBlast and IMGT [140, 153] and the variable region ranging from FWR1 to the end of the J gene was extracted. Base calls within the variable region with a Phred score below 16 were masked and sequences with more than 15 masked nucleotides, stop codons, or frameshifts were not considered for further analyses. Sequence clonality for each participant was analyzed by grouping identical VH/JH gene pairs and by determining the pairwise Levenshtein distance for their CDRH3s. Sequences with a minimal CDRH3 amino acid identity of at least 75 % (considering the shortest CDRH3) were assigned to one clone group. 100 rounds of input sequence randomization and clonal assignment were performed and the result with the lowest number of remaining unassigned (non-clonal) sequences was selected for downstream analyses. All clones were cross-validated by the investigators taking shared mutations and light chain information into account.

8.3.11. Antibody sequence selection for cloning and production

Antibodies were selected for cloning based on two approaches. The similarity approach was based on matching the sequences against 868 and 52 sequences from SARS-CoV-2-binding antibodies retrieved from the CoVAbDab (21.08.20, [154]) and [62]), respectively. Similarity restrictions were sequences with identical VH/JH combination, a CDRH3 length difference ≤ 2 AA, and a CDRH3 Levenshtein distance ≤ 3 AA in comparison to at least one SARS-CoV-2-binding antibody (18 in total). The second approach was the random approach, based on a selection performed to yield at least 6 random antibody sequences per individual including at least 3 different clones and at least 3 non-clonal sequences. In case of less than 3 clones, random non-clonal sequences were used to fill up the selection.

8.3.12. Antibody cloning and production of SARS-CoV-2-specific B cells

Antibody cloning and production of SARS-CoV-2-specific antibodies from the sorted B cells followed the protocol described in “8.1.5. Antibody cloning and production from single cell sorted B cells” and [135] with some changes: PCR amplification for SLIC assembly was performed with extended forward primers based on 2nd PCR primers [56] covering the complete endogenous leader sequence of all heavy and light chain V genes [135] and reverse primers specific for the 5’ end of heavy and light chain constant regions. The heavy chain variable regions of the IgG^- sorted B cell subsets were cloned into IgG1 expression vectors.

9. Results

Part I

9.1 Parts of the methods and used materials described here and discussed in *10. Discussion*-Part *I* are included in [63, 133, 134]. This includes text as well as all figures. See also *14. Detailed description of work performed for this thesis.*

9.1. In-depth B cell analysis

An in-depth analysis of B cell development, antigenic responses and dynamics can shape our understanding of (1) elicited antibodies post vaccination and their protectivity (2) frequency and features of antigen-specific antibodies and (3) antibody-application for prevention and treatment of diseases [50]. Since pathogen encounters substantially shape the composition of B cells in our overall B cell repertoires among the different subsets, we need advanced techniques that allow us to analyze the antigen-specific B cell response and characterize the overall B cell repertoire [155]. For this, we isolated peripheral B cells from healthy and infected individuals and sorted single antigen-specific B cells and B cells in bulk from the antigen-experienced B cell (IgG^+) and naïve B cell compartment (Figure 4). We extracted sequence information of both datasets to identify differences or similarities regarding levels of SHM, CDR3 lengths, B cell clonalities and V gene distribution (Figure 4). Here, I describe both protocols in detail and demonstrate their application in two studies that aimed to characterize the B cell response against Ebola virus and HIV-1, respectively.

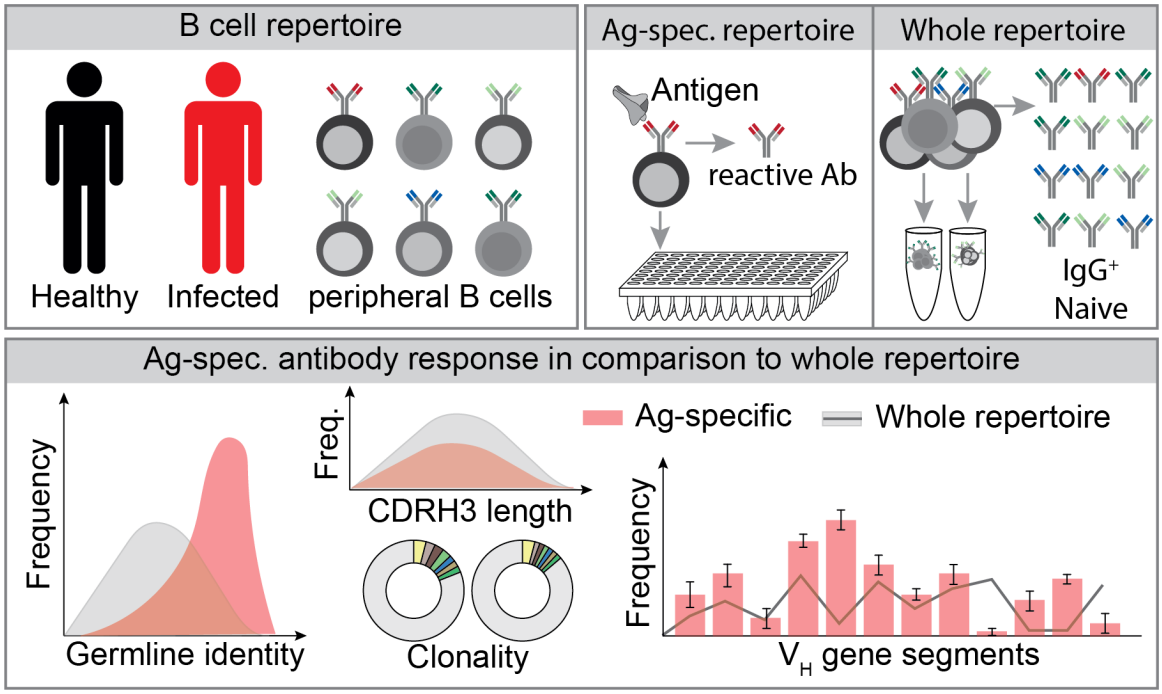

Figure 4: In-depth B cell repertoire analyses

We were interested in analyzing and characterizing the B cell repertoires of healthy and infected individuals by extracting antigen-reactive, antigen-experienced (IgG^+) and naïve B cells from the overall pool of peripheral B cells. Using fluorescently-labeled pathogen-derived baits we sorted single cells in 96-well plates. By sorting IgG^+ and naïve B cells and performing NGS, we generated large sequencing data-sets on whole subset-repertoires. We looked for differences and similarities in germline identity to exploit SHM-levels, CDR3-lengths, sequence-clonalities and V-gene distribution.

9.1.1. Pathogen-specific single B cell analysis

For the detection of human pathogen-specific B cells, we enriched B cells using magnetic beads (MACS) followed by quantitative and qualitative multi-parametric fluorescence activated cell sorting. PBMCs were isolated from peripheral blood by density centrifugation and mixed with magnetic microbeads that were conjugated to monoclonal anti-CD19 antibodies. Using a strong magnet $CD19^+$ B cells were selected and incubated with a FACS-antibody mixture including fluorescently labeled bait-protein. This allowed for bait-specific cell sorting in a single cell manner into 96-well plates (Figure 5, A).

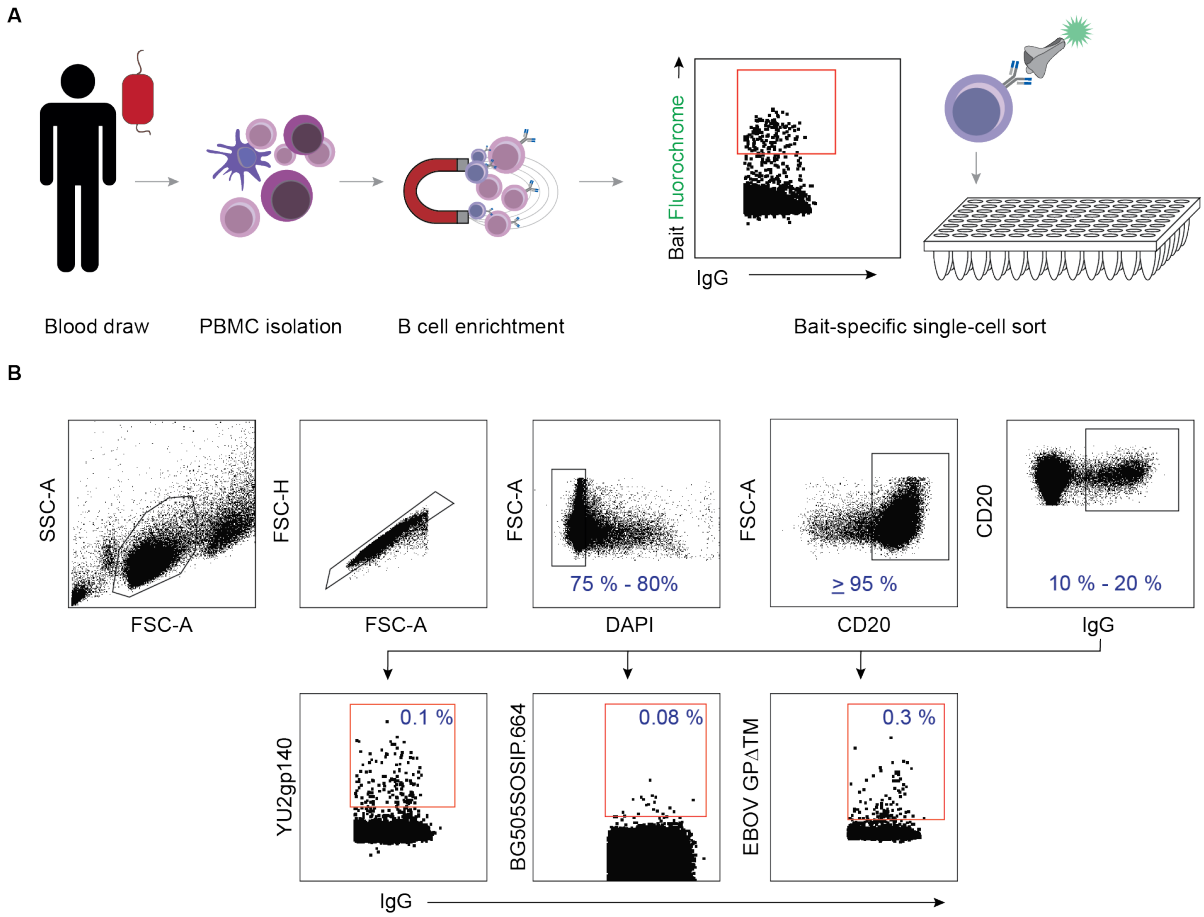

Figure 5: Isolation of pathogen specific single B cells

(A) Overview of the main steps to isolate pathogen-specific B cells. After blood draw, PBMCs were isolated and enriched for $CD19^+$ cells. Using a fluorochrome-conjugated bait protein in combination with IgG, FACS allowed for identification and isolation of pathogen-reactive single B cells. (B) Flow cytometry analysis displaying the gating strategy for antigen-specific single cell sort. Lymphocytes were identified in forward- and side-scatter followed by single, live cells using FSC-H, FSC-A and DAPI. Purified B cells were stained with anti-CD20 and anti-IgG antibodies. $YU2_{gp140}$ and $BG505_{SOSIP.664}$ were used as bait-protein to isolate HIV-1 reactive cells and EBOV GPΔTM for Ebola virus. Figure was adapted from [135] with data from [63] and [134].

Displaying the cells in forward-scatter-area (FSC-A) and side-scatter-area, lymphocytes are identified. Doublets were excluded using the forward-scatter-height (FSC-H) and FSC-A parameter. $DAPI^-$ events accounted for viable cells, which ranged between 75 % and 80 %. Purification efficiency of the magnetic $CD19^+$ cell enrichment was extrapolated from the $CD20^+$ cell proportion of >95 %. Of those B cells 10 % to 20 % were IgG^+ B cells and the population of interest here for pathogen-specific binding. We successfully established this workflow for single cell sorts of IgG^+ B cells that bound to the HIV-1 bait proteins $YU2_{gp140}$ and $BG505_{SOSIP.664,}$ respectively. Binding frequency of IgG^+ B cells to the bait proteins was higher for $YU2_{gp140}$ (0.1 %) compared to $BG505_{SOSIP.664}$ (0.08 %) (Figure 5, B) [63]. This protocol was

also used to sort *Zaire ebolavirus* glycoprotein (lacking the transmembrane domain; EBOV GP Δ TM) reactive IgG^+ cells (0.3 %) (Figure 5, B) [134]. The isolation of pathogen-specific single B cells was the first step and foundation for the protocol for effective high-throughput isolation of fully human antibodies targeting infectious pathogens by Gieselmann & Kreer *et al.* 2021.

9.1.2. B cell receptor analysis of bulk sorted B cell subsets

From the isolated pathogen-specific B cells we amplified heavy and light chain information to perform sequence analysis [56, 135]. We looked for clonal relationships by grouping sequences with identical VH/JH gene pairs and similar CDRH3 amino acids. We assessed CDRH3 length and hydrophobicity as well as V gene germline identities. To identify unusual antibody features in terms of CDR3 regions, somatic hypermutation or restriction to certain V genes we needed a B cell receptor sequence data set representative for the overall receptor repertoire in this individual to use as reference for comparison [50, 62, 63, 134]. Here, we established a protocol for the generation of a reference sequence data set of the naïve and antigen-experienced B cell repertoire. For the generation of red blood cell- and thrombocyte-concentrates after blood donation in the blood bank, buffy coats were produced as by-products and contain a concentrated composition of immune cells. Here, 24 Buffy coats were collected for PBMC and B cell isolation. Buffy coat volumes ranged from 51 to 63 ml and contained 683.5 million PBMCs in total on average, determined by cell counting after PBMC isolation by density gradient solution. After B cell enrichment using CD19 microbeads, cells were counted and stained for FACS analysis. Antigen-experienced B cells were defined here as $DAPI^-$, CD20+, IgG^+ cells and naïve B cells as $DAPI^-$, $CD20^+$, IgM^+, IgD^+, $CD27^-$, IgG^- cells (Figure 6, A). Measured from 24 samples, buffy coats contained on average 7.9 % B cells, 0.6 % IgG^+ B cells and 1.4 % naïve B cells (Figure 6, A). Using these parameter we determined the initial buffy coat volume needed to sort 1x 10^5 antigen-experienced B cells (3.7 ml) and 1x 10^5 naïve B cells (1.5 ml) (Figure 6, A). Staining and sorting strategy was applied to whole blood samples taking a PBMC concentration of ~1 x 10^6 PBMCs/1 ml whole blood [135] into account compared to a Buffy coat concentration of 12 x 10^6 PBMCs/1 ml.

A

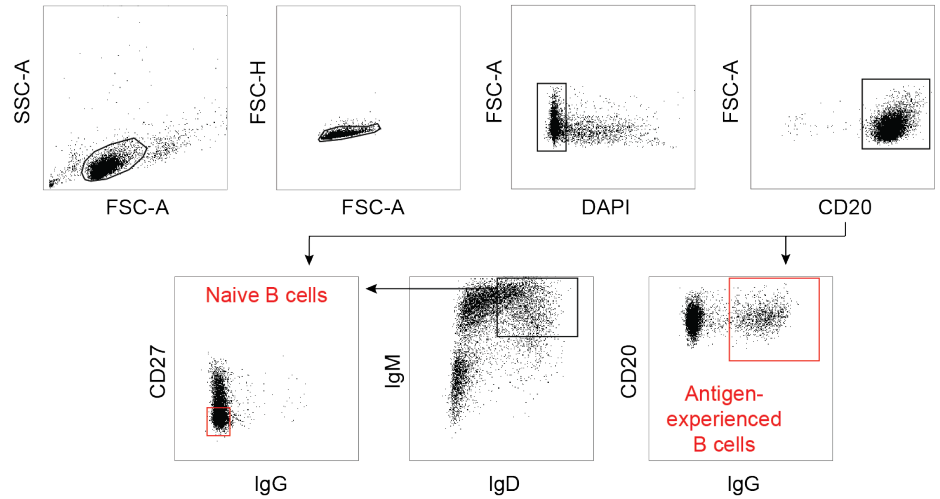

	(ml) BC volume	(x10⁶) per BC PBMC count	(%) B cells per BC			(ml) BC for 10⁵ cells	
			CD19/20⁺	**IgG⁺**	**Naive**	**IgG⁺ B cells**	**Naive B cells**
Top value	63.0	1,438.4	21.6	1.7	3.7	16.2	7.7
Bottom value	51.0	192.0	2.4	0.1	0.1	0.3	0.1
Median	58.0	668.4	6.8	0.5	1.0	2.2	1.0
Mean	58.0	683.5	7.9	0.6	1.4	3.7	1.5
SD	2.9	374.2	4.7	0.5	1.0	4.3	1.7

B

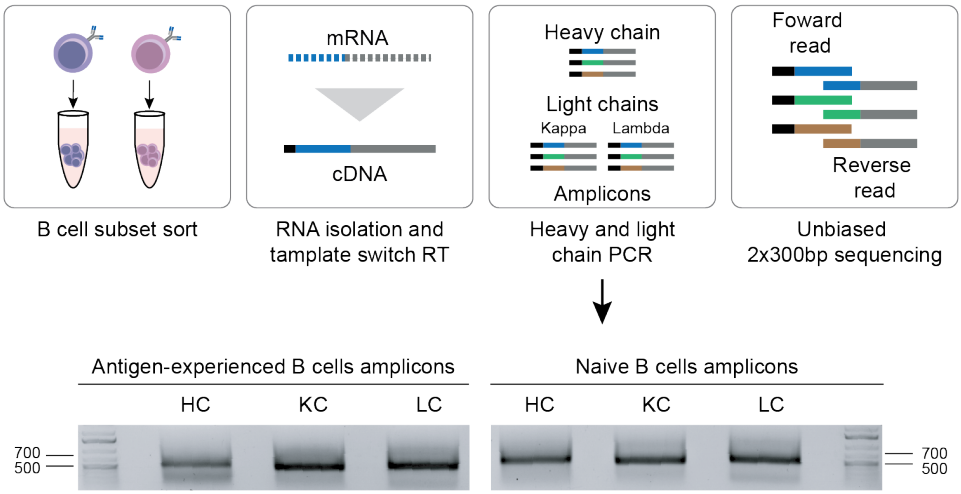

Figure 6: Establishing a protocol for the generation of a reference sequence data set of the naïve and antigen-experienced B cell repertoire.

(A) Gating strategy for antigen-experienced B cells (Dapi$^-$, CD20$^+$, IgG$^+$) and naïve B cells (Dapi$^-$, CD20$^+$, IgM$^+$, IgD$^+$, CD27$^-$, IgG$^-$). Table showing buffy coat (n=24) parameter assessed by cell count and flow cytometry analysis to determine the amount of buffy coat for 10^5 cells per subset. SD indicates the standard deviation. (B) Overview of the main steps for an unbiased NGS-protocol including subset sort, RNA isolation, heavy and light chain amplification (amplicons between 500-700 bp; see gel picture) and unbiased 2x300 bp *I*llumina sequencing.

To extract the BCR sequence information we established an unbiased NGS-protocol starting with the isolation of RNA of the sorted cells followed by cDNA generation by template-switch reverse transcription (RT). Heavy and light chain variable region PCRs were performed and amplicons (500-700 bp) were purified and used for library preparation before Ilumina MiSeq 2x 300 bp sequencing (Figure 6, B). We conclude that buffy coats are an easily accessible source for PBMCs and B cells from healthy individuals to generate a large reference sequence data set.

9.1.3 B cell analyses to decipher the EBOV GP-specific B cell response

The recombinant vesicular stomatitis virus (VSV)-based vector carrying the *Zaire ebolavirus* (EBOV) glycoprotein (rVSV-ZEBOV) was one of the most promising vaccine candidates against lethal EBOV infections. However, a comprehensive analysis, including single-cell analysis, of the rVSV-ZEBOV B cell immune response was lacking. Therefore, we investigated the humoral immune response in six rVSV-ZEBOV-immunized individuals and performed in-depth B cell and sequence analysis in four individuals (EV01, EV03, EV04, EV05). We sorted EBOV GPΔTM-reactive IgG^+ single B cells (Figure 7, a) and analyzed 1,507 heavy- and 261 light- variable regions and detected a polyclonal B cell response with 49, 42, 51 and 45 individual B cell clones in study participants EV01, EV03, EV04 and EV05, respectively (Figure 7, b. and c). We observed similarities among all study participants in V gene family-distribution (Figure 7, d), CDR3 length and germline identity. The mean germline identity for the heavy chains ranged from 90.6 % to 94.2 % and for the light chains slightly higher from 93.9 % to 95.9 % (Figure 7, e).

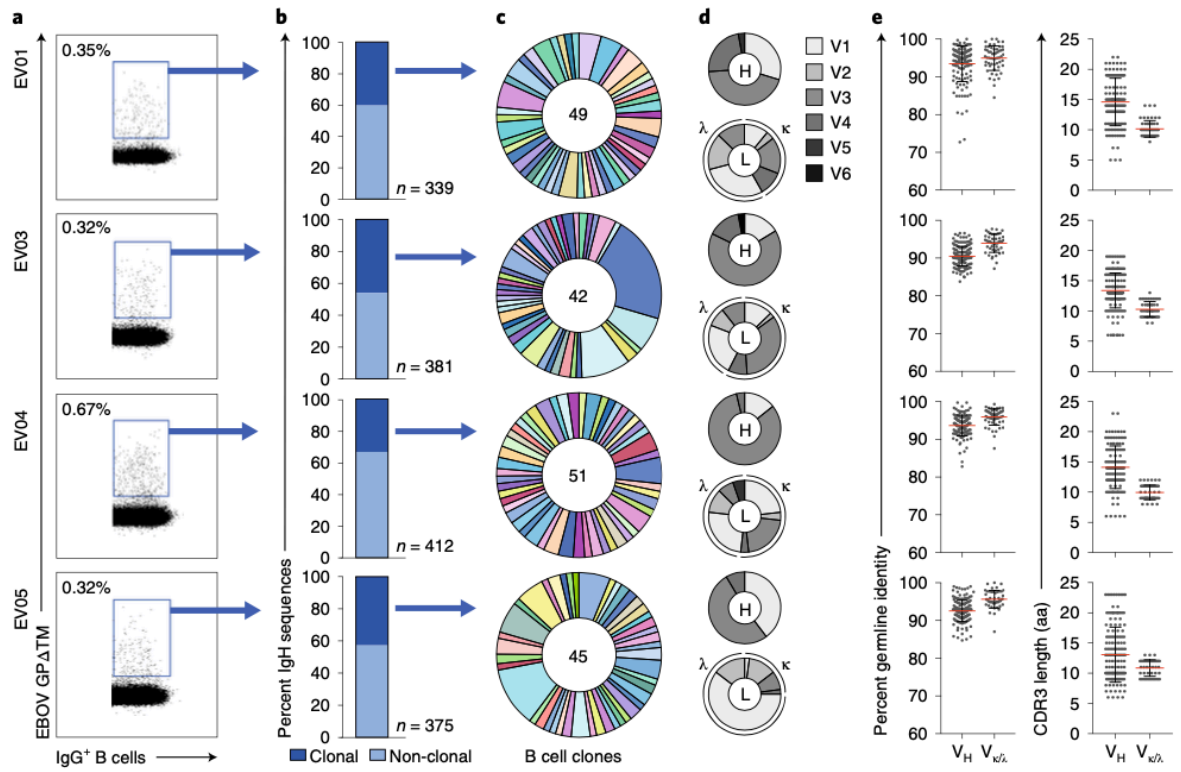

Figure 7: EBOV GPΔTM-specific single B cell sorts and subsequent sequence analysis

(a) Flow cytometry analysis displaying final sorting gate of EBOV GPΔTM reactive CD20$^+$, IgG$^+$ B cells from individuals EV01 and EV03-05. (b) Percentage distribution of clonal and non-clonal sequences. (c) B cell clones with total clone number displayed in the center of the pie chart. (d) V gene family distribution of heavy (H) and light (L) chains of all unique clones (e) Dot plots depicting germline identities (%) and CDR3 lengths (aa) for heavy and light chains, respectively of all clonal sequences. (Figure from [134], Figure 2).

Additionally, we generated a reference sequence data set by isolating 250,000 antigen-experienced B cells (CD20$^+$, IgG$^+$) for all four donors (Figure 8) and performing NGS analysis on the heavy chains (Figure 9) [134].

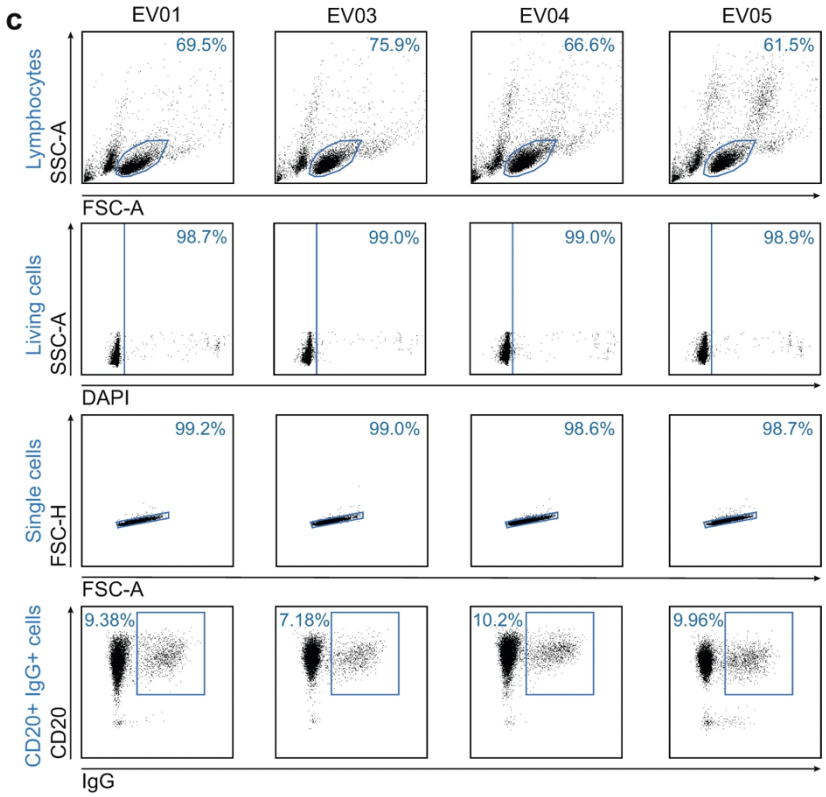

Figure 8: Gating strategy to sort antigen-experienced B cells to generate an unbiased NGS-data set as reference repertoire in rVSV-ZEBOV-vaccinated donors.

(c) FACS plots of the gating strategy for the cell population for NGS analysis: In total 250,000 $CD20^{+}$, IgG^{+} B cells for each rVSV-ZEBOV-vaccinated donor were bulk sorted into collection tubes (Figure from [134], Extended data figure 2).

We compared EBOV GPΔTM-reactive cells (blue) and donor-matched antigen-experienced B cell reference (gray) for differences in CDRH3 length and V-gene germline identity. Differences were small ranging from 0.8 to 1.3 amino acids (aa) for the mean CDRH3 lengths and −0.9 to 1.0 % for mean V gene germline identity (Figure 9, f). However, comparing the variable gene segment distribution, a prominent increase in frequency for the variable gene segment IGHV3-15 (green) was revealed (Figure 9, g). Among the antigen-experienced B cell reference, IGHV3-15 was only detectable with an average frequency of 1.3 %, whereas we observed a significant 5.4-, 6.4-, 4.8- and 9.9-fold increase for EV01, EV03, EV04 and EV05, respectively [134].

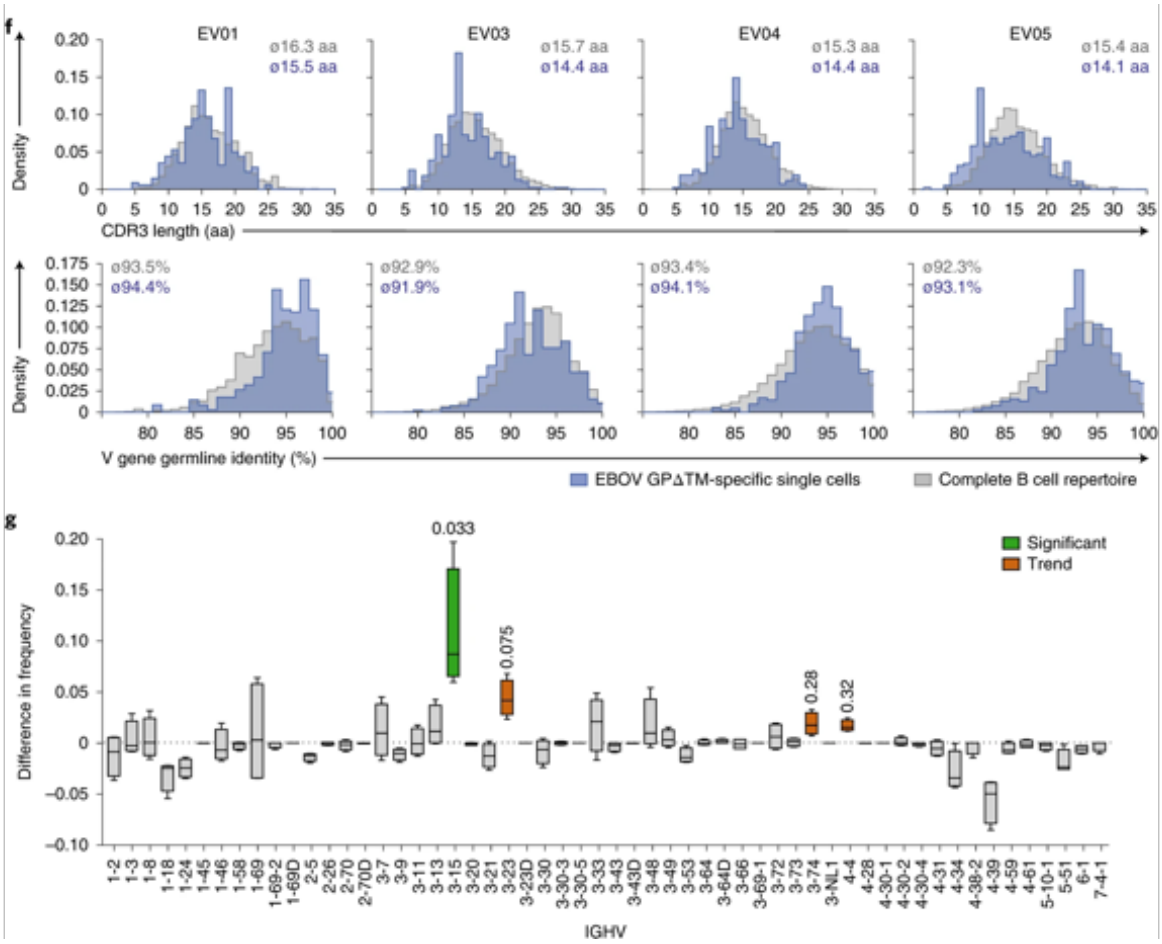

Figure 9: Comparison of the EBOV GPΔTM-specific B cell response to bulk-sorted IgG-positive cells of the corresponding donor

(f) Comparing sequence characteristics between EBOV GPΔTM-specific B cells (blue) and the IgG-postive B cell repertoire (gray) of the different individuals. Heavy chain CDR3 amino acid length (top) and V gene segment identity (bottom) are displayed. (Ø) indicates mean values determined for aa lengths and V gene germline identities. (**g**) Divergence of heavy chain V gene segment frequencies between the overall B cell IgG repertoire and EBOV GPΔTM-specific B cells from four independent samples of rVSV-ZEBOV-immunized individuals. Boxes contain 50% of available data points, with the line displaying the median values and whiskers representing 75% of the difference between the highest or lowest value. To determine if the increase of frequency is significant, a resampling approach based on a one-sided Mann–Whitney U-test with $\alpha = 0.05$ and Bonferroni correction for multiple testing was utilized (Figure from [134], Figure 2.).

We conclude that rVSV-ZEBOV-administration results in a polyclonal B cell response, eliciting antibodies with similar characteristics among the study participants.

9.1.4 B cell analyses to decipher the HIV-1 Env-reactive B cell response

Patient IDC561 was identified as elite HIV-1 neutralizer ranking among the top 1 % of a cohort of 2,274 individuals. We sorted HIV-1 IgG^+ Env-bait-reactive single B cells from this patient and obtained and analyzed 812 IgG^+ heavy chain sequences (Figure 10). One of the isolated B cells expressed an antibody that we named 1-18. It was a novel IGHV1-46 derived CD4

binding site antibody with exceptional potency and breadth with a coverage of 97% on a 119-virus panel and an IC50 of 0.048 µg/ml. The monotherapy with 1-18 was able to fully suppress viremia in HIV-1 $YU2_{gp140}$-infected mice and neutralize typical escape mutants *in vitro* and *in vivo* with infected mice harboring viral variants due to a pretreatment with other CD4bs bNAbs [63].

To describe the antigen-experienced B cell repertoire of the patient, we generated reference sequence data out of $CD20^+$, IgG^+ B cells. Comparison of the reference antigen-experienced B cell repertoire (gray) with the Env-reactive B cells (blue) revealed longer CDRH3s (Figure 10, F) and higher levels of SHM with a median germline identity of 88.4 % of the Env-reactive B cells compared to 95.3 % in the reference data set (Figure 10, G). Furthermore, we observed an enrichment for the VH gene segments IGHV1-46, 1-69 and 4-4 (Figure 10, H) [63]. We conclude that the antibody repertoire of the elite neutralizer IDC561 harbors exceptionally potent and broad antibody clones with notably higher levels of SHM.

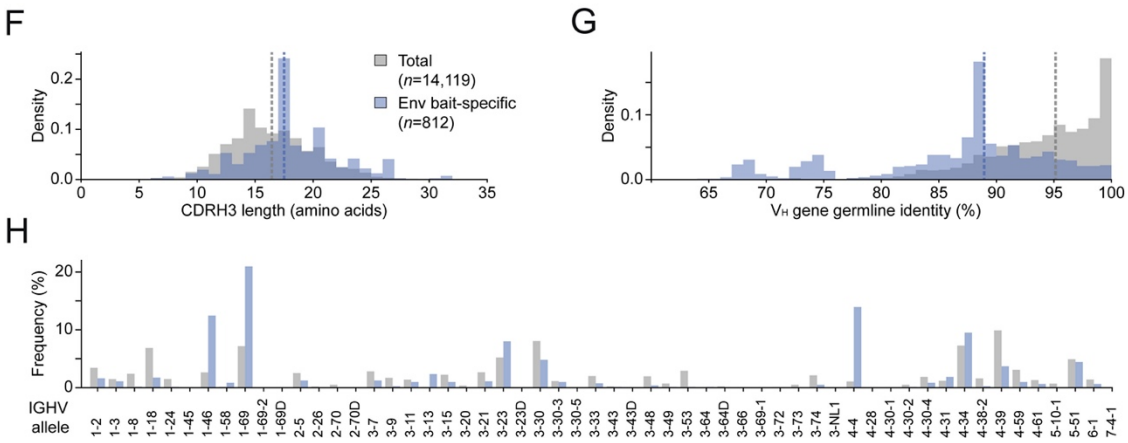

Figure 10: Comparison of the Env-specific response of IDC561 to the overall B cell repertoire of the same donor.

(F–H) Comparison of bulk-sorted IgG^+ B cells of IDC561 and Env-reactive B cells (F) displays CDRH3 lengths (G) displays VH gene germline identity (H) shows VH allele distribution. Dashed lines indicate medians (Figure from [63], Figure S1).

Part II

All described methods and used materials described here and discussed in *10.Discussion-Part II* are included in [62]. This includes text as well as all figures. See also *14. Detailed description of work performed for this thesis.*

9.2 B cell analysis of SARS-CoV-2 infected individuals

9.2.1 Isolation of SARS-CoV-2 reactive B cells from SARS-CoV-2 infected individuals.

When the SARS-CoV-2 pandemic emerged, we set out to investigate the antibody response against SARS-CoV-2 and isolate SARS-CoV-2 reactive and SARS-CoV-2 neutralizing antibodies to identify potential therapeutic agents. Thus, we collected blood samples from SARS-CoV-2 infected individuals. First, we collected blood from seven patients at a single timepoint between 8 and 36 days after diagnosis (IDCnC2, IDFnC2, IDHbnC1, IDHbnC2, IDHbnC3, IDHbnC4, IDHbnC5) (Figure 11, A). We purified IgG from plasma and tested for SARS-CoV-2 binding by ELISA against the full trimeric S ectodomain and neutralizing IgG activity against authentic SARS-CoV-2. Half-maximal effective concentrations (EC50) ranged from 3.1–96.1 µg/mL and inhibitory concentrations (IC100) between 78.8 and 1,500 µg/mL (Figure 11, B).

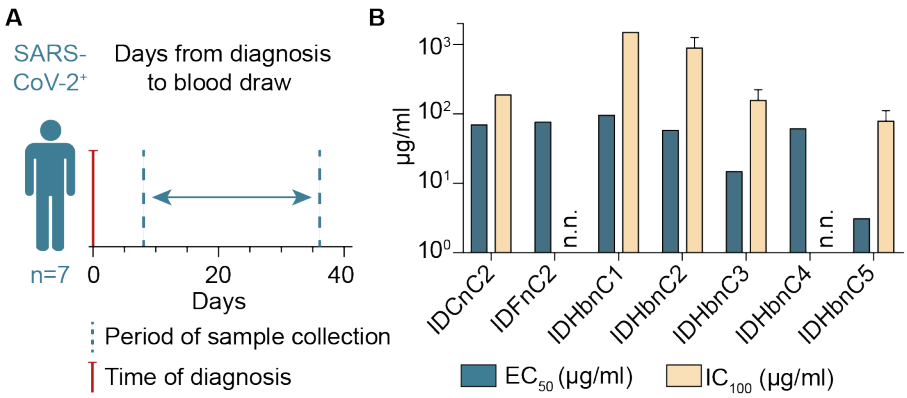

Figure 11: Blood sample collection from SARS-CoV-2 infected individual.

(**A**) Illustration displaying the period of sample collection of 7 SARS-CoV-2 infected study participants including time of diagnosis. (**B**) displayed as bar plots: binding to the trimeric SARS-CoV-2 S ectodomain by ELISA (EC50) and neutralization activity against authentic SARS-CoV-2 measured by the complete inhibition of VeroE6 cell infection (IC100) of plasma-purified IgG samples. Statistics include arithmetic or geometric means including the SD of duplicates or quadruplicates for EC50 and IC100, respectively. n.n., stands for: no neutralization as defined by IC100 > 1,500 µg/mL IgG (adapted from [156]; Figure 1).

We established a SARS-CoV-2 specific sorting strategy by using fluorescently labeled SARS-CoV-2 spike protein (Figure 12, A) and isolated 1,751 IgG^{+} SARS-CoV-2 S-protein-reactive single cells. Frequency for S protein-reactive cells among the five patients ranged between 0.04% (±0.06) and 1.02% (±0.11) (Figure 12, B). Analyzing heavy and light chain sequences, we observed a polyclonal antibody response with 22%–45% clonally related sequences per individual and 2–29 members per identified B cell clone (Figure 12 C). We conclude that SARS-CoV-2 infection initiates a polyclonal B cell response in all studied individuals.

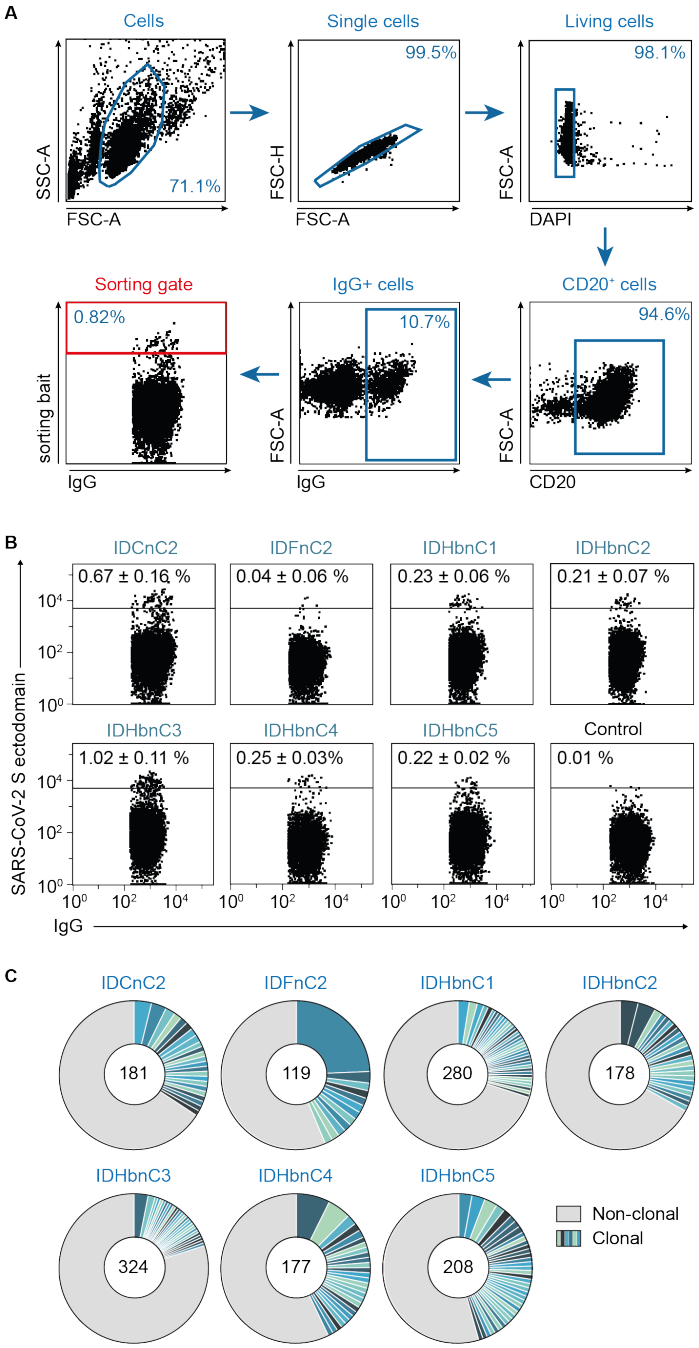

Figure 12: SARS-CoV-2 S-reactive B cell isolation and clonal analysis.

(A) To identify SARS-CoV-2 specific B cells we stained $CD19^+$ B cells, isolated by MACS, with DAPI, CD20, IgG and fluorescently-labeled S-ectodomain protein. We excluded doublets by FSC-A vs. FSC-H. $DAPI^-$ $CD20^+$ IgG^+ cells were gated and cells positive for SARS-CoV-2 S ectodomain were sorted in a single cell manner into 96-well plates. (B) Dot plots of S-ectodomain protein frequencies of the single cell sorts for all seven patients. Depicted numbers with standard deviation indicate average frequencies of S-reactive B cells. (**C**) Pie charts displaying clonal relationships of S-reactive B cells for all seven patients. Numbers in the center of the charts annotade productive heavy-chain sequences (adapted from [156] Figure 1, Figure S1).

9.2.2. Longitudinal blood samples from additional SARS-CoV-2-infected individuals

From additional five infected individuals we obtained blood at three time points ranging from 8-69 days after diagnosis (Figure 13, A). Values for S-ectodomain binding (EC50) and SARS-CoV-2 neutralization (IC100) for the time points ranged from 1.54–129 µg/mL and 78.8–1,500 µg/mL (Figure 13, B). Applying the same FACS strategy to the five patients at the three timepoints we isolated additional 2,562 IgG$^+$ SARS-CoV-2 S-protein-reactive single B cells and amplified IgG$^+$ heavy and light chains for in depth analysis of the SARS-CoV-2 B cell response. We observed S-reactive B cell frequencies up to 0.65 %, with higher frequencies at later time points (Figure 13, C). In terms of clonality, we observed that fifty-one percent of all clones were detected repeatedly spanning the three time points. We suggested that SARS-CoV-2 S-reactive B cells persist spanning the time of investigation of 2.5 months. Looking at the individual time points, the portion of clonally related sequences ranged from 18 – 67 % across patients and remained constant, showing minor decreases over time (Figure 13, D). We conclude that a S-reactive B cell immune response develops shortly after SARS-CoV-2 infection and that B cell clones stay detectable over time.

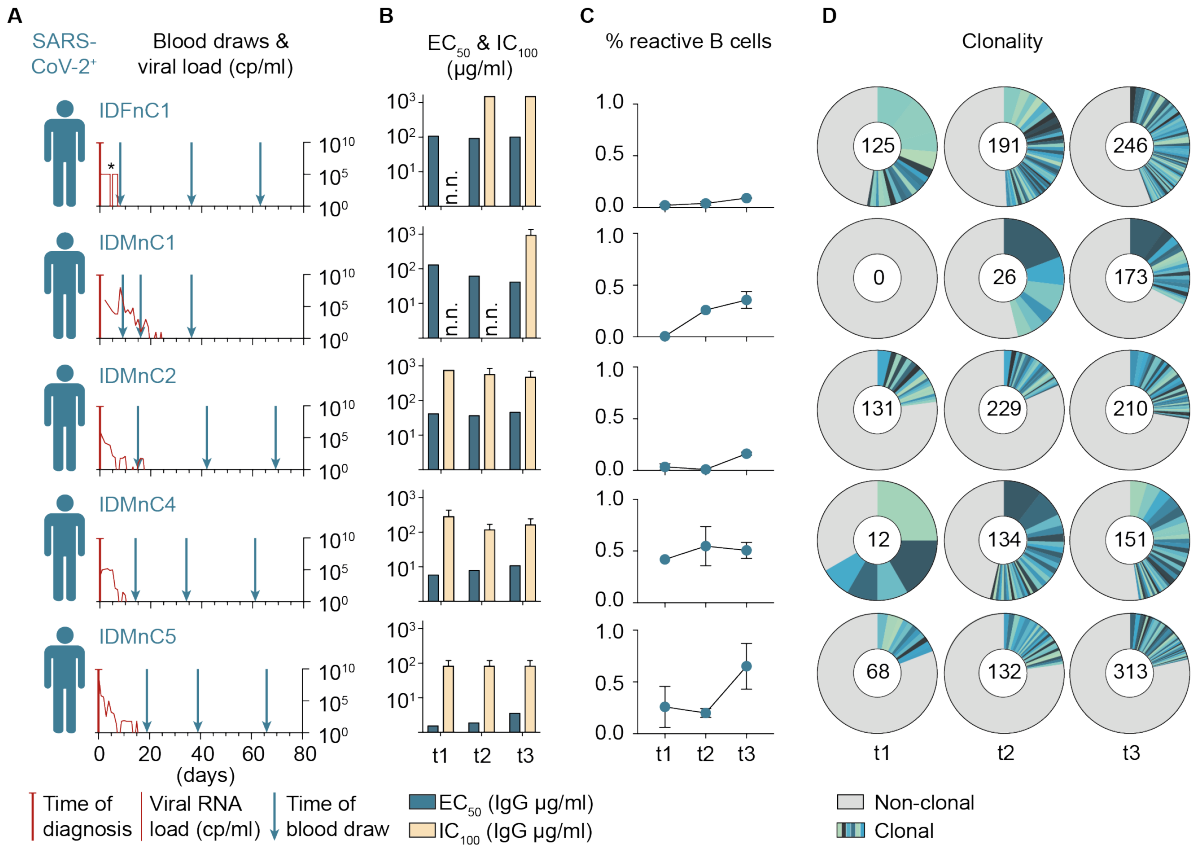

Figure 13: Longitudinal sample collection

(A) Illustration displaying the period of sample collection of additional five patients at three different timepoints including the time of diagnosis and copies [cp] per milliliter for the viral RNA load values from nasopharyngeal swabs (right x-axis). Of note here: (*) The viral load for IDFnC1 was given as positive or negative result. (B) Binding to the trimeric SARS-CoV-2 S ectodomain was assessed by ELISA (EC50) and neutralization activity (IC100) against wildtype SARS-CoV-2 by complete inhibition of VeroE6 cell infection for all timepoints of purified plasma IgGs. n.n. stands for: no neutralization by IC100 > 1,500 µg/mL IgG. Statistics included arithmetic or geometric means with SD of duplicates or quadruplicates for EC50 and IC100, respectively. (C) Frequency of SARS-CoV-2 S ectodomain-reactive IgG^+ B cells at the three different time points. (D) Pie charts show clonal relationship over time. Numbers in the center of the charts indicate productive heavy-chain sequences per time point (adapted from [156] Figure 1, Figure S1).

In total our study comprised 12 SARS-CoV-2 infected individuals and S-protein specific cell sorting allowed for the generation of 6,587 productive heavy and light chains. We observed a broad spectrum of VH gene segments, normally distributed CDRH3-lengths, symmetrical CDRH3 hydrophobicity distributions, and an enrichment of the IgG1 isotype (Figure 14). Furthermore, to compare the SARS-CoV-2 specific B cell response to healthy repertoire data, we generated a large NGS reference data set from 48 healthy individuals (samples collected before the COVID-19 pandemic). The reference NGS data set resulted from 10^5 bulk sorted antigen-experienced B cells for each individual as described in *Part I 9.1.2.*. The comparison revealed an overrepresentation of IGHV 3-30 and that VH genes of S-reactive B cells were, on average, less mutated than VH genes from healthy IgG^+ repertoires (median identity of 98.3 versus 94.3, $p < 0.0001$) (Figure 14).

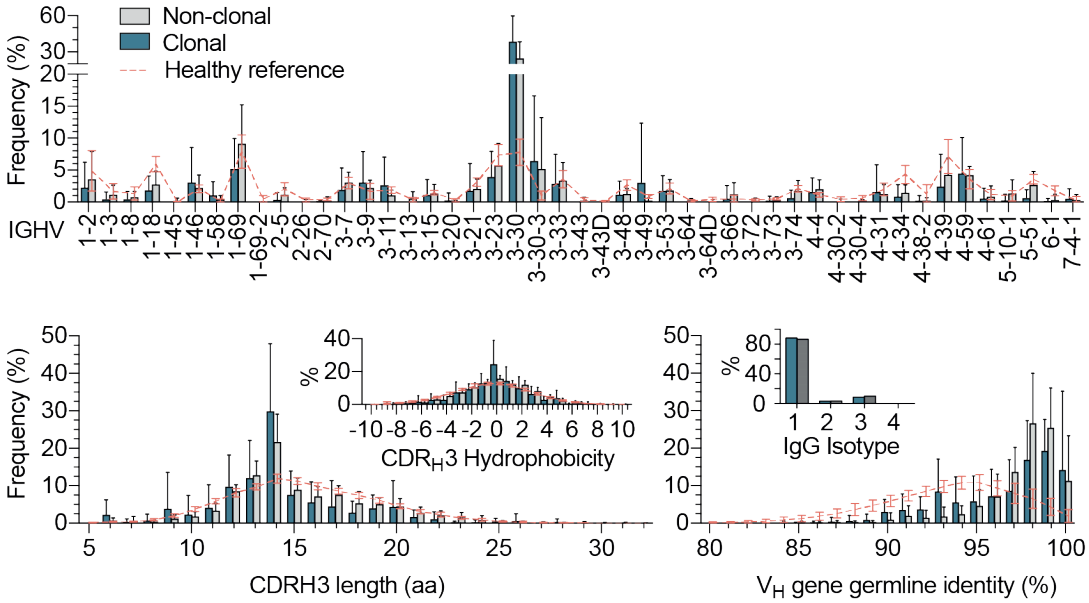

Figure 14: Analysis of all productive heavy chains extracted from the S-protein specific isolated B cells from all 12 study participants.

Displayed on the top are frequencies of VH gene segments with bars for clonal and non-clonal sequences. On the bottom, displayed are CDRH3 length, hydrophobicity and VH gene germline identity and IgG isotype of clonal and non-clonal sequences from all 12 individuals and time points. NGS reference data from 48 healthy individuals (collected before the COVID-19 pandemic) are depicted as a red line. Calculated for the bar and line plots are mean and SD values (Figure adapted from [62]; Figure 2 €).

We produced 255 antibodies from all 12 patients and identified 79 reactive antibodies with 27 neutralizing antibodies among 9 of 12 individuals by determining the neutralization activity against authentic SARS-CoV-2. We analyzed the repertoire characteristics of neutralizing and non-neutralizing antibodies and showed a broad distribution of VH gene segments (Figure

15). Notably, 31 of 79 binding and 10 of 27 neutralizing antibodies demonstrated high germline identities of 99–100% (Figure 15). We conclude that SARS-CoV-2 infection elicits antibodies with a broad spectrum of different V genes with a preference for IGHV 3-30 and low degree of somatic mutations.

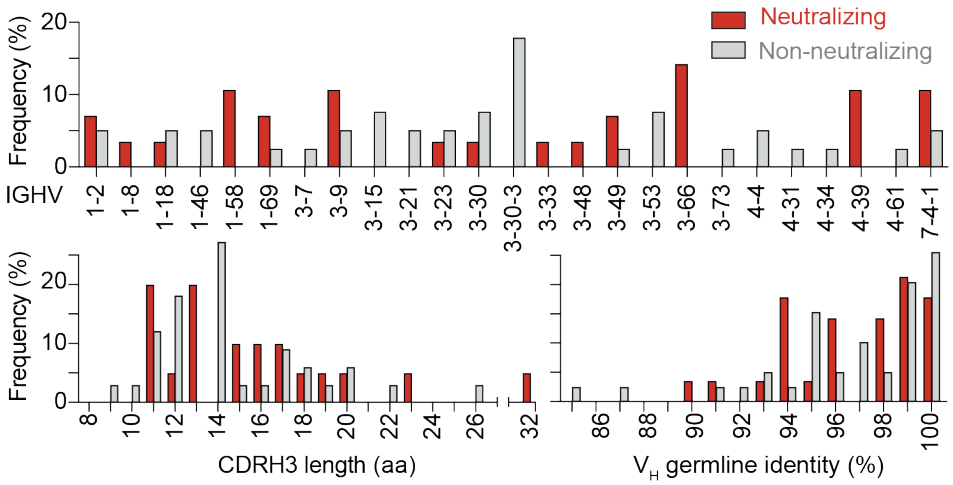

Figure 15: Analysis of productive heavy chains grouped by the categories of neutralizing and non-neutralizing antibodies.

Top: V gene distribution for non-neutralizing and neutralizing antibodies. Frequency values resulted from clonal sequence groups that were collapsed and treated as one sample to determine frequencies. Bar plot on the left shows CDRH3 length and on the right V gene germline identity of the heavy chains of non-neutralizing and neutralizing antibodies (adapted from [62]; Figure 3 (G)).

9.2.3. Identification of potential SARS-CoV-2 precursor sequences

It was the low rate of somatic mutations among the binding and neutralizing antibodies that shaped the idea to search for potential precursor B cells in the naïve human B cell repertoire of the 48 healthy and pre-pandemic donors (Figure 16). To this end, we bulk-sorted 10^5 naïve B cells per donor and applied the established NGS-protocol described previously (see Figure 6). We generated a total of 455,423 unique heavy chains, 170,781 kappa and 91,505 lambda chains. We matched our identified 79 S-protein reactive antibodies against the naïve repertoire and looked for similarities (Figure 16, A).

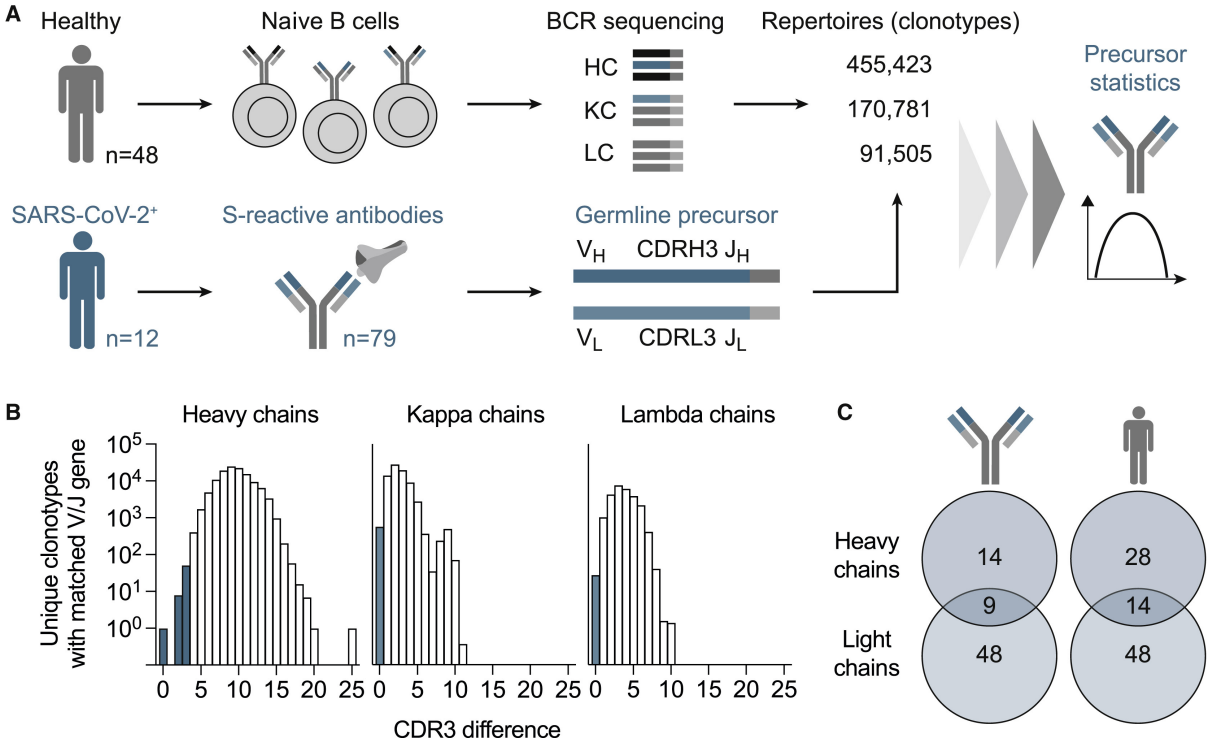

Figure 16: Identifying sequences from SARS-CoV-2 S-reactive antibodies in a NGS sequencing data set from pre-pandemic naïve B cells

(A) Strategy for sequence precursor identification from healthy naive B cell receptor repertoires. Within the large data set generated from the naïve B cells of 48 healthy individuals, sampled before the pandemic, we searched for sequence matches of heavy and light chains from 79 S-reactive antibodies isolated from 12 SARS-CoV-2 infected study participants. (B) Number of clonotypes in healthy naive B cell receptor repertoires (n = 48) with matched V/J genes from SARS-CoV-2-binding antibodies (n = 79), plotted against the CDR3 difference. Bars of included potential sequence precursors are highlighted in shades of blue. For heavy chains, CDR3s were allowed to differ 1 aa in length and contain up to 3 aa mutations. For light chains, only identical CDR3s were counted. (C) Number of different antibody heavy and light chains for which precursors were matched and number of different individuals from which precursor sequences were isolated. Numbers in overlapping circles indicate that both heavy and light chains were detected. (Figure from [62]; Figure 5)

The alignment revealed highly similar sequences (CDRH3s with 1 aa divergence in length and up to 3 aa differences) and even one identical CDRH3 sequence. We found potential precursor sequences of 9 antibodies in 14 healthy individuals (Figure 16, C). Furthermore, among these potential precursor sequences we found similarities to three potent neutralizing antibodies (CnC2t1p1_B4, HbnC3t1p1_G4, and HbnC3t1p2_B10). We conclude that potential SARS-CoV-2 precursor sequences are present in the naïve B cell compartment. This experiment was the foundation for the following study where we searched for more indicators for a pre-existing immune response against SARS-CoV-2 ([143], Submitted and currently under review at iScience (Dec. 2021)).

Part III

All described methods and used materials described here and discussed in *10.Discussion-Part III* are included in [142] that is (as of December 2021) under review at the *iScience* journal and available at biorxiv.org (https://doi.org/10.1101/2021.09.08.459398). This includes text as well as all figures and tables. See also *14. Detailed description of work performed for this thesis.*

9.3 Determining pre-existing B cell immunity against SARS-CoV-2

9.3.1. Antibody pairs composed of SARS-CoV-2-reactive antibody sequences and chains derived from naïve B cell antibodies

As shown in Figure 15, we identified potential unpaired heavy- and/or light-chain precursor sequences of potent SARS-CoV-2-reactive antibodies in a NGS data set of naïve and pre-pandemic B cells. This study was conducted on sequence level only and solely based on sequence-similarity, however, still raising the question whether naïve B cells can encode for antibodies that do not require further affinity maturation for a potent SARS-CoV-2 reactivity (Figure 16 and Figure 17) [62]. To address this question experimentally, we produced 31 antibodies composed of a pre-pandemic heavy or light chain obtained from naïve B cells and a heavy or light chain from SARS-CoV-2-reactive mAbs derived from convalescent individuals [62]. We tested these combined antibodies for S protein binding by ELISA and SARS-CoV-2 neutralization by testing against pseudovirus SARS-CoV-2 (Figure 18).

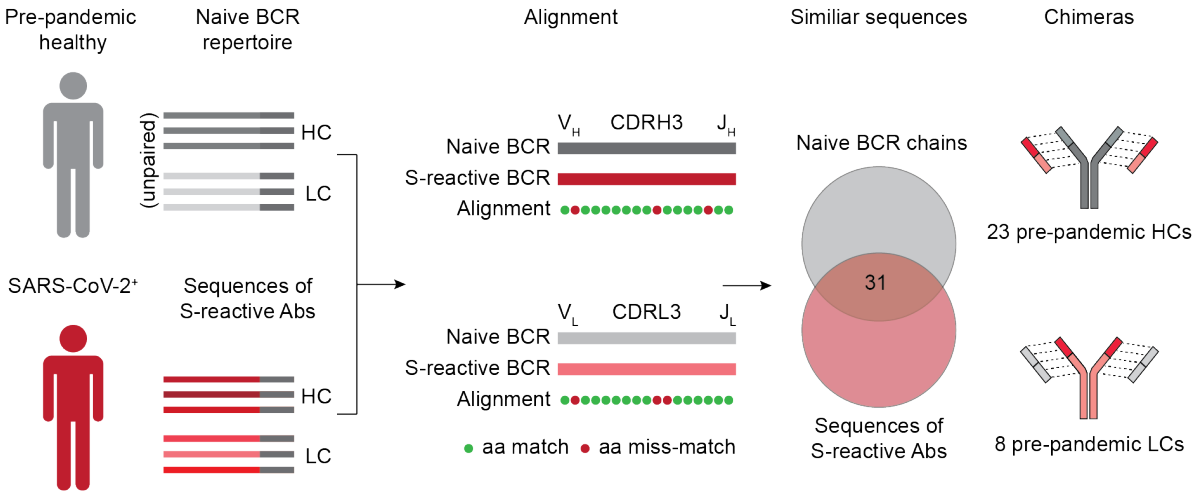

Figure 17: Pre-pandemic naïve and SARS-CoV-2 reactive chain chimeras

Scheme for identifying heavy and light chain sequences in a pre-pandemic naïve B cell repertoire that are similar to heavy and light chains of SARS-CoV-2 reactive antibodies.

Differences between the V gene and CDR3 region between NGS-derived and original chains range ranged from 0 to 5 and 0 to 3 amino acids, respectively. With the exception of mAbs CnC2t1p1_B4 and MnC2t1p1_C12, pairing of pre-pandemic light chains with the original heavy chains retained binding and neutralization activity (Figure 18). In 20 out of 23 chimeric mAbs, pairing of pre-pandemic heavy chains with the original light chain resulted in loss of binding and neutralization activity. However, for one antibody (MnC2t1p1_C12) pairing of the original light chain with 3 out of 13 pre-pandemic heavy chains resulted in retained binding activity suggesting that these heavy chains can assemble SARS-CoV-2 spike protein reactive antibodies (Figure 18). We conclude that some naïve B cells can express heavy or light chains that can be parts of SARS-CoV-2-reactive antibodies without the need for further affinity maturation.

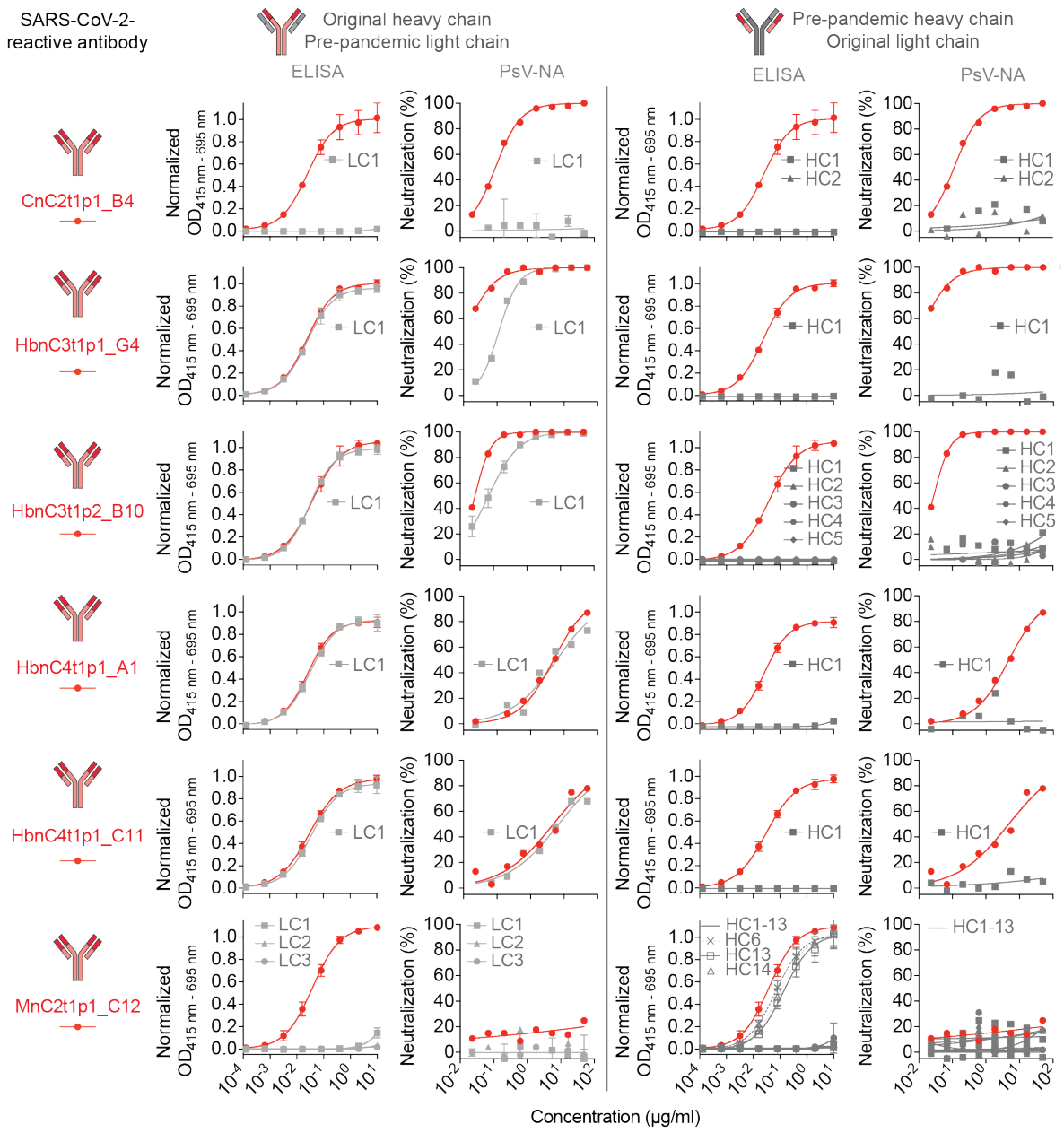

Figure 18: Pre-pandemic naïve B cells express SARS-CoV-2-reactive heavy or light chains

Plots display binding and neutralzation activtiy against SARS-CoV-2 of 6 previously described SARS-CoV-2-reactive antibodies (red) and 31 combined antibodies that are build out of heavy or light chain of the original SARS-CoV-2-reactive antibodies paired with a NGS-derived heavy (darker grey) or light (grey) chain. Binding activity against SARS-CoV-2 was determined by ELISA and neutraliation assay were conducted with pseudovirus (PsV-NA). Each antibody was produced in at least duplicates. ELISAs and neutralization assays were performed with biological replicates. Symbols depict means and error bars indicate standard deviation.

9.3.2. Testing pre-pandemic plasma and polyclonal IgG samples for reactivity against SARS-CoV-2

To investigate whether SARS-CoV-2-reactive antibodies are present in the plasma of unexposed individuals, we investigated pre-pandemic blood samples from 150 donors. Between August and November of 2019, we generated a biobank out of 150 buffy coats by isolating and storing plasma and PBMCs from each donor. The donors were considered unexposed and pre-pandemic as the COVID-19 outbreak was not before December 2019 (Figure 19). Donors ranged in age between 18 and 66 years with a mean age of 30.6 and median age of 27 years (Figure 19 and Table 1). 49.3 % of donors were male and 50.7 % female (Figure 19 and Table 1).

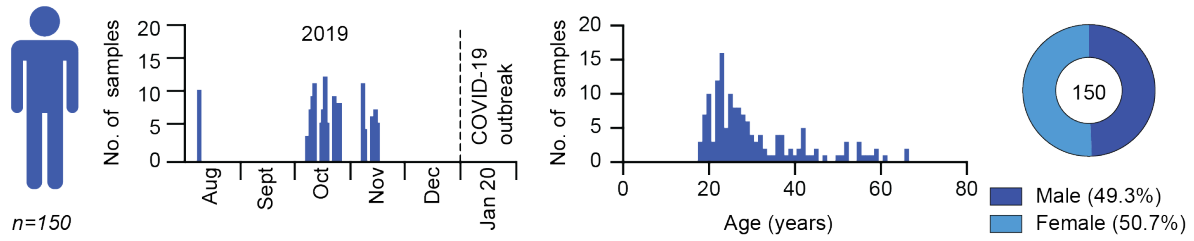

Figure 19: Pre-pandemic sample collection

150 donors were sampled before the SARS-CoV-2 pandemic between August and November of 2019. Pre-pandemic blood samples were collected in form of buffy coats and plasma and PBMCs were isolated and stored. Gender and age distribution of donors are shown as pie chart and bar plots.

Table 1: Demographical characteristics of blood donors

Sample	Date of blood draw	Age	Gender	Sample	Date of blood draw	Age	Gender	Sample	Date of blood draw	Age	Gender
Pre001	08.08.2019	26	w	Pre052	16.10.2019	28	w	Pre103	24.10.2019	34	m
Pre002	08.08.2019	28	w	Pre053	16.10.2019	38	m	Pre104	25.10.2019	32	w
Pre003	08.08.2019	26	w	Pre054	16.10.2019	41	w	Pre105	25.10.2019	23	w
Pre004	08.08.2019	26	w	Pre055	16.10.2019	22	w	Pre106	25.10.2019	23	w
Pre005	08.08.2019	36	w	Pre056	16.10.2019	29	m	Pre107	25.10.2019	23	w
Pre006	08.08.2019	45	m	Pre057	16.10.2019	23	w	Pre108	25.10.2019	26	m
Pre007	08.08.2019	61	m	Pre058	16.10.2019	23	w	Pre109	25.10.2019	26	m
Pre008	08.08.2019	23	w	Pre059	16.10.2019	21	w	Pre110	25.10.2019	33	w
Pre009	08.08.2019	37	m	Pre060	17.10.2019	23	w	Pre111	25.10.2019	32	m
Pre010	08.08.2019	56	m	Pre061	17.10.2019	26	m	Pre112	25.10.2019	42	m
Pre011	08.08.2019	32	m	Pre062	17.10.2019	22	w	Pre113	07.11.2019	36	m
Pre012	07.10.2019	23	m	Pre063	17.10.2019	22	w	Pre114	07.11.2019	36	m
Pre013	07.10.2019	30	m	Pre064	17.10.2019	22	w	Pre115	07.11.2019	24	w
Pre014	07.10.2019	23	m	Pre065	17.10.2019	42	w	Pre116	07.11.2019	22	w
Pre015	07.10.2019	31	w	Pre066	17.10.2019	28	m	Pre117	07.11.2019	23	w
Pre016	09.10.2019	20	w	Pre067	17.10.2019	28	m	Pre118	07.11.2019	24	m
Pre017	09.10.2019	30	m	Pre068	17.10.2019	21	w	Pre119	07.11.2019	22	m
Pre018	09.10.2019	19	m	Pre069	17.10.2019	21	m	Pre120	07.11.2019	43	m
Pre019	09.10.2019	28	w	Pre070	17.10.2019	23	w	Pre121	07.11.2019	24	m
Pre020	09.10.2019	27	w	Pre071	17.10.2019	24	m	Pre122	07.11.2019	23	w
Pre021	09.10.2019	39	m	Pre072	17.10.2019	29	m	Pre123	07.11.2019	31	w
Pre022	09.10.2019	22	w	Pre073	18.10.2019	19	w	Pre124	07.11.2019	33	m
Pre023	09.10.2019	37	m	Pre074	18.10.2019	25	w	Pre125	08.11.2019	51	m
Pre024	10.10.2019	36	m	Pre075	18.10.2019	26	w	Pre126	08.11.2019	25	w
Pre025	10.10.2019	29	m	Pre076	18.10.2019	27	w	Pre127	08.11.2019	66	w
Pre026	10.10.2019	27	m	Pre077	18.10.2019	66	m	Pre128	08.11.2019	26	w
Pre027	10.10.2019	29	m	Pre078	18.10.2019	29	w	Pre129	08.11.2019	25	w
Pre028	10.10.2019	22	m	Pre079	22.10.2019	20	w	Pre130	12.11.2019	19	w
Pre029	10.10.2019	23	w	Pre080	22.10.2019	22	m	Pre131	12.11.2019	30	m
Pre030	10.10.2019	25	w	Pre081	22.10.2019	25	w	Pre132	12.11.2019	30	m
Pre031	10.10.2019	20	w	Pre082	22.10.2019	57	w	Pre133	12.11.2019	47	w
Pre032	10.10.2019	22	m	Pre083	22.10.2019	18	m	Pre134	12.11.2019	37	w
Pre033	10.10.2019	29	m	Pre084	22.10.2019	18	w	Pre135	12.11.2019	55	w
Pre034	11.10.2019	42	m	Pre085	22.10.2019	52	m	Pre136	12.11.2019	59	m
Pre035	11.10.2019	27	m	Pre086	22.10.2019	52	m	Pre137	14.11.2019	25	m
Pre036	11.10.2019	27	m	Pre087	22.10.2019	37	w	Pre138	14.11.2019	23	w
Pre037	11.10.2019	55	m	Pre088	22.10.2019	20	m	Pre139	14.11.2019	20	m
Pre038	11.10.2019	50	m	Pre089	23.10.2019	20	m	Pre140	14.11.2019	27	w
Pre039	11.10.2019	55	m	Pre090	23.10.2019	27	w	Pre141	14.11.2019	20	m
Pre040	11.10.2019	31	m	Pre091	23.10.2019	19	m	Pre142	14.11.2019	42	m
Pre041	11.10.2019	25	w	Pre092	23.10.2019	25	w	Pre143	14.11.2019	35	w
Pre042	11.10.2019	22	w	Pre093	23.10.2019	27	m	Pre144	14.11.2019	42	w
Pre043	11.10.2019	32	m	Pre094	23.10.2019	39	m	Pre145	15.11.2019	40	m
Pre044	11.10.2019	45	m	Pre095	23.10.2019	25	w	Pre146	15.11.2019	59	w
Pre045	11.10.2019	28	w	Pre096	23.10.2019	20	w	Pre147	15.11.2019	52	w
Pre046	15.10.2019	19	w	Pre097	23.10.2019	58	m	Pre148	15.11.2019	41	m
Pre047	15.10.2019	25	w	Pre098	24.10.2019	18	w	Pre149	15.11.2019	24	w
Pre048	15.10.2019	20	m	Pre099	24.10.2019	22	w	Pre150	15.11.2019	23	m
Pre049	15.10.2019	44	m	Pre100	24.10.2019	19	m	EV005	16.12.2016	44	m
Pre050	15.10.2019	28	w	Pre101	24.10.2019	20	w	EV006	20.01.2017	45	m
Pre051	15.10.2019	23	m	Pre102	24.10.2019	19	w				

We aimed to conduct a variety of different immunoassays that are illustrated in Figure 20. Next to commercially available immunoassays and in house ELISA for the detection of IgG, IgM and IgA-binding against SARS-CoV-2 S ectodomain (S1/S2), HKU1 and OC43, we established an additional binding assay using cell surface expressed full-length SARS-CoV-2 S protein (Figure 20). Neutralization activity was tested against SARS-CoV-2 pseudoviruses and wildtype live viruses (Figure 20). Furthermore, we purified IgGs from all 150 plasma samples and performed in house ELISA and neutralization assays as indicated in the illustrational overview (Figure 20). Due to the different performed immunoassays and large data sets, we summarized the data in Figure 24 in form of a heatmap.

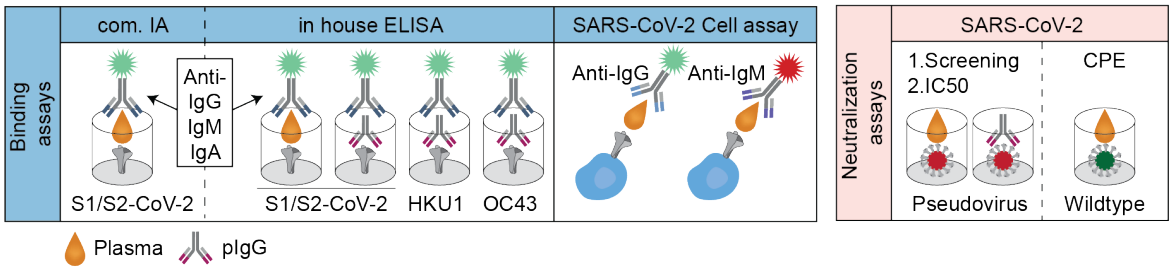

Figure 20: Overview on applied immunoassays.

We purified IgGs from 150 plasma samples and conducted different immunoassays with both the plasma and IgG sample. We performed commercially available immonoassay (com. IA), in house ELISA against S1/S2 and cell surface expressed SARS-CoV-2 S for binding reactivity. Neutralisation was tested in single and serial-dilutions against pseudo-and wildtype-virus.

First, we performed ELISA binding assays and commercially available immunoassays with all 150 plasma samples against soluble SARS-CoV-2 S protein (S1/S2). We tested for IgG, IgM and IgA-binding. The corresponding purified IgG samples were additionally tested against HKU1 (S1/S2) and OC43 (S1/S2) (Figure 21).

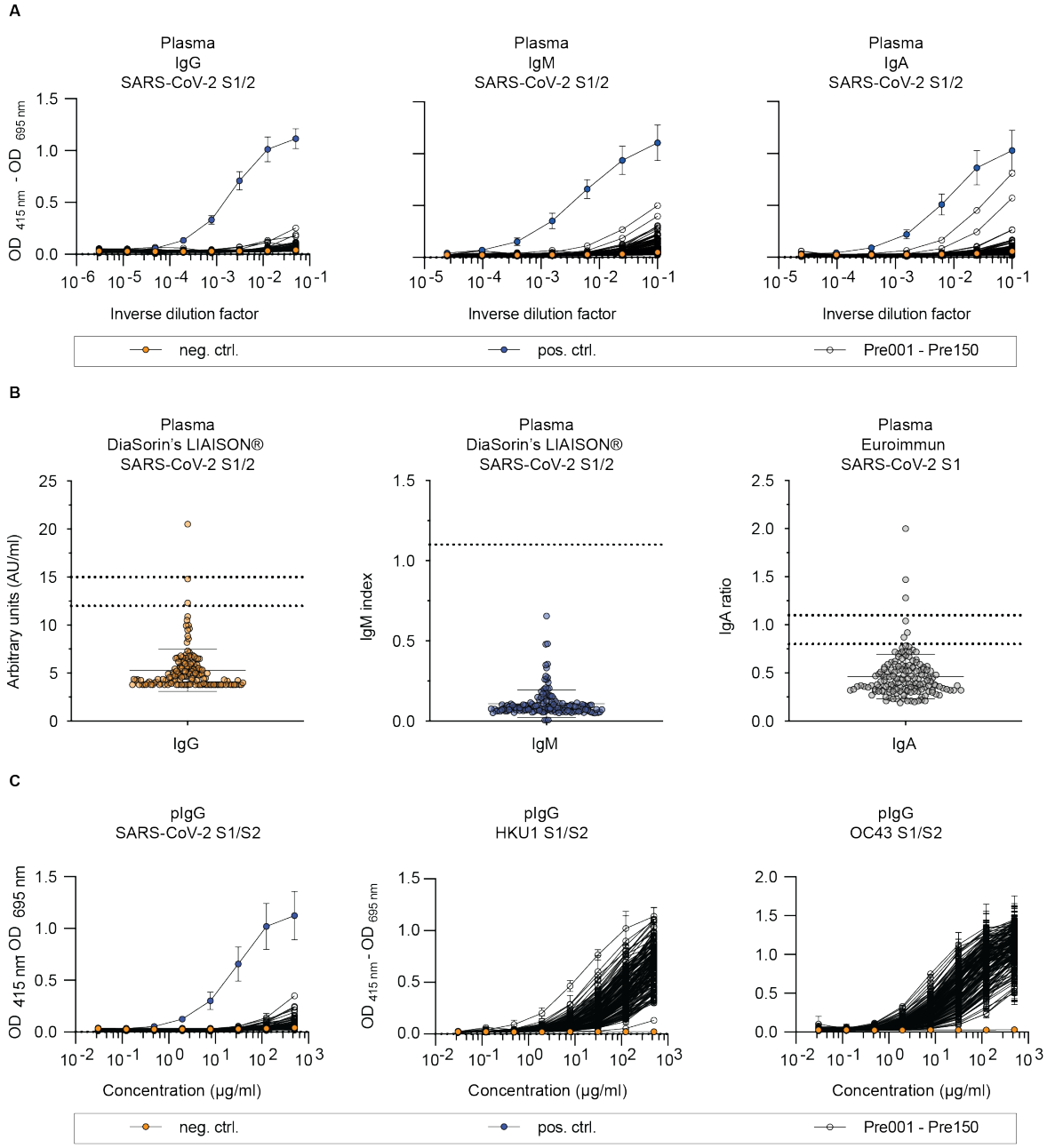

Figure 21: Binding immunoassays of 150 plasma and purified IgG samples

(A) 150 plasma samples were tested for binding against SARS-CoV-2 (S1/S2). We distinguished binding in 1:4 serial dilutions of secreted IgG, IgM and IgA. Starting dilution for the plasma samples were 1:20 for IgG detection and 1:10 for IgM and IgA detection. Ebola surface protein was used as negative control (orange) and plasma from convalescent patient HbnC003 as positive control (blue). (B) 150 plasma samples were tested for IgG, IgM and IgA binding against SARS-CoV-2. We used the automated DiaSorin's LIAISON® for IgG and IgM measurement and the automated Euroimmun Analyzer I system for IgA measurement (only S1 subunit) (C) 150 purified IgG samples were tested for binding against SARS-CoV-2 (S1/S2), HKU1 (S1/S2) and OC43 (S1/S2). We distinguished binding in 1:4 serial dilutions with a starting dilution of 500 µg/ml. Ebola surface protein was used as negative control (orange) and purified IgG from convalescent patient HbnC003 as positive control (blue) for SARS-CoV (S1/S2).

To establish the cell-surface assay, we transfected HEK293T cells with plasmids encoding SARS-CoV-2 S-protein. We identified the successfully transfected cells by gating into mCherry^{+} cells (Figure 22). All 150 plasma samples were prepared in 4-serial dilutions ranging from 1:50, 1:200, 1:800, 1:3200, 1:12800 and 1:51200 comprising a total of 912 samples analyzed on a BD ARIAFusion instrument. Binding of IgG and IgM was detected using an anti-IgG-Fc and anti-IgM antibody. Plasma from a convalescent donor was used as positive control to determine the optimal gating settings to distinguish negative from positive events (Figure 22). The signal in IgG and IgM was the strongest in the 1:50 dilution with gradual loss of signal intensity in the higher dilutions (Figure 22). Representative displayed here is the plasma sample Pre001 showing only very few events at a dilution of 1:50 to 1:800 in the lower right gating-square that was considered positive according to the positive control (Figure 22).

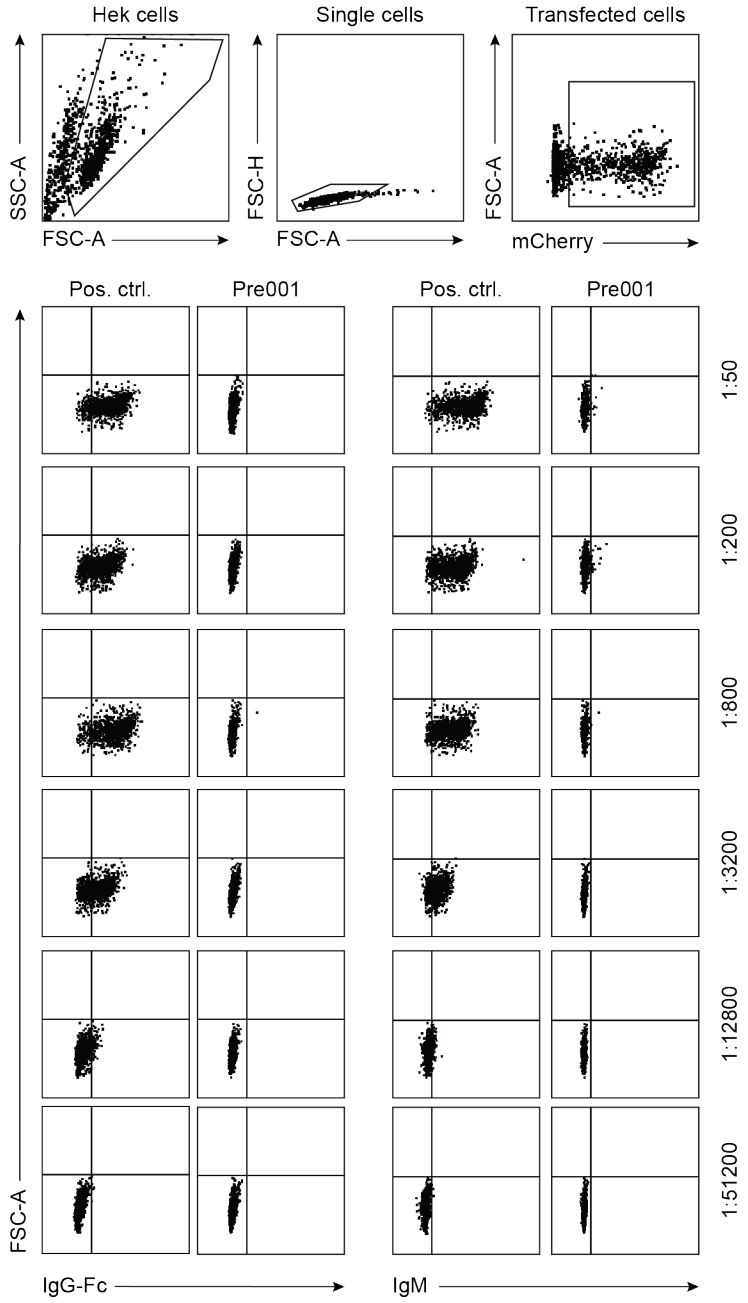

Figure 22: Gating strategy for cell-surface-expressed S-protein immunoassay

HEK293T cells were displayed in FSC-A and SSC-A and doublets were excluded using FSC-A vs. FSC-H. Transfection efficacy was determined by the expression of the reporter gene mCherry. Transfected cells with plasma dilutions are analyzed for IgG-Fc and IgM binding. Plasma sample from a SARS-CoV-2 infected and recovered donor was used as positive control. Pre001 from our cohort was used as representative sample.

We tested all 150 plasma samples against pseudovirus and authentic SARS-CoV-2 (Figure 23, A). For the assay with authentic virus we diluted the plasma samples 1:10 and exposed VeroE6 cells to authentic SARS-CoV-2 virus in the presence of our plasma samples and detected the presence of CPE as indicator for neutralization. Uninfected VeroE6 cells and infected VeroE6 cells in the presence of a potent mAb (C6) served as negative control (Figure 23, A (1, 3)). There was no sign of CPE, whereas the absence of a potent antibody (Figure 23, A (2)) resembled the same level of CPE as observed for all 150 pre-pandemic plasma samples (Figure 23, A (4)), indicating no neutralization activity. Pseudovirus single assays were performed with all 150 plasma samples and resulted in no neutralization for all samples (Figure 23, B), except for samples Pre027 and Pre035, which showed more than >50 % neutralization activity in the 1:10 single dilution assay and were therefore re-tested in serial dilutions with pseudovirus, to exclude any plasma related background activity from the single dilution assay (Figure 23, B). Neutralization activity was not confirmed. Purified IgG samples were tested in a single concentration and serial dilution for those samples exceeding neutralizing activity above 50 %. 6 Samples were re-tested and neutralization was not confirmed (Figure 23, C).

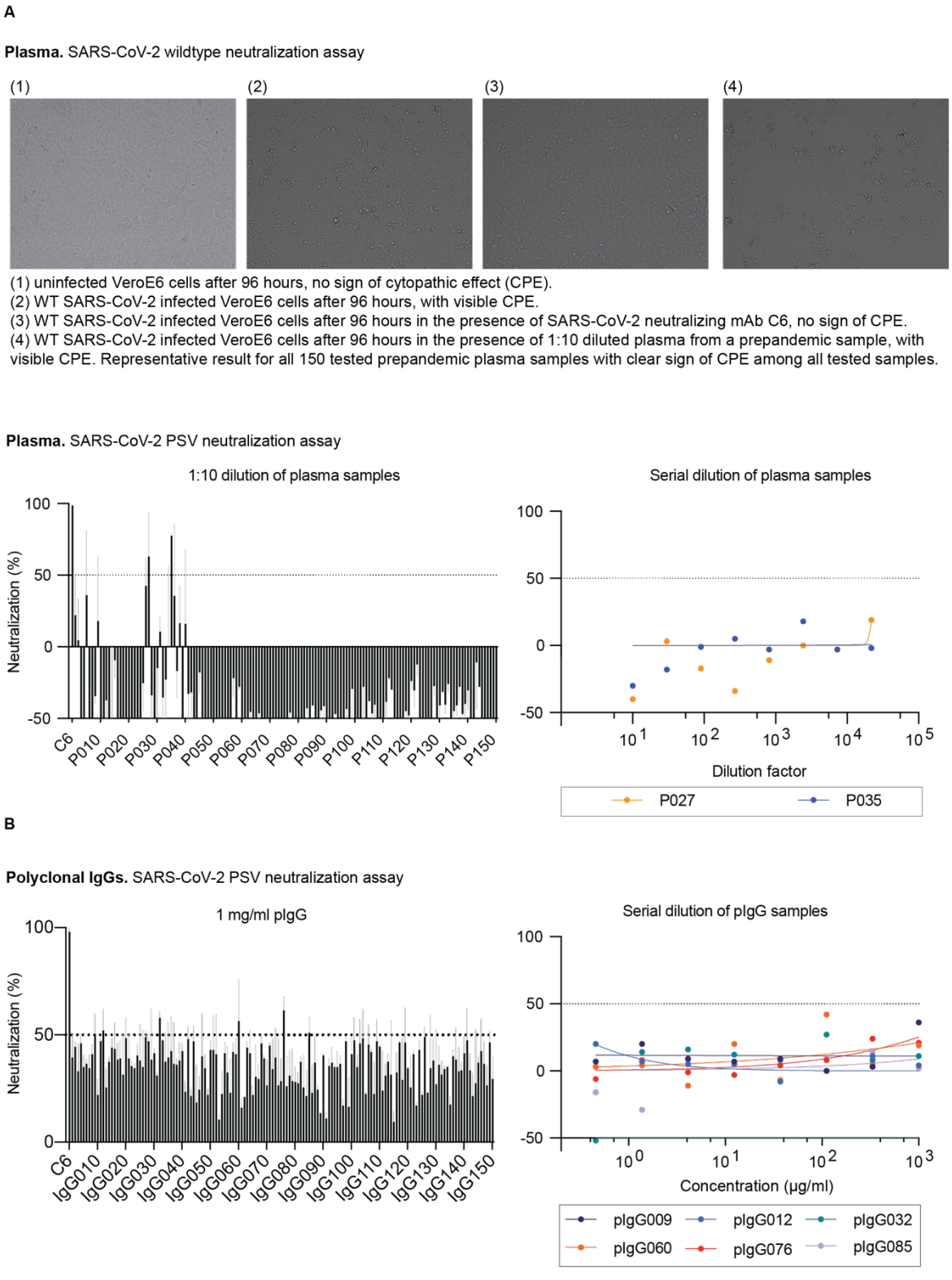

Figure 23: Neutralization activity of plasma and polyclonal IgGs against SARS-CoV-2

Neutralization assay conducted on plasma samples (A) and displayed in (B) polyclonal IgGs against authentic SARS-CoV-2 (wildtype) and/or pseudovirus (PSV). Samples were tested in duplicate experiments (wildtype) or in duplicates in a single experiment (pseudovirus). As positive control we used the SARS-CoV-2 neutralizing antibody C6. Bars and circles of graph plots show means and error bars indicate standard deviation.

Data sets from all conducted experiments on the 150 plasma and corresponding pIgG samples are summarized in the heatmap (Figure 24). The results of binding-analysis to soluble or cell surface expressed SARS-CoV-2 S proteins showed mostly no or only minor binding of IgG, IgM and IgA in plasma samples. The samples Pre033-IgA, Pre051-IgG, Pre074-IgA, Pre084-IgM and Pre097-IgA showed binding in one single assay (Figure 24). However, binding detected by immunoassays could not be confirmed in the flow-cytometry approach utilizing cell surface expressed full-length S protein (Figure 24). In CAs, donor Pre004 exhibited weak plasma IgG activity to full lengths S protein. While the corresponding pIgG sample showed strong reactivity to HKU1 and OC43 S proteins, we saw no binding to SARS-CoV-2 trimeric S protein. Furthermore, neutralization assays of pIgG against SARS-CoV-2 pseudovirus was performed at a concentration of 1 mg/ml. PIgG of six donors (Pre009, Pre012, Pre032, Pre060, Pre076, Pre085) exhibited neutralization activity of SARS-CoV-2 pseudovirus by ≥ 50 %. However, when tested in serial dilutions neutralization activity of these samples could not be confirmed (Figure 23 and Figure 24). Summarized, in our study cohort of 150 samples from adult individuals obtained before the COVID-19 outbreak we detected no or only minimal binding reactivity against SARS-CoV-2 and no neutralization activity. We conclude that there is no evidence of a pre-existing SARS-CoV-2 related B cell immune response on plasma level in healthy adults.

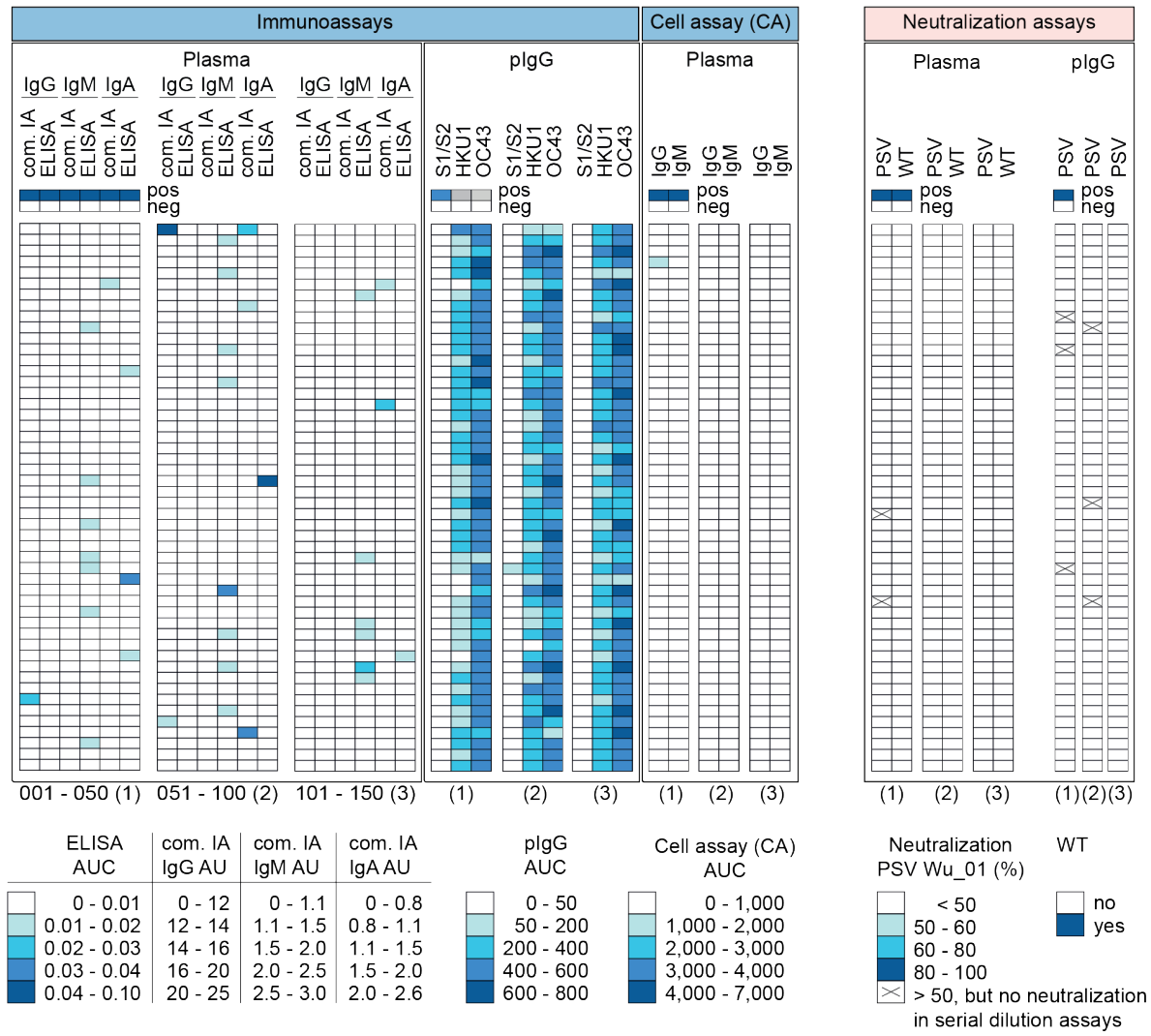

Figure 24: Heatmap summarizing performed binding and neutralization assays from all 150 plasma and pIgG samples of the 150 donors

Heat map illustrating binding (AUC or AU) and neutralization activity (% or CPE) of pre-pandemic plasma samples and pIgG against SARS-CoV-2 and endemic HCoVs (HKU1 and OC43) S proteins or authentic SARS-CoV-2 (wildtype; WT) and pseudovirus (PSV Wu_01), respectively (see also Figure 20 to 22).

9.3.3 Evaluating the presence of SARS-CoV-2-reactive B cells in pre-pandemic samples

With the in-depth serological testing of SARS-CoV-2 directed reactivity in the plasma from the 150 donors, potential reactivity on a cellular level was not covered. We hypothesized, that if SARS-CoV-2-reactive B cells were present in non-exposed individuals, this may only be the case to such a low extent that a SARS-CoV-2 specific-bait sort would be required to identify these cells. To investigate the presence of SARS-CoV-2 -reactive B cells, we performed single B cell sorts of 40 donors sampled before the pandemic (Figure 25).

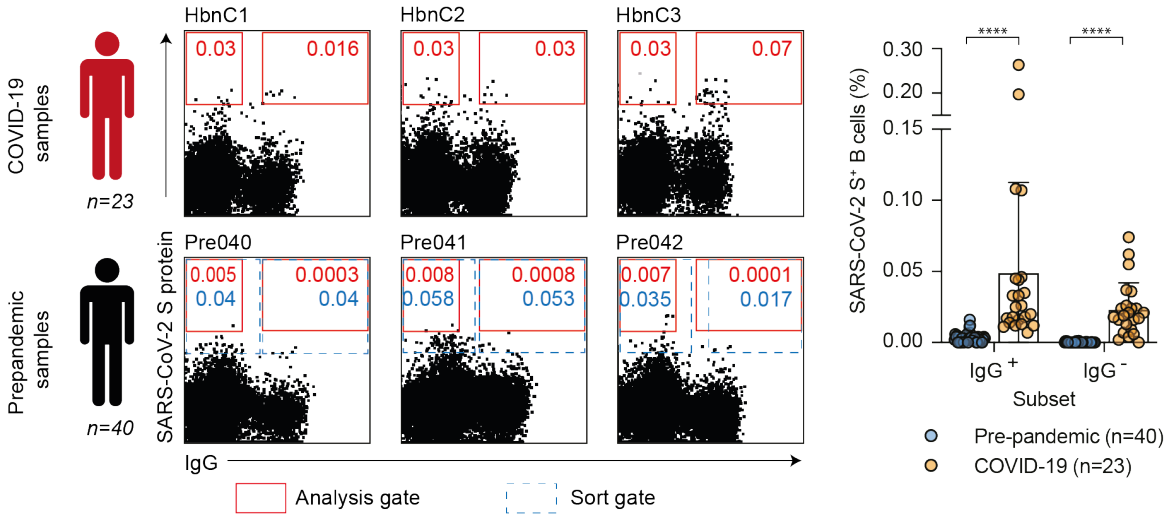

Figure 25: Lack of SARS-CoV-2-reactive B cells

Representative dot plots of SARS-CoV-2-reactive, CD19+CD20+, IgG+ and IgG- B cells of COVID-19 samples compared to pre-pandemic samples. Depicted numbers indicate frequencies of S protein reactive B cells (see also Figure 23). Red colored gate indicates gating strategy for analysis and doted gate indicates actual sorting gate. Dot plot bar graph displays the mean ± SD frequency of SARS-CoV-2-reactive, IgG+ and IgG- B cells in 40 pre-pandemic and 23 COVID-19 samples (*P < 0.05, **P < 0.01, ***P < 0.001 and ****P < 0.0001; unpaired two-tailed t test).

38 pre-pandemic samples from our cohort of 150 samples and two pre-pandemic samples annotated as EV05 and EV06 (Figure 26 and Table 1) were prepared for SARS-CoV-2 specific single B cell sorts and therefore stained as previously described in Kreer & Zehner *et al.* 2020 (also see Figure 12). All samples were gated for lymphocytes, singlets, DAPI$^-$ cells for viability and CD20$^+$ cells for B cells. Compared to the SARS-CoV-2 specific B cell sorts as shown in Figure 12 we also included here SARS-CoV-2-reactive B cells that are IgG$^-$ and IgG$^+$ (Figure 26). We compared the frequencies of 23 COVID-19 convalescent donors to our cohort of 40 pre-pandemic donors. The frequencies of SARS-CoV-2-reactive IgG$^+$ and IgG$^-$ B cells isolated from pre-pandemic blood samples were significantly lower (p value < 0.0001) (Figure 25).

Frequencies of COVID-19 convalescent donors ranged from 0.002 to 0.065 % for IgG^+ (median 0.02 %) and 0.007 to 0.39 % for IgG^- (median 0.031 %) B cells (Figure 25). Applying the same analysis gate of the COVID-19 convalescent samples to our pre-pandemic samples, frequencies ranged from 0 to 0.0013 % for IgG^+ (median 0.0001 %) and from 0 to 0.016 for IgG^- (median 0.003 %) B cells (Figure 25 and Figure 26). Therefore, we conclude that, if present at all, SARS-CoV-2-reactive B cells have a significantly lower frequency in pre-pandemic samples. We reasoned that gate settings applied for COVID-19 convalescent samples may exclude reactive B cells with low spike affinity which may be present in individuals unexposed to SARS-CoV-2. To assure that such cells do not remain undetected, we adjusted the actual sorting gate (Figure 25 and Figure 26) to isolate a total of 8,174 putatively SARS-CoV-2-reactive single B cells, of which 3,852 were IgG^+ and 4,322 IgG^- cells (Figure 26 and Figure 27).

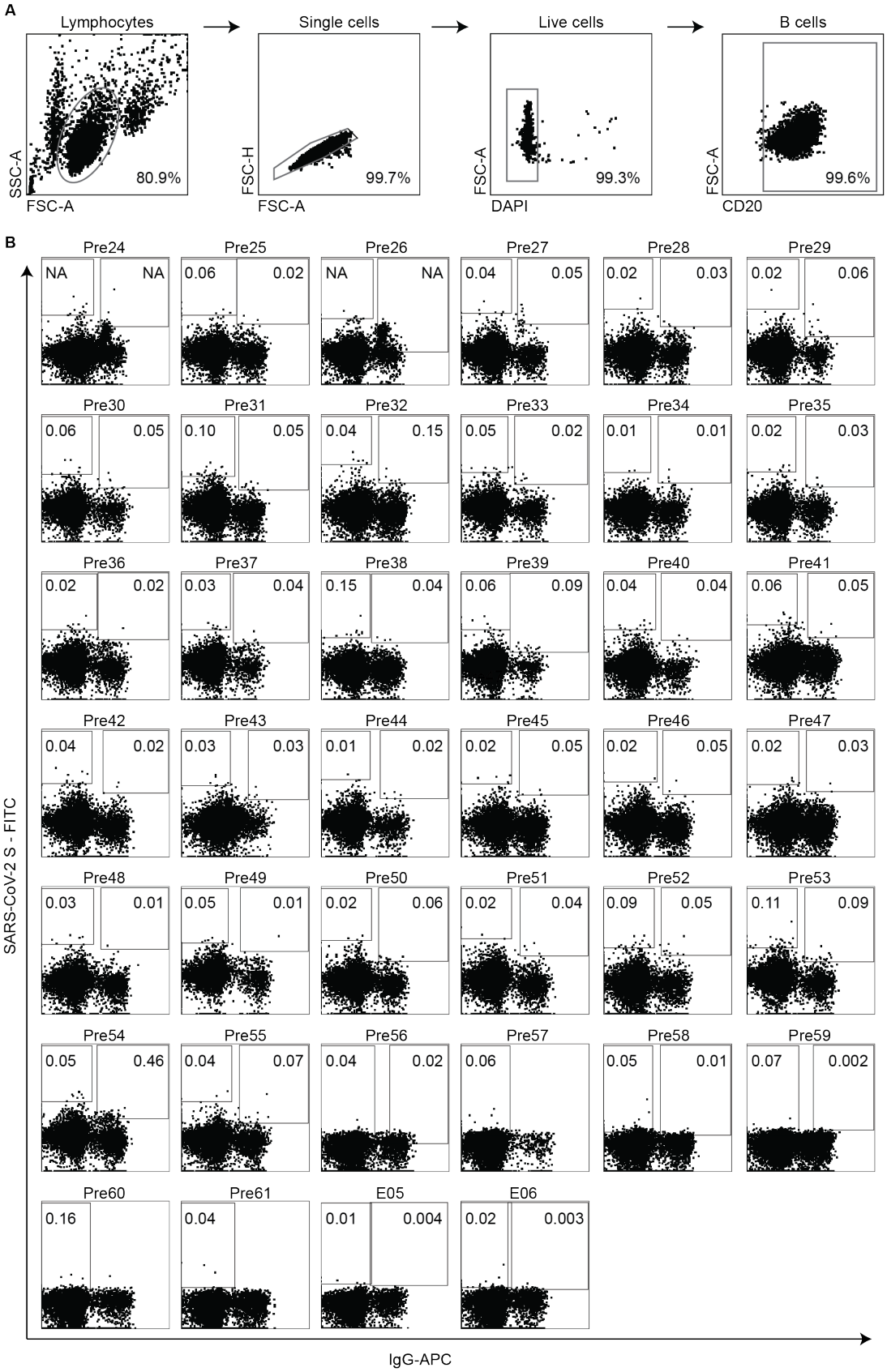
A
Lymphocytes
SSC-A
FSC-A
80.9%
Single cells
FSC-H
FSC-A
99.7%
Live cells
FSC-A
DAPI
99.3%
B cells
FSC-A
CD20
99.6%
B
Pre24 NA NA
Pre25 0.06 0.02
Pre26 NA NA
Pre27 0.04 0.05
Pre28 0.02 0.03
Pre29 0.02 0.06
Pre30 0.06 0.05
Pre31 0.10 0.05
Pre32 0.04 0.15
Pre33 0.05 0.02
Pre34 0.01 0.01
Pre35 0.02 0.03
Pre36 0.02 0.02
Pre37 0.03 0.04
Pre38 0.15 0.04
Pre39 0.06 0.09
Pre40 0.04 0.04
Pre41 0.06 0.05
Pre42 0.04 0.02
Pre43 0.03 0.03
Pre44 0.01 0.02
Pre45 0.02 0.05
Pre46 0.02 0.05
Pre47 0.02 0.03
Pre48 0.03 0.01
Pre49 0.05 0.01
Pre50 0.02 0.06
Pre51 0.02 0.04
Pre52 0.09 0.05
Pre53 0.11 0.09
Pre54 0.05 0.46
Pre55 0.04 0.07
Pre56 0.04 0.02
Pre57 0.06
Pre58 0.05 0.01
Pre59 0.07 0.002
Pre60 0.16
Pre61 0.04
E05 0.01 0.004
E06 0.02 0.003
SARS-CoV-2 S - FITC
IgG-APC

Figure 26: Gating strategy and single cell sorts of SARS-CoV-2-reactive B cell subsets

(A) FACS plots with the gating strategy for single cell sorts of SARS-CoV-2-reactive, IgG^+ and IgG^- B cells. (B) Individual FACS plots displaying sorting gates and frequencies of SARS-CoV-2-reactive, IgG^+ and IgG^- B cells from 40 donors.

Of those we amplified a total of 5,432 productive heavy chain sequences, of which 2,789 sequences accounted for IgG and 2,643 for IgM heavy chains, respectively (Figure 27). Sequence analyses showed that in each individual 0 to 58 % of the sequences were clonally related with a mean clone number of 8.1 clones per individual and a mean clone size of 2.9 members per clone (Figure 27).

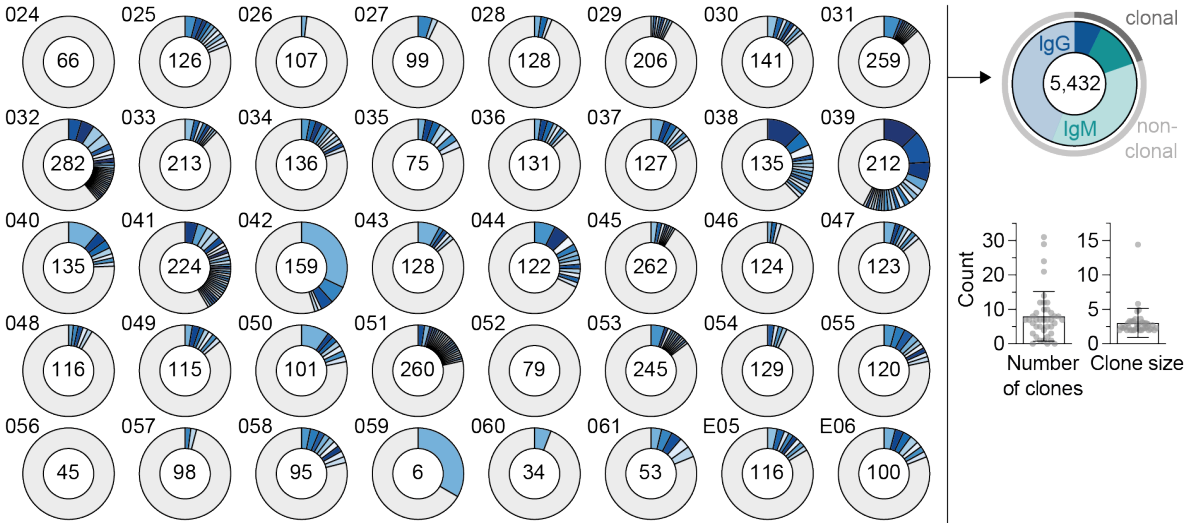

Figure 27: Clonal analysis

Clonal relationship of heavy chain sequences amplified from single SARS-CoV-2-reactive IgG^+ and IgG^- B cells isolated from 40 donors sampled before the pandemic. Individual clones are displayed in different colors of blue, grey and white. In the center of each pie chart, numbers of productive heavy chain sequences are illustrated. Presentation of clone sizes are proportional to the total number of productive heavy chain sequences per clone.

VH gene segment distribution, CDRH3 length and VH gene germline identities showed no notable divergence from a reference antigen-experienced IgG and naïve IgM repertoire data set [62] (Figure 28). The lack of this divergence in combination with the FACS data suggested the absence of SARS-CoV-2-reactive B cells in pre-pandemic samples.

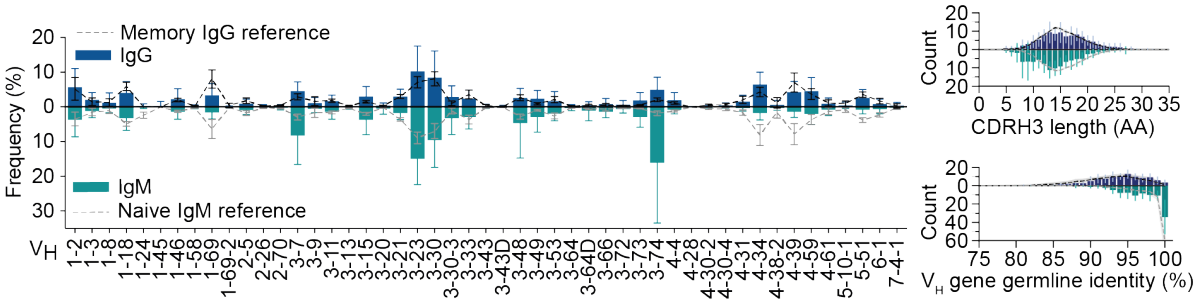

Figure 28: Sequence analysis and comparison to a reference data set

VH gene distribution, VH gene germline identity and CDRH3 length distribution in amino acids (AA) were separately determined for IgG and IgM. Distributions were calculated per individual. Bar and line plots show mean SD.

9.3.4. Monoclonal antibodies isolated from pre-pandemic samples are not reactive against SARS-CoV-2

To investigate the presence of SARS-CoV-2-reactive B cells in pre-pandemic samples on a functional level, we selected 200 antibody candidates among 36 donors from single cell sorted B cells for antibody production and functional analysis (Figure 29). The selection was performed based on sequence similarity (see Methods section) to 920 SARS-CoV-2-reactive antibodies deposited in the CoVAbDab (n = 18) and on random sequence selection (n = 182) (Figure 29). The similarity selection included sequences with identical VH/JH combinations, low level of CDRH3 length differences, and Levenshtein distances between isolated and deposited BCR sequences. The random selection included clonal and non-clonal sequences and aimed to ensure an equal selection of BCR sequences among different donors and clonotypes. In total, we successfully produced 158 monoclonal antibodies (81 IgM-, 77 IgG-derived) as IgG1 isotypes for functional testing.

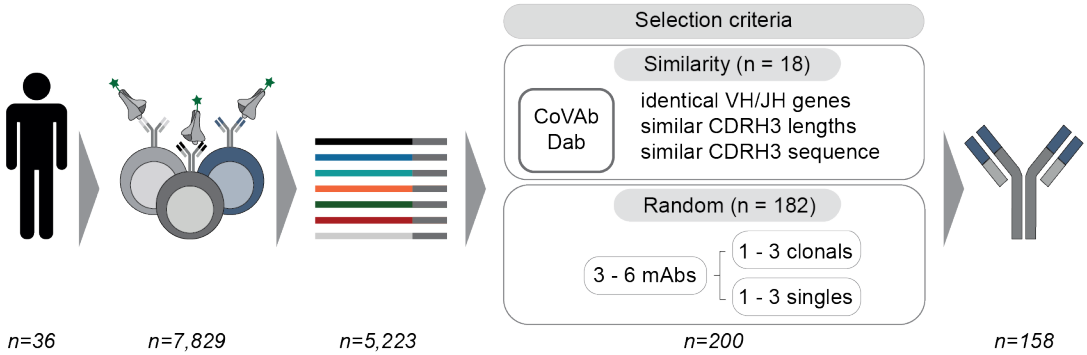

Figure 29: Selection of antibody sequences from pre-pandemic samples for monoclonal antibody production

Illustration demonstrating the sequence selection for downstream antibody production. Sequences were selected for antibody production based on similarity to antibody sequences published in the CoVAbDab and on random selection. From 8,174 SARS-CoV-2-reactive IgG^+ and IgG^- B cells, 5,432 productive heavy chain sequences were amplified. For antibody production, 18 HC sequences were selected based on similarity selection and 182 HC sequences were selected based on random selection. In total 158 antibodies were produced.

First, binding activity of these antibodies to SARS-CoV-2 S protein was tested, followed by ELISA with HKU1 and OC43 S proteins for the analysis of cross-reactivity. ELISA curves of all samples are displayed in Figure 30 (Figure 30 and Figure 31, A). As summarized in the heatmap (Figure 31, A), monoclonal antibodies showed no binding or cross-reactivity against SARS-CoV-2, HKU-1 or OC43 S proteins (Figure 30 and Figure 31, A).

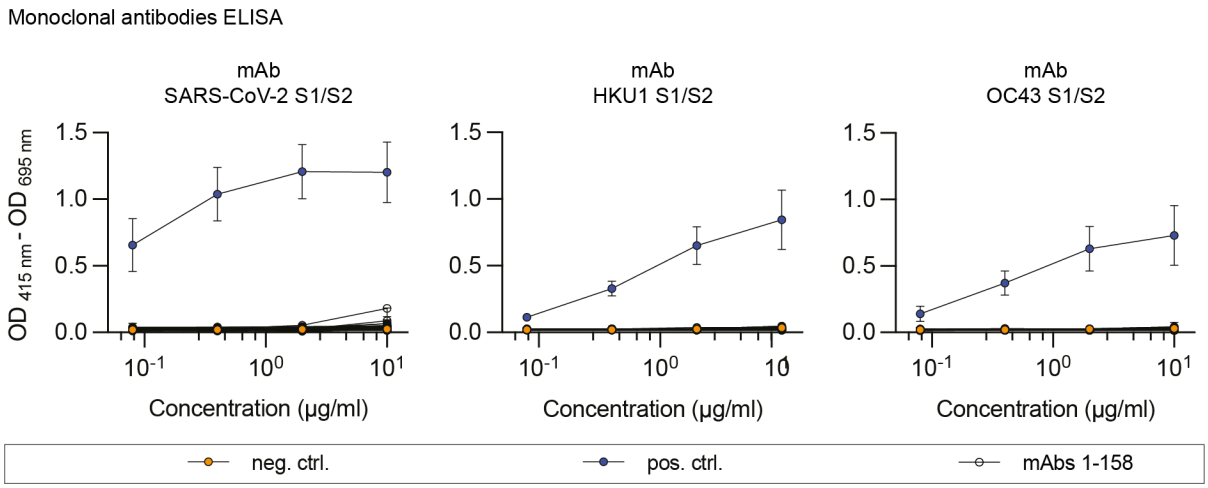

Figure 30: Monoclonal antibodies tested for binding against SARS-CoV-2 and endemic HCoVs by ELISA

158 monoclonal antibodies were tested for binding against SARS-CoV-2 (S1/S2), HKU1 (S1/S2) and OC43 (S1/S2). We distinguished binding in 1:4 serial dilutions with a starting dilution of 50 µg/ml. An HIV1 monoclonal antibody was used as negative control (orange) and the monoclonal antibody C6 for SARS-CoV-2 as positive control. For HKU1 and OC43, polyIgG from Pre091 severed as positive control (blue). ELISAs were performed in duplicate experiments. Error bars indicate standard deviation.

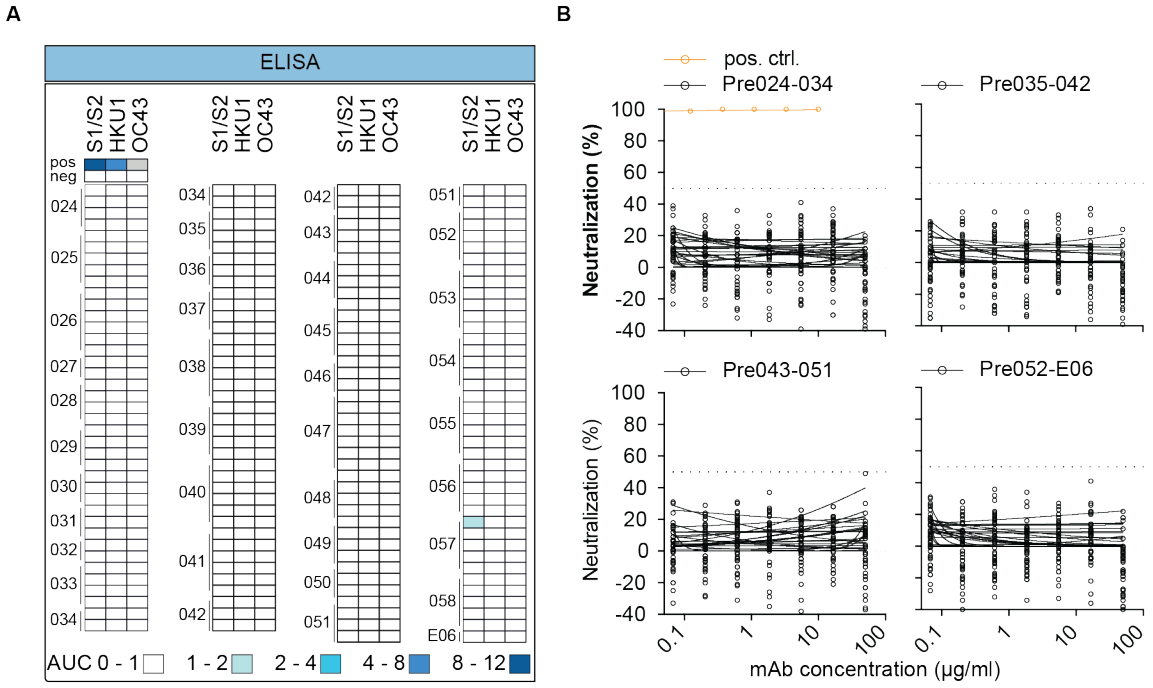

Figure 31: Monoclonal antibodies isolated from pre-pandemic samples show no reactivtiy against SARS-CoV-2 and endemic HCoVs

(A) Heat map visualizing binding (AUC) and neutralization activity (%) of monoclonal antibodies isolated from pre-pandemic blood samples against SARS-CoV-2 and endemic HCoVs (HKU1 and OC43) S proteins or SARS-CoV-2 pseudovirus (PSV Wu_01), respectively. Numbers on the left refer to donors and each row represent one antibody. ELISAs were performed in duplicate experiments and the AUC is presented as geometric mean of duplicates. Samples were tested in duplicates and the average of neutralization is presented. (B) Neutralization activity against SARS-CoV-2 pseudovirus (PSV Wu_01) was performed for all mAbs by serial dilution assays.

Next, all 158 monoclonal antibodies were tested for neutralization activity against SARS-CoV-2 pseudovirus in single concentrations of 50 µg/ml (data not shown) and in serial dilutions (Figure 30, B). None of the produced antibodies showed neutralizing activity up to concentrations of 50 µg/ml (Figure 30, B). In line with the lack of binding activity, we conclude that putatively SARS-CoV-2-S$^+$ B cells from pre-pandemic samples do not encode for SARS-CoV-2-reactive B cell receptors. Taken together, our detailed analysis of the B cell response, spanning plasma and cellular level, provides no evidence for a pre-existing B cell immune response against SARS-CoV-2 in healthy adults.

10. Discussion

The generation of highly pathogen-specific neutralizing antibodies by B cells is critical for a potent, rapid and long-term immune response and protection. The B cell receptor repertoire is shaped by pathogen encounters and can differ across individuals. A detailed understanding of the B cell receptor repertoire and the pathogen-specific antibody response is relevant for therapeutic approaches and vaccine designs [157, 158]. Pathogens like influenza virus, hepatitis C virus (HPV) and HIV-1 are highly variable viruses requiring a vaccine that elicits an antibody response that can overcome the genetic diversity, the fast mutation rates, glycan shield of the envelope protein and the limited accessibility of conserved epitopes [159, 160]. Although these mechanisms are some of the underlying causes for vaccine failure, potent and broadly neutralizing antibodies have been isolated from infected and vaccinated individuals [59, 161, 162]. Demonstrating that the human immune system, in principle, is able to effectively respond to the viral escape mechanisms. Therefore, identification and isolation of B cells targeting specific pathogens does not only inform on the general immune response but also offers a potential therapy option or may improve currently available therapies and influence vaccine design approaches [163, 164]. Therefore, advancing current available techniques promotes the analysis and characterization of the humoral immune response.

Part I:

The first part of this thesis therefore described the high-throughput protocol for the isolation, amplification and production of pathogen-specific human antibodies using fluorescently labeled bait-proteins, optimized PCR primer sets [56] and recombinant antibody production [135]. Through a combination of magnetic microbeads and fluorescent proteins conjugated to antibodies, analyzed using a FACS instrument we identified and isolated HIV-1 and EBOV specific antibodies including antibody 1-18 a promising candidate for HIV-1 therapy [63]. The correct choice of bait-protein, in accordance with the scientific questions addressed, is one critical step. For example, $BG505_{SOSIP.664}$ $YU2_{gp140}$ -trimer and monomeric $YU2_{gp120}$ are two very common HIV-1 bait proteins used for single cell sort approaches and differ strongly in isolation efficiencies for bnAbs targeting certain epitopes of the HIV-1 envelope [165]. This way, B cells reactive against certain structures on the choice of bait-protein are automatically preselected in the sort. To overcome this form of bias it is ideal to sort with both bait proteins, however insufficient amount of blood products and cells can be a limitation. To improve sort efficiency and reduce background signal in the target population it is possible to label the bait-protein of choice with two different fluorochromes as we did for our most recent SARS-CoV-2 specific cell sorts by labeling the S-protein with DyLight488 and Dylight650 and sort double positive B cells only [166]. Subsequently we performed a reverse transcription followed by

amplification of the heavy and light chain V gene regions using seminested multiplex PCR. Multiplex primer design is an additional critical step here as they need to cover all known V genes, sequences with high levels of SHM and insertions and deletions as described for many bNAbs. Thus, we developed openPrimeR, an R-based primer-design tool and generated an optimized multiplex PRC primer set that excels other previously published primer sets in V gene coverage and amplification of highly mutated sequences. When tested side by side with the same template cDNA of HIV-1-reactive B cells the overall coverage was substantially higher for the openPrimeR-designed primer identifying sequences that could not be identified with either one of the two alternative common primer sets [56, 137, 167].

Furthermore, we generated B cell receptor reference data sets to describe pathogen-specific and pathogen-driven B cell receptor alterations. For this method advanced bio-informatic knowledge is essential to analyze millions of different antibody sequences. For example, NGS techniques such as illumina dye sequencing are ideal for high-throughput analysis but often suffer from shorter read lengths and high error rates [50, 168]. To overcome this, we introduced unique molecular identifiers (UMIs) during cDNA generation. Using this approach, we generated large sequencing data sets that, although still small compared to the overall B cell repertoire, offered a broad and in-depth repertoire analysis compared to the throughput limit to tens of thousands of the single cell approach. However, it should be considered that heavy and light chain pairing information could not be retained which is essential for native antibody cloning and production. We bulk-sorted B cell subsets and analyzed repertoire characteristics like clonal distributions, V gene usage and somatic hypermutation (V gene identity). In our cohort of rVSV-ZEBOV-immunized individuals we observed an increase of V gene segment IGHV3-15 and IGLV1-40 among the neutralizing pathogen-specific B cells compared to the overall antigen-experienced B cell repertoire. We made a similar observation for HIV-1 Env-reactive B cells of patient IDC561 compared to the donor-matched antigen-experienced B cell reference with an enrichment for IGHV1-46, 1-69 and 4-4 [63]. Studies have shown that antibodies targeting specific epitopes prefer a specific set of VH genes and have overall structural similarities [169]: as in antibodies directed against the hemagglutinin stem region of influenza virus prefer VH1-69, VH1-18 and VH6-1 [170-173]. Same is reported for HCV with antibodies targeting the E2 antigenic region 3 harboring VH1-69 [174-176]. VH1-46 is described for rotavirus antibodies directed against virus protein 6 (VP6) [177]. HIV-1 bNabs against the gp120 CD4 binding site (CD4bs) tend to the V genes VH1-2 and VH1-46 consistent with our report of 1-18 the VH1-46-derived CD4bs antibody [178, 179]. As well previously described is VH1-69 in HIV-1 antibodies targeting the coreceptor-binding site on gp120 or the conserved heptad repeat 1 (HR1) region and membrane proximal external region (MPER) of gp41 [180, 181]. It is well described that specific antibody features, such as specific

CDR3 lengths, certain amino acid residues at certain positions defined by V gene usage, are required to achieve a broad and potent neutralization [182]. Some of these antibody features are predetermined in the BCR-repertoire of the naïve B cell compartment with germline-encoded sequence characteristics [183]. These insights can influence vaccine design substantially as the administered immunogen is designed to elicit potent antibodies. Germline-targeting vaccine design is a theoretical approach to generate potential precursor B cells [184] by priming with an immunogen templated from known neutralizing and potent Abs to stimulate cell precursors followed by boosts to generate mature potent Abs [185]. Taken together, describing antibody repertoires across individuals and identifying pathogen-dependent alterations promotes the search for the ideal immunogen to elicit the best immune response.

Part II:

Efficient high-throughput protocols for the isolation of potent antigen-specific antibodies and advanced techniques for the study of the humoral immune response were used to meet the high demand for understanding the immune response against SARS-COV-2. We and others identified SARS-CoV-2 neutralizing antibodies mostly targeting the RBD of the S-protein to block viral ACE2 binding for entry [121-125, 186-188]. Successful impairment and prevention of SARS-CoV-2 infection in animal models once more underlines the relevance of antibodies as therapeutic agents [122, 189, 190].

We isolated and analyzed more than 4,000 SARS-CoV-2 reactive B cells by using DyLight488-labeled SARS-CoV-2 spike protein as bait for FACS-analysis. Among these reactive B cells, we found highly potent neutralizing antibodies and determined low concentrations of 0.04 µg/ml needed to fully block viral infections. Sequence analysis showed a rather polyclonal B cell response in all studied patients which was consistent with other studies [191]. Since our study included longitudinal samples, we observed that SARS-CoV-2 S-reactive IgG^+ B cell developed rapidly after infection and that the detected B cell clones at the first timepoint stayed detectable over the study period. However, one major observation due to the longitudinal analysis was an interesting contrast to what we overserved so far in most of our HIV-1 bNAb-studies, namely the limited degree of somatic mutation of SARS-CoV-2-neutralizing antibodies. In the five patients analyzed in detail, we showed little mutational enrichment or B cell expansion over time which is also confirmed by other studies such as Nielsen *et al.* 2020. They described naïve B cell derived sequences from healthy human control data with mostly unmutated IGHV genes, whereas the IgG compartment showed elevated SHM. SARS-COV-2 seroconverted patients however, revealed a polyclonal IgG B cell response with little to no SHM [191]. 10 of our 27 neutralizing SARS-CoV-2 antibodies have V-gene identities ranging

from 99 - 100%. Based on our observation we hypothesized that the virus is cleared so rapidly that B cell stimulation was not stimulated to its full extent since these low mutated antibodies can already prevent antigenic germinal center activation, a step essential for affinity maturation [192, 193]. Recent publications however, investigated the humoral immune response after SARS-CoV-2 infection over a longer period and reported changes in the memory B cell compartment after 6.2 months. Antibodies expressed by those B cells had higher levels of SHM, favorable adaptions to mutations in the RBD and an increasement in potency [194, 195]. The timeframe in our study between 8 and 36 days after diagnosis was too short to observe this prolonged affinity maturation.

High V gene identity was not restricted to neutralizing SARS-CoV-2 antibodies as we observed less mutated VH genes of all SARS-CoV-2 reactive antibodies compared to the healthy IgG repertoire. This comparison also revealed a VH3-30 V gene enrichment among the SARS-CoV-2-reactive cells. Barnes *et al.* 2020 [196] defined a new recurrent anti-SARS-CoV-2 antibody class with the V genes VH3-53/VH3-66 and reported similarity to a SARS-CoV antibody carrying the V gene VH3-30 [187, 196]. This is interesting because they describe the usage of distinct RBD-binding modes common among antibodies derived from VH3-53/VH3-66 and VH3-30 suggesting that binding occurs based on V gene-derived features [196]. Observations like this can help predict antibody information on a functional level extrapolated by sequence information alone [196]. Since there were studies reporting the isolation of weak binding SARS-CoV-2 antibodies from infection-naïve individuals [197] together with our results on low mutated SARS-CoV-2 reactive antibodies in reconvalescent patients, we searched for sequence similarities between S-protein reactive antibody derived sequences and the healthy naïve B cell repertoire. We were able to identify similar heavy and/or light-chain sequences of potent SARS-CoV-2-neutralizing antibodies in every individual. Thus, we hypothesized that these matches resemble potent precursor B cells that were present prior to an infection with SARS-CoV-2 and that could rapidly expand upon infection. However, we could not exclude that these sequence similarities result from pre-exposure to other endemic human coronaviruses and actual functionality of those antibodies needs to be evaluated and whether they provide a potential background immunity. This finding was the foundation for the comprehensive investigation on pre-existing immunity against SARS-CoV-2 in a large pre-pandemic cohort of healthy adults.

Part III:

A pre-existing immunity against SARS-CoV-2 could substantially influence our understanding of protective immunity, susceptibility to infection and COVID-19 disease severity [198-200]. Various studies quickly provided information on pre-existing T cell immunity against SARS-

CoV-2, but the presence of a pre-existing B cell immunity remains to be resolved [192, 201-203].

Reviewing recently published studies on pre-existing B cell immunity in SARS-CoV-2 unexposed individuals provides partially conflicting results. For example, some investigations using serum samples detected SARS-CoV-2 cross-reactive antibodies and pre-existing humoral immunity in uninfected individuals [204-207]. Cross-reactive humoral immune responses were mostly observed against S protein structures within the S2 subunit, the N protein or against ORF polypeptides like non-structural proteins protein 2 (NSP2) and 15 (NSP15), which are largely conserved among endemic HCoVs and SARS-CoV-2. The frequency of cross-reactive serum responses varies substantially between the individual studies. For example, several of these investigations reported an overall seroprevalence of cross-reactive serum responses in 10% to 20% in unexposed individuals [205, 207, 208] and another study observed antibody responses in more than 90% of all samples analyzed [204]. Differences in the frequency of cross-reactive serum responses between these studies were due to differences in the cohort composition and varying sensitivities of the diagnostic assays used. These studies also controversially discussed the extent to which previous immunity against HCoVs influences COVID-19 severity and susceptibility. Thereby, considering seasonal and geographical transmission patterns [205-207].

In contrast, in other studies, cross-reactive serum and B cell responses against SARS-CoV-2 were rarely shown in pre-pandemic samples and opposed a clinically relevant pre-existing B cell immunity [148, 208-211]. Most of the studies to date only analyzed plasma or serum and enriched or PBMC secreted IgG fractions of pre-pandemic samples [148, 204-211]. The studies lacked the overall analysis of B cells from the naïve B cell compartment as well as the isolation of putatively SARS-CoV-2-reactive B cells including the characterization of recombinant monoclonal antibodies derived from these cells. Studies that were solely based on plasma or serum level may have missed pre-existing potent naïve B cell precursors and low frequency memory B cells which did not contribute sufficient amounts of functionally detectable antibodies to plasma Ig fractions. In our dataset, we therefore covered a comprehensive analysis of plasma and IgG fractions and investigated the presence of SARS-CoV-2-reactive B cell precursors, and memory B cells, including the characterization of respective monoclonal antibodies. As described in *Part II* of my thesis we isolated SARS-CoV-2-reactive antibodies from convalescent individuals and identified highly similar sequences in a large sequence dataset of naive B cell receptor repertoires derived from pre-pandemic samples [62]. However, the publication did not include any functional data. Our data supported the hypothesis that some of these chains can be components of SARS-CoV-2-reactive

antibodies without requiring further affinity maturation. This was in line with previous observations reporting that the readily detected antibody response in some individuals might used existing antibody heavy or light chains with certain CDR3 recombination patterns or germline encoded sequence features [62, 125, 196, 212, 213].

In line with this, some studies reported the successful isolation of SARS-CoV-2 neutralizing antibodies from the human naïve B cell compartment using antigen-specific single B cell sorts or phage display [214, 215]. Feldman *et al*. 2021 used diverse SARS-CoV-2 spike protein subdomains as bait for the isolation by FACS of single SARS-CoV-2 and sarbecovirus-reactive naïve B cells. They determined a median frequency of 0.0025 % for RBM-reactive naïve B cells and the subsequent BCR sequence analyses revealed a polyclonal response with diverse gene usage for heavy and light chains. They furthermore observed an increase in the mean repertoire frequency of 20 % for IGHV3-9 in most donors [215]. Finally, some of their produced and tested monoclonal antibodies from naïve B cell precursors showed also binding and neutralization activity against circulating SARS-CoV-2 variants of concern (B.1.1.7, B.1.351 and B.1.617.2) as well as bat-derived coronaviruses. Bertoglio *et al.* 2021 performed phage display as approach to isolate the antibody candidate STE73-2E9 from naïve B cell libraries that targets the ACE2-RBD interface without cross-reactivity to other coronaviruses and neutralizes authentic SARS-CoV-2 wildtype virus with an IC50 of 0.43 nM. However, since phage display is based on random sequence recombination, this work provides no proof that SARS-CoV-2-reactive antibodies develop naturally in the naive B cell compartment [214]. While we performed various immunological and functional assays determining SARS-CoV-2 binding and neutralization activity as well as cross-reactivity to HCoV-HKU1 and HCoV-OC43, we found no evidence of any plasma or IgG reactivity against SARS-CoV-2 in pre-pandemic samples. We comprehensively tested plasma binding activity of IgG, IgM and IgA immunoglobulin isotypes against diverse beta coronavirus S proteins (SARS-CoV-2 S1 and S1/S2, HCoV-HKU1 and HCoV-OC43 S) by in house and commercially available ELISAs. We confirmed our ELISA results by implementing a flow cytometry-based assay using cell-surface-expressed S protein and by performing SARS-CoV-2 pseudo- as well as wildtype neutralization assays. While we observed slight binding activity against the SARS-CoV- S Protein in 3 % of analyzed plasma samples (5/150), no neutralization activity was observed in our pre-pandemic samples. This is consistent with recently published data that disagreed on a broad pre-existing B cell immunity, since they reported an overall prevalence of cross-reactive serum responses against the SARS-CoV-2 S protein or the S1 subdomain below 5 % [148, 208-211, 216]. Additionally, the published data from Anderson *et al.* 2021 and Poston *et al.* 2021 indicated a lack of SARS-CoV-2 neutralization activity in pre-pandemic serum sample and no evidence for a protection from disease severity by hCoV-reactive

antibodies [209, 210]. It should be noted that some of the compared studies differed in cohort composition and experimental assays. For instance, Ng *et al.* 2020 detected serum neutralization activity in unexposed children, adolescents, and pregnant women, who were included in our study cohort [205]. Of note, the individuals involved in our cohort were not tested for a recent HCoV infections prior to blood sampling. Therefore, we could not rule out that previous HCoV infections may have been determinants for the detection of cross-reactivity to SARS-CoV-2 in the plasma samples. In line with this, recent HCoV infections may have elicited a transient serum cross-reactivity against SARS-CoV-2 that was not detected in our data and experimental design. Moreover, HCoV infections appeared with higher prevalence in children and young adolescents who were not included in our study cohort [207, 217, 218].

To investigate the presence of a potential pre-existing immunity on a cellular level, we conducted antigen-specific single cell sorts with 40 donors and isolated a total of 8,174 putatively SARS-CoV-2-reactive B cells. We compared the frequencies of putatively SARS-CoV-2-reactive B cells in pre-pandemic samples with the frequencies in COVID-19 convalescent samples and observe very low frequencies, which was consistent with our findings from binding and neutralization screening of plasma samples and polyclonal IgG. We chose the native, full trimeric SARS-CoV-2 S protein as bait and adjusted the sorting gate according to the low frequencies. It can be argued that application of an alternative bait proteins e.g., the S2 subunit would have been a better choice [148, 205, 208, 211]. Although we aimed to apply the most stringent gating strategy for cell sorting, we cannot fully exclude the possibility that isolated cells also included SARS-CoV-2-non-reactive B cells. Sequence analyses revealed a diverse heavy chain V gene usage, normally distributed CDRH3 lengths and VH gene germline identities similar to the naïve BCR receptor repertoire of healthy individuals sampled before the pandemic. We found no enrichment of specific V genes as the case for some antibodies of SARS-CoV-2 convalescent individuals that can harbor enrichments in IGHV3-30, IGHV3-53 or IGHV3-63 [125, 196, 212]. Furthermore, we recombinantly produced and tested 158 monoclonal antibodies and detected no relevant reactivity against SARS-CoV-2 and endemic HCoV S proteins. Of note, we only produced a small proportion (n=158) of amplified and functional BCR sequences (n=5,223) and while we applied defined selection-criteria for antibody production, we cannot rule out that SARS-CoV-2-reactive BCR sequences indeed were present among isolated sequences amplified but simply not selected by our bio-informatical approach. Taken together, a pre-existing B cell immunity against pathogens can be a critical determinant of clinical outcome of infections and vaccination strategies. We and others investigated towards the presence and relevance of a pre-existing B cell immunity against SARS-CoV-2 in unexposed individuals and the results are

partly conflicting. While a pre-existing B cell immunity against SARS-CoV-2 was reported in certain study cohorts including children, adolescents or pregnant women, our comprehensive and detailed analysis of the B cell response, on plasma and cellular level, yielded no comparable evidence in a large cohort of healthy adults.

11. Conclusion

A key component of an effective and long-term immune response is the generation of potent, neutralizing antibodies that target pathogens and that are elicited upon infection or vaccination [219]. A detailed analysis of the human B cell response is critical for our understanding and the development of immune-mediated approaches to overcome global medical challenges as we are currently facing with the emerge of the novel COVID-19 pandemic [88]. The first part of this thesis described the technical foundation for the detailed analysis of the B cell repertoires in healthy or infected individuals. A reliable and reproduceable identification and isolation of B cell subsets is crucial for the analysis of evolutionary and developmental aspects of B cell repertoire composition and characteristics [135]. This way we revealed a convergence of antibody sequences across immune-challenged (infected or vaccinated) individuals offering molecular insights into shared features and differences in human B cell responses to pathogens [62, 63, 134, 135]. The urgent need for novel therapeutic agents and monoclonal antibodies as promising candidates was the rational for the isolation of new potent antibodies directed against Ebola virus, HIV-1 and SARS-CoV-2 [62, 63, 134]. Finally, we were able to provide valuable data regarding pre-existing immunity against SARS-CoV-2. Our comprehensive analysis on plasma and B cell level in a cohort of healthy adults provided no evidence to support the presence of a pre-existing immunity (Ercanoglu et al., Submitted and currently under review in iScience (Dec. 2021).

12. References

1. Janeway, C.A., Jr. and R. Medzhitov, *Innate immune recognition.* Annu Rev Immunol, 2002. **20**: p. 197-216.
2. Beutler, B., *Not "molecular patterns" but molecules.* Immunity, 2003. **19**(2): p. 155-6.
3. Beutler, B., *Inferences, questions and possibilities in Toll-like receptor signalling.* Nature, 2004. **430**(6996): p. 257-63.
4. Vivier, E. and B. Malissen, *Innate and adaptive immunity: specificities and signaling hierarchies revisited.* Nat Immunol, 2005. **6**(1): p. 17-21.
5. Gellert, M., *Molecular analysis of V(D)J recombination.* Annu Rev Genet, 1992. **26**: p. 425-46.
6. Murphy, K., Paul Travers, Mark Walport, Charles Janeway, *Janeway's Immunobiology*. 9 ed. 2017, New York: Garland Science.
7. Haynes, B.F., et al., *B-cell-lineage immunogen design in vaccine development with HIV-1 as a case study.* Nat Biotechnol, 2012. **30**(5): p. 423-33.
8. Galson, J.D., et al., *Studying the antibody repertoire after vaccination: practical applications.* Trends Immunol, 2014. **35**(7): p. 319-31.
9. Behring, v.E.K., Shibasaburo, *Über das Zustandekommen der Diphterie-Immunität und der Tetanus-Immunität bei Thieren. .* Dtsch Med Wochenschr 1890(49): p. 1113-1114.
10. Ehrlich, P., *Die Seitenkettentheorie und ihre Gegner.* Münchner Med Wochenschr, 1901. **2123-2124**.
11. Cooper, M.D., R.D. Peterson, and R.A. Good, *Delineation of the Thymic and Bursal Lymphoid Systems in the Chicken.* Nature, 1965. **205**: p. 143-6.
12. Cooper, M.D., et al., *The functions of the thymus system and the bursa system in the chicken.* J Exp Med, 1966. **123**(1): p. 75-102.
13. Owen, J.J., M.D. Cooper, and M.C. Raff, *In vitro generation of B lymphocytes in mouse foetal liver, a mammalian 'bursa equivalent'.* Nature, 1974. **249**(455): p. 361-3.
14. Cooper, M.D., *A life of adventure in immunobiology.* Annu Rev Immunol, 2010. **28**: p. 1-19.
15. Edelman, G.M., *Antibody structure and molecular immunology.* Scand J Immunol, 1991. **34**(1): p. 1-22.
16. Wu, T.T. and E.A. Kabat, *An analysis of the sequences of the variable regions of Bence Jones proteins and myeloma light chains and their implications for antibody complementarity.* J Exp Med, 1970. **132**(2): p. 211-50.
17. Zan, H. and P. Casali, *Editorial: Epigenetics of B Cells and Antibody Responses.* Front Immunol, 2015. **6**: p. 656.
18. Keyt, B.A., et al., *Structure, Function, and Therapeutic Use of IgM Antibodies.* Antibodies (Basel), 2020. **9**(4).
19. Valenzuela, N.M. and S. Schaub, *The Biology of IgG Subclasses and Their Clinical Relevance to Transplantation.* Transplantation, 2018. **102**(1S Suppl 1): p. S7-S13.
20. Gutzeit, C., K. Chen, and A. Cerutti, *The enigmatic function of IgD: some answers at last.* Eur J Immunol, 2018. **48**(7): p. 1101-1113.
21. Woof, J.M. and M.A. Kerr, *The function of immunoglobulin A in immunity.* J Pathol, 2006. **208**(2): p. 270-82.
22. Kelly, B.T. and M.H. Grayson, *Immunoglobulin E, what is it good for?* Ann Allergy Asthma Immunol, 2016. **116**(3): p. 183-7.
23. Lefranc, M.P., et al., *IMGT, the international ImMunoGeneTics database.* Nucleic Acids Res, 1999. **27**(1): p. 209-12.
24. Harris, L.J., et al., *The three-dimensional structure of an intact monoclonal antibody for canine lymphoma.* Nature, 1992. **360**(6402): p. 369-72.
25. Andre M. Vale, J.F.K., Alberto Nobrega, Harry W. Schroeder, *Chapter 7 - Development and Function of B Cell Subsets*, in *Molecular Biology of B Cells*, T.H. Frederick W. Alt, Andreas Radbruch, Michael Reth, Editor. 2015: Academic Press. p. Pages 99-119.

26. Nagasawa, T., *Microenvironmental niches in the bone marrow required for B-cell development.* Nat Rev Immunol, 2006. **6**(2): p. 107-16.
27. Schroeder, H.W., Jr., *Similarity and divergence in the development and expression of the mouse and human antibody repertoires.* Dev Comp Immunol, 2006. **30**(1-2): p. 119-35.
28. Halliley, J.L., et al., *Long-Lived Plasma Cells Are Contained within the CD19(-)CD38(hi)CD138(+) Subset in Human Bone Marrow.* Immunity, 2015. **43**(1): p. 132-45.
29. Tedder, T.F., *CD19: a promising B cell target for rheumatoid arthritis.* Nat Rev Rheumatol, 2009. **5**(10): p. 572-7.
30. Klasener, K., et al., *CD20 as a gatekeeper of the resting state of human B cells.* Proc Natl Acad Sci U S A, 2021. **118**(7).
31. Pierpont, T.M., C.B. Limper, and K.L. Richards, *Past, Present, and Future of Rituximab-The World's First Oncology Monoclonal Antibody Therapy.* Front Oncol, 2018. **8**: p. 163.
32. Kosmas, C., et al., *Anti-CD20-based therapy of B cell lymphoma: state of the art.* Leukemia, 2002. **16**(10): p. 2004-15.
33. Hardy, R.R. and K. Hayakawa, *B cell development pathways.* Annu Rev Immunol, 2001. **19**: p. 595-621.
34. Seifert, M. and R. Kuppers, *Human memory B cells.* Leukemia, 2016. **30**(12): p. 2283-2292.
35. Yoshikawa, K., et al., *AID enzyme-induced hypermutation in an actively transcribed gene in fibroblasts.* Science, 2002. **296**(5575): p. 2033-6.
36. Longerich, S., et al., *AID in somatic hypermutation and class switch recombination.* Curr Opin Immunol, 2006. **18**(2): p. 164-74.
37. Macallan, D.C., et al., *B-cell kinetics in humans: rapid turnover of peripheral blood memory cells.* Blood, 2005. **105**(9): p. 3633-40.
38. Schur, P.H., *IgG subclasses. A historical perspective.* Monogr Allergy, 1988. **23**: p. 1-11.
39. Vidarsson, G., G. Dekkers, and T. Rispens, *IgG subclasses and allotypes: from structure to effector functions.* Front Immunol, 2014. **5**: p. 520.
40. Pabst, O. and E. Slack, *IgA and the intestinal microbiota: the importance of being specific.* Mucosal Immunol, 2020. **13**(1): p. 12-21.
41. Sutton, B.J., et al., *IgE Antibodies: From Structure to Function and Clinical Translation.* Antibodies (Basel), 2019. **8**(1).
42. Sethna, Z., et al., *OLGA: fast computation of generation probabilities of B- and T-cell receptor amino acid sequences and motifs.* Bioinformatics, 2019. **35**(17): p. 2974-2981.
43. Nutt, S.L., et al., *The generation of antibody-secreting plasma cells.* Nat Rev Immunol, 2015. **15**(3): p. 160-71.
44. Lu, L.L., et al., *Beyond binding: antibody effector functions in infectious diseases.* Nat Rev Immunol, 2018. **18**(1): p. 46-61.
45. Smyth, M.J., et al., *Activation of NK cell cytotoxicity.* Mol Immunol, 2005. **42**(4): p. 501-10.
46. Huber, V.C., et al., *Fc receptor-mediated phagocytosis makes a significant contribution to clearance of influenza virus infections.* J Immunol, 2001. **166**(12): p. 7381-8.
47. Vanderven, H.A., et al., *Fc functional antibodies in humans with severe H7N9 and seasonal influenza.* JCI Insight, 2017. **2**(13).
48. Dunkelberger, J.R. and W.C. Song, *Complement and its role in innate and adaptive immune responses.* Cell Res, 2010. **20**(1): p. 34-50.
49. van Erp, E.A., et al., *Fc-Mediated Antibody Effector Functions During Respiratory Syncytial Virus Infection and Disease.* Front Immunol, 2019. **10**: p. 548.
50. Kreer, C., et al., *Exploiting B Cell Receptor Analyses to Inform on HIV-1 Vaccination Strategies.* Vaccines (Basel), 2020. **8**(1).

51. Vanshylla, K., et al., *Kinetics and correlates of the neutralizing antibody response to SARS-CoV-2 infection in humans.* Cell Host Microbe, 2021. **29**(6): p. 917-929 e4.
52. Wiesner, M., et al., *Conditional immortalization of human B cells by CD40 ligation.* PLoS One, 2008. **3**(1): p. e1464.
53. Pasqualini, R. and W. Arap, *Hybridoma-free generation of monoclonal antibodies.* Proc Natl Acad Sci U S A, 2004. **101**(1): p. 257-9.
54. Kwakkenbos, M.J., et al., *Stable long-term cultures of self-renewing B cells and their applications.* Immunol Rev, 2016. **270**(1): p. 65-77.
55. Setliff, I., et al., *High-Throughput Mapping of B Cell Receptor Sequences to Antigen Specificity.* Cell, 2019. **179**(7): p. 1636-1646 e15.
56. Kreer, C., et al., *openPrimeR for multiplex amplification of highly diverse templates.* J Immunol Methods, 2020. **480**: p. 112752.
57. Little, M., et al., *Of mice and men: hybridoma and recombinant antibodies.* Immunol Today, 2000. **21**(8): p. 364-70.
58. Smith, S.L., *Ten years of Orthoclone OKT3 (muromonab-CD3): a review.* J Transpl Coord, 1996. **6**(3): p. 109-19; quiz 120-1.
59. Grilo, A.L. and A. Mantalaris, *The Increasingly Human and Profitable Monoclonal Antibody Market.* Trends Biotechnol, 2019. **37**(1): p. 9-16.
60. Reff, M.E., et al., *Depletion of B cells in vivo by a chimeric mouse human monoclonal antibody to CD20.* Blood, 1994. **83**(2): p. 435-45.
61. Arin, M.J., et al., *Anti-CD20 monoclonal antibody (rituximab) in the treatment of pemphigus.* Br J Dermatol, 2005. **153**(3): p. 620-5.
62. Kreer, C., et al., *Longitudinal Isolation of Potent Near-Germline SARS-CoV-2-Neutralizing Antibodies from COVID-19 Patients.* Cell, 2020. **182**(6): p. 1663-1673.
63. Schommers, P., et al., *Restriction of HIV-1 Escape by a Highly Broad and Potent Neutralizing Antibody.* Cell, 2020. **180**(3): p. 471-489 e22.
64. Caskey, M., et al., *Viraemia suppressed in HIV-1-infected humans by broadly neutralizing antibody 3BNC117.* Nature, 2015. **522**(7557): p. 487-91.
65. Scheid, J.F., et al., *HIV-1 antibody 3BNC117 suppresses viral rebound in humans during treatment interruption.* Nature, 2016. **535**(7613): p. 556-60.
66. Schoofs, T., et al., *HIV-1 therapy with monoclonal antibody 3BNC117 elicits host immune responses against HIV-1.* Science, 2016. **352**(6288): p. 997-1001.
67. Kaplon, H. and J.M. Reichert, *Antibodies to watch in 2021.* MAbs, 2021. **13**(1): p. 1860476.
68. Saxena, D., et al., *Atoltivimab/maftivimab/odesivimab (Inmazeb) combination to treat infection caused by Zaire ebolavirus.* Drugs Today (Barc), 2021. **57**(8): p. 483-490.
69. Sidebottom, D.B. and D. Gill, *Ronapreve for prophylaxis and treatment of covid-19.* BMJ, 2021. **374**: p. n2136.
70. Pelegrin, M., M. Naranjo-Gomez, and M. Piechaczyk, *Antiviral Monoclonal Antibodies: Can They Be More Than Simple Neutralizing Agents?* Trends Microbiol, 2015. **23**(10): p. 653-665.
71. Panda, S. and J.L. Ding, *Natural antibodies bridge innate and adaptive immunity.* J Immunol, 2015. **194**(1): p. 13-20.
72. Moldt, B., et al., *Highly potent HIV-specific antibody neutralization in vitro translates into effective protection against mucosal SHIV challenge in vivo.* Proc Natl Acad Sci U S A, 2012. **109**(46): p. 18921-5.
73. Shingai, M., et al., *Passive transfer of modest titers of potent and broadly neutralizing anti-HIV monoclonal antibodies block SHIV infection in macaques.* J Exp Med, 2014. **211**(10): p. 2061-74.
74. Gautam, R., et al., *A single injection of anti-HIV-1 antibodies protects against repeated SHIV challenges.* Nature, 2016. **533**(7601): p. 105-109.
75. Julg, B., et al., *Broadly neutralizing antibodies targeting the HIV-1 envelope V2 apex confer protection against a clade C SHIV challenge.* Sci Transl Med, 2017. **9**(406).
76. Jacob, S.T., et al., *Ebola virus disease.* Nat Rev Dis Primers, 2020. **6**(1): p. 13.

77. Dowell, S.F., et al., *Transmission of Ebola hemorrhagic fever: a study of risk factors in family members, Kikwit, Democratic Republic of the Congo, 1995. Commission de Lutte contre les Epidemies a Kikwit.* J Infect Dis, 1999. **179 Suppl 1**: p. S87-91.
78. Mulangu, S., et al., *A Randomized, Controlled Trial of Ebola Virus Disease Therapeutics.* N Engl J Med, 2019. **381**(24): p. 2293-2303.
79. Gaudinski, M.R., et al., *Safety, tolerability, pharmacokinetics, and immunogenicity of the therapeutic monoclonal antibody mAb114 targeting Ebola virus glycoprotein (VRC 608): an open-label phase 1 study.* Lancet, 2019. **393**(10174): p. 889-898.
80. Heppner, D.G., Jr., et al., *Safety and immunogenicity of the rVSVG-ZEBOV-GP Ebola virus vaccine candidate in healthy adults: a phase 1b randomised, multicentre, double-blind, placebo-controlled, dose-response study.* Lancet Infect Dis, 2017. **17**(8): p. 854-866.
81. Forsythe, S.S., et al., *Twenty Years Of Antiretroviral Therapy For People Living With HIV: Global Costs, Health Achievements, Economic Benefits.* Health Aff (Millwood), 2019. **38**(7): p. 1163-1172.
82. Silva, B.F., et al., *Adverse effects of chronic treatment with the Main subclasses of highly active antiretroviral therapy: a systematic review.* HIV Med, 2019. **20**(7): p. 429-438.
83. Caskey, M., et al., *Antibody 10-1074 suppresses viremia in HIV-1-infected individuals.* Nat Med, 2017. **23**(2): p. 185-191.
84. Mendoza, P., et al., *Combination therapy with anti-HIV-1 antibodies maintains viral suppression.* Nature, 2018. **561**(7724): p. 479-484.
85. Edupuganti, S., et al., *Feasibility and Successful Enrollment in a Proof-of-Concept HIV Prevention Trial of VRC01, a Broadly Neutralizing HIV-1 Monoclonal Antibody.* J Acquir Immune Defic Syndr, 2021. **87**(1): p. 671-679.
86. Gilbert, P.B., et al., *Basis and Statistical Design of the Passive HIV-1 Antibody Mediated Prevention (AMP) Test-of-Concept Efficacy Trials.* Stat Commun Infect Dis, 2017. **9**(1).
87. Zhu, N., et al., *A Novel Coronavirus from Patients with Pneumonia in China, 2019.* N Engl J Med, 2020. **382**(8): p. 727-733.
88. Cucinotta, D. and M. Vanelli, *WHO Declares COVID-19 a Pandemic.* Acta Biomed, 2020. **91**(1): p. 157-160.
89. Weiss, S.R. and J.L. Leibowitz, *Coronavirus pathogenesis.* Adv Virus Res, 2011. **81**: p. 85-164.
90. Hamre, D. and J.J. Procknow, *A new virus isolated from the human respiratory tract.* Proc Soc Exp Biol Med, 1966. **121**(1): p. 190-3.
91. McIntosh, K., et al., *Recovery in tracheal organ cultures of novel viruses from patients with respiratory disease.* Proc Natl Acad Sci U S A, 1967. **57**(4): p. 933-40.
92. McIntosh, K., et al., *Coronavirus infection in acute lower respiratory tract disease of infants.* J Infect Dis, 1974. **130**(5): p. 502-7.
93. Su, S., et al., *Epidemiology, Genetic Recombination, and Pathogenesis of Coronaviruses.* Trends Microbiol, 2016. **24**(6): p. 490-502.
94. Peiris, J.S., et al., *Coronavirus as a possible cause of severe acute respiratory syndrome.* Lancet, 2003. **361**(9366): p. 1319-25.
95. W.H., O. *Summary table of SARS cases by country, November 1, 2002-August 7, 2003*. 2021; Available from: https://www.who.int/publications/m/item/summary-of-probable-sars-cases-with-onset-of-illness-from-1-november-2002-to-31-july-2003.
96. Zaki, A.M., et al., *Isolation of a novel coronavirus from a man with pneumonia in Saudi Arabia.* N Engl J Med, 2012. **367**(19): p. 1814-20.
97. Control, E.C.f.D.P.a., *Distribution of confirmed cases of MERS-CoV by place of infection and month of onset, from March 2012 to 2 December 2019.* 2021.
98. Stadnytskyi, V., et al., *The airborne lifetime of small speech droplets and their potential importance in SARS-CoV-2 transmission.* Proc Natl Acad Sci U S A, 2020. **117**(22): p. 11875-11877.

99. Echternach, M., et al., *Impulse Dispersion of Aerosols during Singing and Speaking: A Potential COVID-19 Transmission Pathway.* Am J Respir Crit Care Med, 2020. **202**(11): p. 1584-1587.
100. Edwards, D.A., et al., *Exhaled aerosol increases with COVID-19 infection, age, and obesity.* Proc Natl Acad Sci U S A, 2021. **118**(8).
101. Chen, N., et al., *Epidemiological and clinical characteristics of 99 cases of 2019 novel coronavirus pneumonia in Wuhan, China: a descriptive study.* Lancet, 2020. **395**(10223): p. 507-513.
102. Wang, D., et al., *Clinical Characteristics of 138 Hospitalized Patients With 2019 Novel Coronavirus-Infected Pneumonia in Wuhan, China.* JAMA, 2020. **323**(11): p. 1061-1069.
103. Chan, J.F., et al., *A familial cluster of pneumonia associated with the 2019 novel coronavirus indicating person-to-person transmission: a study of a family cluster.* Lancet, 2020. **395**(10223): p. 514-523.
104. Ksiazek, T.G., et al., *A novel coronavirus associated with severe acute respiratory syndrome.* N Engl J Med, 2003. **348**(20): p. 1953-66.
105. Naqvi, A.A.T., et al., *Insights into SARS-CoV-2 genome, structure, evolution, pathogenesis and therapies: Structural genomics approach.* Biochim Biophys Acta Mol Basis Dis, 2020. **1866**(10): p. 165878.
106. Chazal, N., *Coronavirus, the King Who Wanted More Than a Crown: From Common to the Highly Pathogenic SARS-CoV-2, Is the Key in the Accessory Genes?* Front Microbiol, 2021. **12**: p. 682603.
107. Wrapp, D., et al., *Cryo-EM structure of the 2019-nCoV spike in the prefusion conformation.* Science, 2020. **367**(6483): p. 1260-1263.
108. Bianchi, M., et al., *Sars-CoV-2 Envelope and Membrane Proteins: Structural Differences Linked to Virus Characteristics?* Biomed Res Int, 2020. **2020**: p. 4389089.
109. Thomas, S., *The Structure of the Membrane Protein of SARS-CoV-2 Resembles the Sugar Transporter SemiSWEET.* Pathog Immun, 2020. **5**(1): p. 342-363.
110. Schoeman, D. and B.C. Fielding, *Coronavirus envelope protein: current knowledge.* Virol J, 2019. **16**(1): p. 69.
111. Cubuk, J., et al., *The SARS-CoV-2 nucleocapsid protein is dynamic, disordered, and phase separates with RNA.* Nat Commun, 2021. **12**(1): p. 1936.
112. Alanagreh, L., F. Alzoughool, and M. Atoum, *The Human Coronavirus Disease COVID-19: Its Origin, Characteristics, and Insights into Potential Drugs and Its Mechanisms.* Pathogens, 2020. **9**(5).
113. Hoffmann, M., et al., *SARS-CoV-2 Cell Entry Depends on ACE2 and TMPRSS2 and Is Blocked by a Clinically Proven Protease Inhibitor.* Cell, 2020. **181**(2): p. 271-280 e8.
114. Li, W., et al., *Angiotensin-converting enzyme 2 is a functional receptor for the SARS coronavirus.* Nature, 2003. **426**(6965): p. 450-4.
115. Qian, Z., et al., *Innate immune response of human alveolar type II cells infected with severe acute respiratory syndrome-coronavirus.* Am J Respir Cell Mol Biol, 2013. **48**(6): p. 742-8.
116. Fehr, A.R. and S. Perlman, *Coronaviruses: an overview of their replication and pathogenesis.* Methods Mol Biol, 2015. **1282**: p. 1-23.
117. Ziebuhr, J., E.J. Snijder, and A.E. Gorbalenya, *Virus-encoded proteinases and proteolytic processing in the Nidovirales.* J Gen Virol, 2000. **81**(Pt 4): p. 853-79.
118. Schubert, K., et al., *SARS-CoV-2 Nsp1 binds the ribosomal mRNA channel to inhibit translation.* Nat Struct Mol Biol, 2020. **27**(10): p. 959-966.
119. Sethna, P.B., M.A. Hofmann, and D.A. Brian, *Minus-strand copies of replicating coronavirus mRNAs contain antileaders.* J Virol, 1991. **65**(1): p. 320-5.
120. Perlman, S. and J. Netland, *Coronaviruses post-SARS: update on replication and pathogenesis.* Nat Rev Microbiol, 2009. **7**(6): p. 439-50.
121. Brouwer, P.J.M., et al., *Potent neutralizing antibodies from COVID-19 patients define multiple targets of vulnerability.* Science, 2020. **369**(6504): p. 643-650.

122. Cao, Y., et al., *Potent Neutralizing Antibodies against SARS-CoV-2 Identified by High-Throughput Single-Cell Sequencing of Convalescent Patients' B Cells.* Cell, 2020. **182**(1): p. 73-84 e16.
123. Hansen, J., et al., *Studies in humanized mice and convalescent humans yield a SARS-CoV-2 antibody cocktail.* Science, 2020. **369**(6506): p. 1010-1014.
124. Ju, B., et al., *Human neutralizing antibodies elicited by SARS-CoV-2 infection.* Nature, 2020. **584**(7819): p. 115-119.
125. Robbiani, D.F., et al., *Convergent antibody responses to SARS-CoV-2 in convalescent individuals.* Nature, 2020. **584**(7821): p. 437-442.
126. Beigel, J.H., et al., *Remdesivir for the Treatment of Covid-19 - Final Report.* N Engl J Med, 2020. **383**(19): p. 1813-1826.
127. Weinreich, D.M., et al., *REGN-COV2, a Neutralizing Antibody Cocktail, in Outpatients with Covid-19.* N Engl J Med, 2021. **384**(3): p. 238-251.
128. Dougan, M., et al., *Bamlanivimab plus Etesevimab in Mild or Moderate Covid-19.* N Engl J Med, 2021. **385**(15): p. 1382-1392.
129. Gupta, A., et al., *Early Treatment for Covid-19 with SARS-CoV-2 Neutralizing Antibody Sotrovimab.* N Engl J Med, 2021.
130. Polack, F.P., et al., *Safety and Efficacy of the BNT162b2 mRNA Covid-19 Vaccine.* N Engl J Med, 2020. **383**(27): p. 2603-2615.
131. Baden, L.R., et al., *Efficacy and Safety of the mRNA-1273 SARS-CoV-2 Vaccine.* N Engl J Med, 2021. **384**(5): p. 403-416.
132. Sadoff, J., et al., *Safety and Efficacy of Single-Dose Ad26.COV2.S Vaccine against Covid-19.* N Engl J Med, 2021. **384**(23): p. 2187-2201.
133. Kurosaki, T., K. Kometani, and W. Ise, *Memory B cells.* Nat Rev Immunol, 2015. **15**(3): p. 149-59.
134. Ehrhardt, S.A., et al., *Polyclonal and convergent antibody response to Ebola virus vaccine rVSV-ZEBOV.* Nat Med, 2019. **25**(10): p. 1589-1600.
135. Gieselmann, L., et al., *Effective high-throughput isolation of fully human antibodies targeting infectious pathogens.* Nat Protoc, 2021. **16**(7): p. 3639-3671.
136. Ozawa, T., H. Kishi, and A. Muraguchi, *Amplification and analysis of cDNA generated from a single cell by 5'-RACE: application to isolation of antibody heavy and light chain variable gene sequences from single B cells.* Biotechniques, 2006. **40**(4): p. 469-70, 472, 474 passim.
137. Tiller, T., et al., *Efficient generation of monoclonal antibodies from single human B cells by single cell RT-PCR and expression vector cloning.* J Immunol Methods, 2008. **329**(1-2): p. 112-24.
138. von Boehmer, L., et al., *Sequencing and cloning of antigen-specific antibodies from mouse memory B cells.* Nat Protoc, 2016. **11**(10): p. 1908-1923.
139. Sievers, F., et al., *Fast, scalable generation of high-quality protein multiple sequence alignments using Clustal Omega.* Mol Syst Biol, 2011. **7**: p. 539.
140. Ye, J., et al., *IgBLAST: an immunoglobulin variable domain sequence analysis tool.* Nucleic Acids Res, 2013. **41**(Web Server issue): p. W34-40.
141. Vander Heiden, J.A., et al., *pRESTO: a toolkit for processing high-throughput sequencing raw reads of lymphocyte receptor repertoires.* Bioinformatics, 2014. **30**(13): p. 1930-2.
142. Koch, T., et al., *Safety and immunogenicity of a modified vaccinia virus Ankara vector vaccine candidate for Middle East respiratory syndrome: an open-label, phase 1 trial.* Lancet Infect Dis, 2020. **20**(7): p. 827-838.
143. Ercanoglu, M.S., et al., *No substantial pre-existing B cell immunity against SARS-CoV-2 in healthy adults.* bioRxiv, 2021: p. 2021.09.08.459398.
144. St-Jean, J.R., et al., *Human respiratory coronavirus OC43: genetic stability and neuroinvasion.* J Virol, 2004. **78**(16): p. 8824-34.
145. Woo, P.C., et al., *Characterization and complete genome sequence of a novel coronavirus, coronavirus HKU1, from patients with pneumonia.* J Virol, 2005. **79**(2): p. 884-95.

146. Corman, V.M., et al., *Assays for laboratory confirmation of novel human coronavirus (hCoV-EMC) infections.* Euro Surveill, 2012. **17**(49).
147. Kreye, J., et al., *A Therapeutic Non-self-reactive SARS-CoV-2 Antibody Protects from Lung Pathology in a COVID-19 Hamster Model.* Cell, 2020. **183**(4): p. 1058-1069 e19.
148. Song, G., et al., *Cross-reactive serum and memory B-cell responses to spike protein in SARS-CoV-2 and endemic coronavirus infection.* Nat Commun, 2021. **12**(1): p. 2938.
149. Stadlbauer, D., et al., *SARS-CoV-2 Seroconversion in Humans: A Detailed Protocol for a Serological Assay, Antigen Production, and Test Setup.* Curr Protoc Microbiol, 2020. **57**(1): p. e100.
150. Kowarz, E., D. Loscher, and R. Marschalek, *Optimized Sleeping Beauty transposons rapidly generate stable transgenic cell lines.* Biotechnol J, 2015. **10**(4): p. 647-53.
151. Walker, L.M., et al., *Broad and potent neutralizing antibodies from an African donor reveal a new HIV-1 vaccine target.* Science, 2009. **326**(5950): p. 285-9.
152. Crawford, K.H.D., et al., *Protocol and Reagents for Pseudotyping Lentiviral Particles with SARS-CoV-2 Spike Protein for Neutralization Assays.* Viruses, 2020. **12**(5).
153. Lefranc, M.P., et al., *IMGT, the international ImMunoGeneTics information system.* Nucleic Acids Res, 2009. **37**(Database issue): p. D1006-12.
154. Raybould, M.I.J., et al., *CoV-AbDab: the coronavirus antibody database.* Bioinformatics, 2021. **37**(5): p. 734-735.
155. Boonyaratanakornkit, J. and J.J. Taylor, *Techniques to Study Antigen-Specific B Cell Responses.* Front Immunol, 2019. **10**: p. 1694.
156. Kreer, C., et al., *Longitudinal Isolation of Potent Near-Germline SARS-CoV-2-Neutralizing Antibodies from COVID-19 Patients.* Cell, 2020. **182**(4): p. 843-854 e12.
157. Ahmed, R. and D. Gray, *Immunological memory and protective immunity: understanding their relation.* Science, 1996. **272**(5258): p. 54-60.
158. Plotkin, S.A., *Correlates of protection induced by vaccination.* Clin Vaccine Immunol, 2010. **17**(7): p. 1055-65.
159. Chen, F., et al., *VH1-69 antiviral broadly neutralizing antibodies: genetics, structures, and relevance to rational vaccine design.* Curr Opin Virol, 2019. **34**: p. 149-159.
160. Saunders, K.O., et al., *Targeted selection of HIV-specific antibody mutations by engineering B cell maturation.* Science, 2019. **366**(6470).
161. Kaplon, H., et al., *Antibodies to watch in 2020.* MAbs, 2020. **12**(1): p. 1703531.
162. Simek, M.D., et al., *Human immunodeficiency virus type 1 elite neutralizers: individuals with broad and potent neutralizing activity identified by using a high-throughput neutralization assay together with an analytical selection algorithm.* J Virol, 2009. **83**(14): p. 7337-48.
163. Walker, L.M. and D.R. Burton, *Passive immunotherapy of viral infections: 'super-antibodies' enter the fray.* Nat Rev Immunol, 2018. **18**(5): p. 297-308.
164. Graham, B.S., M.S.A. Gilman, and J.S. McLellan, *Structure-Based Vaccine Antigen Design.* Annu Rev Med, 2019. **70**: p. 91-104.
165. Sanders, R.W., et al., *A next-generation cleaved, soluble HIV-1 Env trimer, BG505 SOSIP.664 gp140, expresses multiple epitopes for broadly neutralizing but not non-neutralizing antibodies.* PLoS Pathog, 2013. **9**(9): p. e1003618.
166. Kanika Vanshylla, C.F., Marie Wunsch, Nareshkumar Poopalasingam, Matthijs Meijers, Christoph Kreer, Franziska Kleipass, Denis Ruchnewitz, Meryem S. Ercanoglu, Henning Gruell, Friederike Münn, Kai Pohl, Hanna Janicki, Tobias Nolden, Simone Bartl, Saskia Catherina Stein, Max Augustin, Felix Dewald, Lutz Gieselmann, Philipp Schommers, Thomas F. Schulz, Leif Erik Sander, Manuel Koch, Marta Luksza, Michael Lässig, Pamela J. Bjorkman, Florian Klein, *Discovery of ultrapotent broadly neutralizing antibodies from SARS-CoV-2 elite neutralizers.* Cell Host Microbe, 2021.
167. Ippolito, G.C., et al., *Antibody repertoires in humanized NOD-scid-IL2Rgamma(null) mice and human B cells reveals human-like diversification and tolerance checkpoints in the mouse.* PLoS One, 2012. **7**(4): p. e35497.

168. Greiff, V., et al., *Bioinformatic and Statistical Analysis of Adaptive Immune Repertoires.* Trends Immunol, 2015. **36**(11): p. 738-749.
169. Henry Dunand, C.J. and P.C. Wilson, *Restricted, canonical, stereotyped and convergent immunoglobulin responses.* Philos Trans R Soc Lond B Biol Sci, 2015. **370**(1676).
170. Joyce, M.G., et al., *Vaccine-Induced Antibodies that Neutralize Group 1 and Group 2 Influenza A Viruses.* Cell, 2016. **166**(3): p. 609-623.
171. Pappas, L., et al., *Rapid development of broadly influenza neutralizing antibodies through redundant mutations.* Nature, 2014. **516**(7531): p. 418-22.
172. Sui, J., et al., *Structural and functional bases for broad-spectrum neutralization of avian and human influenza A viruses.* Nat Struct Mol Biol, 2009. **16**(3): p. 265-73.
173. Wheatley, A.K., et al., *H5N1 Vaccine-Elicited Memory B Cells Are Genetically Constrained by the IGHV Locus in the Recognition of a Neutralizing Epitope in the Hemagglutinin Stem.* J Immunol, 2015. **195**(2): p. 602-10.
174. Bailey, J.R., et al., *Broadly neutralizing antibodies with few somatic mutations and hepatitis C virus clearance.* JCI Insight, 2017. **2**(9).
175. Giang, E., et al., *Human broadly neutralizing antibodies to the envelope glycoprotein complex of hepatitis C virus.* Proc Natl Acad Sci U S A, 2012. **109**(16): p. 6205-10.
176. Merat, S.J., et al., *Hepatitis C virus Broadly Neutralizing Monoclonal Antibodies Isolated 25 Years after Spontaneous Clearance.* PLoS One, 2016. **11**(10): p. e0165047.
177. Weitkamp, J.H., et al., *VH1-46 is the dominant immunoglobulin heavy chain gene segment in rotavirus-specific memory B cells expressing the intestinal homing receptor alpha4beta7.* J Immunol, 2005. **174**(6): p. 3454-60.
178. Wu, X., et al., *Focused evolution of HIV-1 neutralizing antibodies revealed by structures and deep sequencing.* Science, 2011. **333**(6049): p. 1593-602.
179. Zhou, T., et al., *Structural Repertoire of HIV-1-Neutralizing Antibodies Targeting the CD4 Supersite in 14 Donors.* Cell, 2015. **161**(6): p. 1280-92.
180. Huang, C.C., et al., *Structural basis of tyrosine sulfation and VH-gene usage in antibodies that recognize the HIV type 1 coreceptor-binding site on gp120.* Proc Natl Acad Sci U S A, 2004. **101**(9): p. 2706-11.
181. Williams, W.B., et al., *HIV-1 VACCINES. Diversion of HIV-1 vaccine-induced immunity by gp41-microbiota cross-reactive antibodies.* Science, 2015. **349**(6249): p. aab1253.
182. Klein, F., et al., *Somatic mutations of the immunoglobulin framework are generally required for broad and potent HIV-1 neutralization.* Cell, 2013. **153**(1): p. 126-38.
183. Lee, J.H., et al., *Vaccine genetics of IGHV1-2 VRC01-class broadly neutralizing antibody precursor naive human B cells.* NPJ Vaccines, 2021. **6**(1): p. 113.
184. Amitai, A., et al., *Defining and Manipulating B Cell Immunodominance Hierarchies to Elicit Broadly Neutralizing Antibody Responses against Influenza Virus.* Cell Syst, 2020. **11**(6): p. 573-588 e9.
185. Steichen, J.M., et al., *HIV Vaccine Design to Target Germline Precursors of Glycan-Dependent Broadly Neutralizing Antibodies.* Immunity, 2016. **45**(3): p. 483-496.
186. Andreano, E., et al., *Extremely potent human monoclonal antibodies from COVID-19 convalescent patients.* Cell, 2021. **184**(7): p. 1821-1835 e16.
187. Pinto, D., et al., *Cross-neutralization of SARS-CoV-2 by a human monoclonal SARS-CoV antibody.* Nature, 2020. **583**(7815): p. 290-295.
188. Seydoux, E., et al., *Analysis of a SARS-CoV-2-Infected Individual Reveals Development of Potent Neutralizing Antibodies with Limited Somatic Mutation.* Immunity, 2020. **53**(1): p. 98-105 e5.
189. Rogers, T.F., et al., *Isolation of potent SARS-CoV-2 neutralizing antibodies and protection from disease in a small animal model.* Science, 2020. **369**(6506): p. 956-963.
190. Zost, S.J., et al., *Potently neutralizing and protective human antibodies against SARS-CoV-2.* Nature, 2020. **584**(7821): p. 443-449.

191. Nielsen, S.C.A., et al., *Human B Cell Clonal Expansion and Convergent Antibody Responses to SARS-CoV-2.* Cell Host Microbe, 2020. **28**(4): p. 516-525 e5.
192. Grifoni, A., et al., *Targets of T Cell Responses to SARS-CoV-2 Coronavirus in Humans with COVID-19 Disease and Unexposed Individuals.* Cell, 2020. **181**(7): p. 1489-1501 e15.
193. Ni, L., et al., *Detection of SARS-CoV-2-Specific Humoral and Cellular Immunity in COVID-19 Convalescent Individuals.* Immunity, 2020. **52**(6): p. 971-977 e3.
194. Gaebler, C., et al., *Evolution of antibody immunity to SARS-CoV-2.* Nature, 2021. **591**(7851): p. 639-644.
195. Muecksch, F., et al., *Affinity maturation of SARS-CoV-2 neutralizing antibodies confers potency, breadth, and resilience to viral escape mutations.* Immunity, 2021. **54**(8): p. 1853-1868 e7.
196. Barnes, C.O., et al., *Structures of Human Antibodies Bound to SARS-CoV-2 Spike Reveal Common Epitopes and Recurrent Features of Antibodies.* Cell, 2020. **182**(4): p. 828-842 e16.
197. Wec, A.Z., et al., *Broad neutralization of SARS-related viruses by human monoclonal antibodies.* Science, 2020. **369**(6504): p. 731-736.
198. Imkeller, K. and H. Wardemann, *Assessing human B cell repertoire diversity and convergence.* Immunol Rev, 2018. **284**(1): p. 51-66.
199. Niu, X., et al., *Longitudinal Analysis of T and B Cell Receptor Repertoire Transcripts Reveal Dynamic Immune Response in COVID-19 Patients.* Front Immunol, 2020. **11**: p. 582010.
200. Schultheiss, C., et al., *Next-Generation Sequencing of T and B Cell Receptor Repertoires from COVID-19 Patients Showed Signatures Associated with Severity of Disease.* Immunity, 2020. **53**(2): p. 442-455 e4.
201. Le Bert, N., et al., *SARS-CoV-2-specific T cell immunity in cases of COVID-19 and SARS, and uninfected controls.* Nature, 2020. **584**(7821): p. 457-462.
202. Mateus, J., et al., *Selective and cross-reactive SARS-CoV-2 T cell epitopes in unexposed humans.* Science, 2020. **370**(6512): p. 89-94.
203. Sette, A. and S. Crotty, *Adaptive immunity to SARS-CoV-2 and COVID-19.* Cell, 2021. **184**(4): p. 861-880.
204. Majdoubi, A., et al., *A majority of uninfected adults show preexisting antibody reactivity against SARS-CoV-2.* JCI Insight, 2021. **6**(8).
205. Ng, K.W., et al., *Preexisting and de novo humoral immunity to SARS-CoV-2 in humans.* Science, 2020. **370**(6522): p. 1339-1343.
206. Sagar, M., et al., *Recent endemic coronavirus infection is associated with less-severe COVID-19.* J Clin Invest, 2021. **131**(1).
207. Woudenberg, T., et al., *Humoral immunity to SARS-CoV-2 and seasonal coronaviruses in children and adults in north-eastern France.* EBioMedicine, 2021. **70**: p. 103495.
208. Nguyen-Contant, P., et al., *S Protein-Reactive IgG and Memory B Cell Production after Human SARS-CoV-2 Infection Includes Broad Reactivity to the S2 Subunit.* mBio, 2020. **11**(5).
209. Anderson, E.M., et al., *Seasonal human coronavirus antibodies are boosted upon SARS-CoV-2 infection but not associated with protection.* Cell, 2021. **184**(7): p. 1858-1864 e10.
210. Poston, D., et al., *Absence of Severe Acute Respiratory Syndrome Coronavirus 2 Neutralizing Activity in Prepandemic Sera From Individuals With Recent Seasonal Coronavirus Infection.* Clin Infect Dis, 2021. **73**(5): p. e1208-e1211.
211. Shrock, E., et al., *Viral epitope profiling of COVID-19 patients reveals cross-reactivity and correlates of severity.* Science, 2020. **370**(6520).
212. Barnes, C.O., et al., *SARS-CoV-2 neutralizing antibody structures inform therapeutic strategies.* Nature, 2020. **588**(7839): p. 682-687.
213. Hurlburt, N.K., et al., *Structural basis for potent neutralization of SARS-CoV-2 and role of antibody affinity maturation.* Nat Commun, 2020. **11**(1): p. 5413.

214. Bertoglio, F., et al., *SARS-CoV-2 neutralizing human recombinant antibodies selected from pre-pandemic healthy donors binding at RBD-ACE2 interface.* Nat Commun, 2021. **12**(1): p. 1577.
215. Feldman, J., et al., *Naive human B cells engage the receptor binding domain of SARS-CoV-2, variants of concern, and related sarbecoviruses.* Sci Immunol, 2021. **6**(66): p. eabl5842.
216. Chau, N.V.V., et al., *Absence of SARS-CoV-2 antibodies in pre-pandemic plasma from children and adults in Vietnam.* Int J Infect Dis, 2021. **111**: p. 127-129.
217. Chiu, S.S., et al., *Human coronavirus NL63 infection and other coronavirus infections in children hospitalized with acute respiratory disease in Hong Kong, China.* Clin Infect Dis, 2005. **40**(12): p. 1721-9.
218. Esper, F., et al., *Evidence of a novel human coronavirus that is associated with respiratory tract disease in infants and young children.* J Infect Dis, 2005. **191**(4): p. 492-8.
219. Fauci, A.S. and H.D. Marston, *PUBLIC HEALTH. Toward an HIV vaccine: A scientific journey.* Science, 2015. **349**(6246): p. 386-7.

13. Declaration

Hiermit versichere ich an Eides statt, dass ich die vorliegende Dissertation selbstständig und ohne die Benutzung anderer als der angegebenen Hilfsmittel und Literatur angefertigt habe. Alle Stellen, die wörtlich oder sinngemäß aus veröffentlichten und nicht veröffentlichten Werken dem Wortlaut oder dem Sinn nach entnommen wurden, sind als solche kenntlich gemacht. Ich versichere an Eides statt, dass diese Dissertation noch keiner anderen Fakultät oder Universität zur Prüfung vorgelegen hat; dass sie - abgesehen von unten angegebenen Teilpublikationen und eingebundenen Artikeln und Manuskripten (siehe detaillierte Beschreibung in *14. Detailed description of work performed for this thesis*) - noch nicht veröffentlicht worden ist sowie, dass ich eine Veröffentlichung der Dissertation vor Abschluss der Promotion nicht ohne Genehmigung des Promotionsausschusses vornehmen werde. Die Bestimmungen dieser Ordnung sind mir bekannt. Darüber hinaus erkläre ich hiermit, dass ich die Ordnung zur Sicherung guter wissenschaftlicher Praxis und zum Umgang mit wissenschaftlichem Fehlverhalten der Universität zu Köln gelesen und sie bei der Durchführung der Dissertation zugrundeliegenden Arbeiten und der schriftlich verfassten Dissertation beachtet habe und verpflichte mich hiermit, die dort genannten Vorgaben bei allen wissenschaftlichen Tätigkeiten zu beachten und umzusetzen. Ich versichere, dass die eingereic4hte elektronische Fassung der eingereichten Druckfassung vollständig entspricht.

Daten präsentiert in der hier vorliegenden Dissertationsschrift wurden bereits in folgenden Publikationen veröffentlich:

Ehrhardt, S. A., M. Zehner, V. Krahling, H. Cohen-Dvashi, C. Kreer, N. Elad, H. Gruell, **M. S. Ercanoglu**, P. Schommers, L. Gieselmann, R. Eggeling, C. Dahlke, T. Wolf, N. Pfeifer, M. M. Addo, R. Diskin, S. Becker and F. Klein (2019). "Polyclonal and convergent antibody response to Ebola virus vaccine rVSV-ZEBOV." Nat Med 25(10): 1589-1600.

Ercanoglu, M. S., L. Gieselmann, S. Dähling, N. Poopalasingam, S. Detmer, M. Koch, M. Korenkov, S. Halwe, M. Klüver, V. Di Cristanziano, H. Janicki, M. Schlotz, J. Worczinski, B. Gathof, H. Gruell, M. Zehner, S. Becker, K. Vanshylla, C. Kreer and F. Klein (2021). "No substantial pre-existing B cell immunity against SARS-CoV-2 in healthy adults." bioRxiv: 2021.2009.2008.459398.

Gieselmann, L., C. Kreer, **M. S. Ercanoglu**, N. Lehnen, M. Zehner, P. Schommers, J. Potthoff, H. Gruell and F. Klein (2021). "Effective high-throughput isolation of fully human antibodies targeting infectious pathogens." Nat Protoc 16(7): 3639-3671.

Kreer, C., M. Zehner, T. Weber, **M. S. Ercanoglu**, L. Gieselmann, C. Rohde, S. Halwe, M. Korenkov, P. Schommers, K. Vanshylla, V. Di Cristanziano, H. Janicki, R. Brinker, A. Ashurov, V. Krahling, A. Kupke, H. Cohen-Dvashi, M. Koch, J. M. Eckert, S. Lederer, N. Pfeifer, T. Wolf, M. Vehreschild, C. Wendtner, R. Diskin, H. Gruell, S. Becker and F. Klein (2020). "Longitudinal Isolation of Potent Near-Germline SARS-CoV-2-Neutralizing Antibodies from COVID-19 Patients." Cell 182(6): 1663-1673.

Schommers, P., H. Gruell, M. E. Abernathy, M. K. Tran, A. S. Dingens, H. B. Gristick, C. O. Barnes, T. Schoofs, M. Schlotz, K. Vanshylla, C. Kreer, D. Weiland, U. Holtick, C. Scheid, M. M. Valter, M. J. van Gils, R. W. Sanders, J. J. Vehreschild, O. A. Cornely, C. Lehmann, G. Fatkenheuer, M. S. Seaman, J. D. Bloom, P. J. Bjorkman and F. Klein (2020). "Restriction of HIV-1 Escape by a Highly Broad and Potent Neutralizing Antibody." Cell 180(3): 471-489 e422.

Köln, den 03.01.2022

Meryem Seda Ercanoglu

14. Detailed description of work performed for this thesis

Parts of this thesis are based on an article that was submitted to the peer-reviewed journal *Nature Medicine:*

Ehrhardt, S. A., M. Zehner, V. Krahling, H. Cohen-Dvashi, C. Kreer, N. Elad, H. Gruell, **M. S. Ercanoglu**, P. Schommers, L. Gieselmann, R. Eggeling, C. Dahlke, T. Wolf, N. Pfeifer, M. M. Addo, R. Diskin, S. Becker and F. Klein (2019). "Polyclonal and convergent antibody response to Ebola virus vaccine rVSV-ZEBOV." Nat Med 25(10): 1589-1600.

I supported this study by conducting FACS-based cell sorts including the pathogen-specific single cell sorts and the bulk-sorts for the repertoire analysis.

Parts of this thesis are based on an article that was submitted to the peer-reviewed journal *Nature Protocols:*

Gieselmann, L., C. Kreer, **M. S. Ercanoglu**, N. Lehnen, M. Zehner, P. Schommers, J. Potthoff, H. Gruell and F. Klein (2021). "Effective high-throughput isolation of fully human antibodies targeting infectious pathogens." Nat Protoc 16(7): 3639-3671.

I supported this study by conducting FACS-based cell sorts including the pathogen-specific single cell sorts and by the subsequent data analysis and design of the FACS-related figure. I provided protocols for the extraction and handling of blood components related to PBMC isolation and protocols for sample preparation of PBMCs and B cells for FACS analysis.

Parts of this thesis are based on an article that was submitted to the peer-reviewed journal *Cell:*

Schommers, P., H. Gruell, M. E. Abernathy, M. K. Tran, A. S. Dingens, H. B. Gristick, C. O. Barnes, T. Schoofs, M. Schlotz, K. Vanshylla, C. Kreer, D. Weiland, U. Holtick, C. Scheid, M. M. Valter, M. J. van Gils, R. W. Sanders, J. J. Vehreschild, O. A. Cornely, C. Lehmann, G. Fatkenheuer, M. S. Seaman, J. D. Bloom, P. J. Bjorkman and F. Klein (2020). "Restriction of HIV-1 Escape by a Highly Broad and Potent Neutralizing Antibody." Cell 180(3): 471-489 e422.

I supported this study by conducting FACS-based cell sorts including the pathogen-specific single cell sorts and the bulk-sorts for the repertoire analysis.

Part of this thesis are based on an article that was submitted to the peer-reviewed journal *Cell:*

Kreer, C., M. Zehner, T. Weber, **M. S. Ercanoglu**, L. Gieselmann, C. Rohde, S. Halwe, M. Korenkov, P. Schommers, K. Vanshylla, V. Di Cristanziano, H. Janicki, R. Brinker, A. Ashurov, V. Krahling, A. Kupke, H. Cohen-Dvashi, M. Koch, J. M. Eckert, S. Lederer, N. Pfeifer, T. Wolf, M. Vehreschild, C. Wendtner, R. Diskin, H. Gruell, S. Becker and F. Klein (2020). "Longitudinal Isolation of Potent Near-Germline SARS-CoV-2-Neutralizing Antibodies from COVID-19 Patients." Cell 182(6): 1663-1673.

I supported this study by isolating and storing PBMCs and plasma from all study participants, by performing IgG-isolation, conducting FACS-based cell sorts including the S-protein specific single cell sorts and the bulk-sorts for the repertoire analysis. I performed experiments for the unbiased B cell repertoire analysis for the 48 healthy individuals to generate a reference sequence data set.

Parts of this thesis are based on an article that was submitted to the peer-reviewed journal *iScience* and that is available on the *bioRxiv* pre-print server:

Ercanoglu, M. S., Gieselmann, L., Dähling S., Poopalasingam N., Detmer S., Koch M., Korenkov M., Halwe S., Klüver M., Di Cristanziano V., Janicki H., Schlotz M., Worczinski J., Gathof B., Gruell H., Zehner M., Becker S., Vanshylla K., Kreer C., Klein F.. (2022). No substantial pre-existing B cell immunity against SARS-CoV-2 in healthy adults. Submitted and currently under review in iScience (Dec. 2021).

I was the lead researcher on this study of which all data are also described in this thesis. All experiments that are described in this thesis were planned, designed and analyzed by myself and Dr. Lutz Gieselmann. All experimental and scientific work has been supported and supervised by Prof. Dr. Florian Klein and Dr. Christoph Kreer. I contributed to all experiments described here but received help by other researchers in some experiments. In the following, I will outline the contribution of other researchers to these experiments:

Sabrina Dähling, supported this study by performing plasmid mini- and maxipreps, transfections, isolation of monoclonal antibodies from culture supernatants, ELISA assays and single cell PCRs. Naresh Poopalasingam, Kanika Vanshylla, Sandro Halwe and Michael Klüver and Stephan Becker supported this study by performing neutralization assays. Susanne Detmer supported this study by performing IgG-isolation from human plasma,

plasmid mini- and maxipreps, transfections, isolation of monoclonal antibodies from culture supernatants and ELISA assays. Manuel Koch supported this study by providing recombinant proteins. Michael Korenkov supported this study by performing colony PCR, plasmid mini- and maxipreps, transfections, isolation of monoclonal antibodies from culture supernatants and ELISA assays. Hannah Janicki and Johanna Worczinski supported this study by performing plasmid mini- and maxipreps, transfections, isolation of monoclonal antibodies from culture supernatants and cell culture. Maike Schlotz supported this study by isolating PBMCs from blood samples and organizing storage of samples. Birgitt Gathof supported this by organizing and providing blood donations of study participants. Veronika Di Cristanziano supported this study by performing commercially available ELISA assays. Matthias Zehner supported this study by performing ELISA assay analysis. Henning Gruell supported this study by revising the manuscript. Christoph Kreer supported this study by performing antibody sequence analyses.